UNIVERSIDADE DE SÃO PAULO
INSTITUTO DE QUÍMICA DE SÃO CARLOS
GRUPO DE BIOANALÍTICA, MICROFABRICAÇÃO E SEPARAÇÕES

Doutorado

Mucus-penetrating polymersomes as a potential lung drug delivery system: preparation, in vitro characterization, and biodistribution tests

Solicitante: Beatriz Nogueira Messias de Miranda
Orientador: Prof. Dr. Emanuel Carrilho

São Carlos - SP
2018

BEATRIZ N. M. MIRANDA

Mucus-penetrating polymersomes as a potential lung drug delivery system: preparation, in vitro characterization, and biodistribution tests

Tese apresentada ao Instituto de Química de São Carlos da Universidade de São Paulo para obtenção do título de Doutor em Ciências.

Área de Concentração: Química Analítica.

Orientador: Prof. Dr. Emanuel Carrilho.

São Carlos - SP

2018

ACKNOWLEDGEMENTS

During the four years of development of this work, one of the themes that caught my attention was Open Inovation. Of course in this thesis, we are dealing with academic work, but I can guarantee that there were many essential collaborators! Undoubtedly, each individual that contributed to the development of this work was essential and enabled these results to be achieved. And for that I will be forever grateful.

I, therefore, thank my supervisor Prof. Dr. Emanuel Carrilho that gave me the opportunity to accomplish my PhD under his guidance, always supporting my inquietude and being a true life-mentor.

My gratitude has to be extended to Dr. Adriano Marim de Oliveira, who accepted me as a student and was very supportive in all extensions. It will be a pleasure to keep working with you.

I thank all the CPG secretary and administrative personel from IQSC, in special, Gislei, Andrea, Vero, Sabrina and Vanessa.

My thesis could not be accomplished without many warm-hearted help and support, from my colleagues Ariane, Leilane, Jordana, Thais, Jocasta, Mayara, Danae, Marília, Aline, Lucilene, Sheila, Giovanna, Maria Helena, Tama, Bianca, Natália, thank you so much for all the support and friendship, gifts that only IPTlândia could give me. I special thank Bruno for all the MatLab and computer related support! I also thank all the administrative support from Gicelma, Elaine, Felipe, Fábia, Izabel, Natália and Kleber. And all the technicians and workers from Bionano.

I would also like to thank Professor David Weitz and his Group for accepting me as a student and for all the support provided. I wish to thank all the members, in especial Dr. Liheng Cai, Dr. Laura Arriaga and Dr. Alireza Abbaspourad for the incredible mentoring and Christina, Vitaly, Max E., Max. Z., Zaira, Jules and Muus for the wonderful memories.

During my internship, I had the pleasure to share the day-to-day with incredible roommates that were essential for such an amazing experience, and made my life so easy and pleasant. Sabrina, Aline and Gabriela, thank you for all the late beer talks, hugs, pictures and Sunday mornings!

Profa. Dra. Iolanda Cuccovia, Profa. Dra. Carlota Yagui and Prof. Dr. Gerhard Wunderlish for access to your laboratory and relevant discussion. Together, I would like to thank Carol, Gustavo, Greicy, Ale, Camila and Wesley. Incredible Drs that helped me on experiments but also contributed greatly on discussion. This thesis would not be accomplished as it is without you. Thank you!!

BioMicS group, that even far was always present. In special, my dear friends and business partners Juliane and Juliana, whom I shared some of the most exciting, and fullfilling business-related situations in my whole life. Thank you for all the learning and friendship! Solve was defnitely one of the most exciting chapters of this thesis!

The research described in this thesis was financed by the Science Without Borders Program, CNPq, and by Fundação de Apoio ao Instituto de Pesquisas Tecnológicas - FIPT, by the Novos Talentos Program. I greatly thank FIPT and IPT for the financial support, access to the IPT's infrastructure and the amazing minds that nurture the Institute. I also thank the Novos Talentos Program committee and founders. In special thanks to Alex, Gisele and Luciana for the great day-to-day work.

Thank you to my family. Vovó Nice, Vovô Sergio, Vovó Idalina that I had the pleasure to share great moments together over the last years, your love and care were essential! And to my dear Vovô Paulo, that is for sure really happy for my now, whenever he is. All my uncles, aunts and cousins, thank you!! And my stepfamily that accepted me 10 years ago with such warm hearts and take care of me as a daugter. Rachel, Silvio, and Livia, tank you so much! Could not ask for a better extended family!

Thank you to my family for all the love and support. Mom and Dad, you are my best inspiration of a successful professional and personal life. I am so lucky to be part of our family. Dezona, that with such a strong nick name, huge heart and one of the most inspiring woman I know, will always be my dear friend and little sister.

My special thanks goes to my partner in life, Lucas. Thank you for all the support, patience, incentive, love and adventures during this important Chapter of my life. In special for being open-minded, positive, constructive and helpful with all of the mountains of advice you've given. Other great adventures are sure to come.

RESUMO

MIRANDA, B. N. M. **Mucus-penetrating polymersomes as a potential lung drug delivery system: preparation, in vitro characterization, and biodistribution tests.** 2018. Tese (Doutorado em Química Analítica) – Instituto de Química de São Carlos, Universidade de São Paulo, São Carlos, 2018.

O muco protege o corpo humano de partículas externas, mas também representa uma barreira para a entrega de controlada de medicamentos através de nanocarregadores. Para ultrapassar a barreira do muco e impedir mucoadesão, nanopartículas sólidas são normalmente revestidas com polímeros inertes, tais como o polietileno glicol (PEG). No entanto, trata-se de um procedimento relativamente complexa. Nesta tese, estudamos métodos para fabricar nanocarreadores com uma excepcional combinação de propriedades, incluindo uma boa capacidade de muco-penetração e uma grande capacidade de carga. Ao contrário dos métodos convencionais de revestimento, usamos um copolímero dibloco, que consiste em dois blocos hidrofóbicos e hidrofílicos, que se auto-organiza em polimerosomos sob hidratação. Devido à inércia do bloco hidrofílico, estes polimerosomos devem ser, por natureza, muco penetradores. Além disso, sua estrutura oca fornece os polimersomos para serem carregados com carga hidrofílica, enquanto a carga hidrofóbica pode ser transportada através da membrana. Por conta da utilização de um polímero hidrolisável na presença de ácido, ácido poli láctico (PLA) como a espinha dorsal copolímero, demonstramos que estes polimerosomos podem liberar o conteúdo, após aplicação do estímulos externo relacionado ao pH. Os experimentos de rastreamento de partículas demonstraram que os polimersomos se difundem mais rápido do que as partículas não revestidas, em muco de intestino de porco, e testes de biodistribuição apresentaram resultados encorajadores para a entrega localizada de fármacos de maneira mais homogênea, melhorando a biodisponibilidade e efeitos terapeuticos. Mais estudos relacionados ao aumento da eficiência de encapsulação e testes de efetividade *in vivo* no tratamento de denças devem ser promovidos. Acreditarmos que combinação das vantages relacionadas à estrutura vesicular dos polimerossomas, estabilidade, e muco penetração possibilitam o desenvolvimento de uma nova plataforma para a entrega controlada de medicamentos na mucosa.

ABSTRACT

MIRANDA, B. N. M. **Mucus-penetrating polymersomes as a potential lung drug delivery system: preparation, in vitro characterization, and biodistribution tests.** 2018. Tese (Doutorado em Química Analítica) – Instituto de Química de São Carlos, Universidade de São Paulo, São Carlos, 2018.

Mucus protects the human body by trapping foreign particulates but also poses a barrier for drug delivery by slowing down the mobility of drug carriers. To design mucus penetrating carriers, solid particles are typically coated with inert polymers such as polyethylene glycol (PEG) to prevent mucoadhesion. However, the solid structure of these particles limits their loading capabilities and the process to coat them requires a complex synthesis. In this thesis we studied methods to fabricate nanocarriers with an exceptional combination of properties including a good mucus-penetration capability and loading capacity of hydrophilic and hydrophobic cargos. Unlike conventional coating methods, we use a diblock copolymer, consisting of both hydrophobic and hydrophilic blocks, which self-assembles into polymersomes under hydration. Because of the inertness of the hydrophilic block, these polymersomes should be mucus-penetrating by nature. Moreover, their hollow structure provides the polymersomes to be loaded with hydrophilic cargo, whereas hydrophobic cargo can be carried through the membrane. Importantly, by using a hydrolysable acid-catalyzed polymer (poly lactic acid, PLA) as the copolymer backbone, we demonstrate that these polymersomes can release contents upon application of external pH stimuli. Particle Tracking experiments demonstrated that polymersomes diffuse faster than uncoated particles in porcine intestine mucus, and biodistribution tests displayed encouraging results towards more homogeneous local drug-delivery, helping bioavailability as well as therapeutic efects. More studies related to the increase of encapsulation efficiency, and *in vivo* disease treatment tests should be promoted. Although we believe that combining the advantages of polymersome carrier, and tunning the membrane composition, this mucus-penetrating carrier we propose may provide as a new platform for mucosal drug delivery.

1. TABLE OF CONTENTS

2. LIST OF FIGURES

OBJECTIVES

The overall goal of this thesis was to contribute to the development of mucus penetrating delivery systems by studying PEG-PLA-based vector platform. Local drug delivery is known to have advantages over the systemic administration, and mucus-penetrating polymersomes appear as a promise into innumerous diseases, such as cystic fibrosis, vaginosis and tumor treatments. This project was focused on the study of the mucus penetrating capability of PEG-b-PLA polymersomes, which motivations are described in Chapter 1; manufacturing methods, downstream techniques as well as characterization of produced vesicles in Chapter 2 and testes of optimisation in the process of carrier formation in Chapter 3; Chapter 4 describes the chemical and physical properties of the porcine intestine mucus which is further used as media for particle tracking experiments to analyze the diffusivity of the polymersomes in comparison to control particles, in Chapter 5, that also demonstrates biodistribution capabilities in comparison to control uncoated particles; while in Chapter 6 the encapsulation and loading of doxorubicin as well as the use of this formulation as a model drug-delivery vehicle was evaluated, together with biological testing.

CHAPTER 1

Aims and motivation

Mucus protects the human body by trapping foreign particulates, acts as a lubricant and selective barrier. At the same time that mucus is essential for protection, its clearance is a critical, physiologically regulated, function of the airways, lungs, eyes, gastrointestinal tract (GI) and female genital tract. In the airways systems, beyond obstruction of airflow, the excessive amount of mucus can be a perfect environment for infection by opportunistic pathogens, contributing to infections.[1] A vicious cycle initiates by mucus accumulation once an inflammatory response triggered by an infection occurs. Such negative effect of change in the physical state of the mucus occurs in other organs as stomach, intestine and female vaginal tract, causing gastric ulcers, inflammatory bowel disease (IBD) and vaginosis, respectively. Bansil *et al.* (2013) studied the influence of mucus microstructure and rheology in infestation and the establishment of colonies by *Helicobacter Pylori* on the mucus epithelial surface of the stomach, directly related to the development of gastric ulcers.[2] Less protective mucus barrier was observed by Schultsz and co-workers (1999) in the intestinal mucus in IBD patients when compared to control.[1] In addition, cervicovaginal mucus (CVM) has its physical state precisely managed according to specific conditions, such as according to the age, fertility cycle, or when semen is present in the vagina, and changes in such control can compromise this physical barrier against vaginal infections.[3]

Other pathophysiological conditions can alter the characteristics or expression of the mucin fibers therefore the composition and properties of mucus secretion. Cancers cells express novel combinations and forms of mucins, which can contribute to the cellular growth, differentiation, transformation, adhesion, invasion, immune surveillance and metastasis, as shown in Figure 1.[4,5] The study of mucin expression patterns and its regulation becomes a potential strategy in finding cancer biomarkers.[4–9]

Figure 1 – Tumors use mucins for invasion, metastasis and protection. a.Tumors use the anti-adhesive effect of mucins to detach from the tumor mass and surrounding stroma and invade. b. Tumors use the adhesive effect of mucins to attach to endothelia and invade. c. Tumors also use mucins to escape immune surveillance

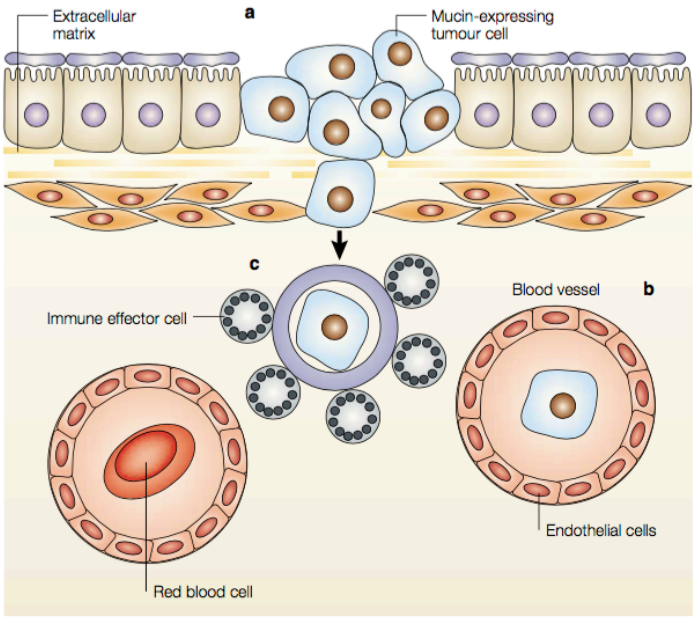

Source: Hollingsworth and Swanson, 2004. Reprinted with permission from Nature Publishing Group.[4]

Therefore, mucosal surfaces are often targeted for locally treating many diseases and its localized drug delivery enables many advantages over the systemic administration, such as reduced systemic side effects and sustained drug levels at target sites.[10] At the same time, mucus poses a barrier for drug delivery by slowing down the mobility of drug carriers, such as solid particles or liposomes. Nanoparticle systems arise as a promising alternative since it may facilitate the delivery of encapsulated therapeutic molecules that suffer from low stability or absorption in mucosal fluids besides its evenly distributed over the site of action.[11–13] Non-uniform delivery can be considered a major problem for the effective prevention and treatment of many diseases, including cystic fibrosis, bronchitis, asthma, sexually transmitted diseases, inflammatory bowel disease and cancer.[11] The achievement of sustained and uniform drug delivery to mucosal surfaces or to its underlying epithelia is possible by the use of mucus-penetrating particles (MPP) that overcome the mucus barrier and its clearance mechanisms;[14] and are generally produced by densely coating solid particles with inert polymers such as polyethylene glycol.[10,15–18] Hanes and co-workers described the benefits of

polyethylene glycol (PEG) coatings in nanoparticles mucus penetration rates compared to uncoated particles.[15] Improvements were later described by Lai *et al.* and complemented by Wang *et al.* who proposed the necessity of high densely coating with low MW of PEG to formulate mucus-penetrating particles.[16,18] Indeed, a nanocarrier covered by PEG limits blood protein tagging, diminishing the probability of being recognized by the immune system and consequently be eliminated. Therefore, low MW PEG produced a sufficiently hydrophilic and uncharged surface that minimizes the mucin-nanoparticle adhesive interactions, allowing particles to diffuse through human mucus.[16,19] However, the solid nature limits the loading capacity and encapsulation efficiency.[20] Moreover, the coating process requires complex synthesis, in which substantial drug loss and polymer degradation could occur.[17]

Here we aim to study a new platform for mucosal drug delivery based on polymersomes. Polymersomes are polymer-vesicles that offer many advantages over other nanostructures, such as loading of hydrophilic and hydrophobic drugs, besides the possibility of carrying larger loading amounts due to its core-shell morphology. The membrane of these polymersomes comprises an amphiphilic diblock copolymer of poly(ethylene-glycol)-b-polylactic acid (PEG-b-PLA). The hydrophilic block, PEG, makes these polymersomes non-sticky to mucus, whereas the hydrophobic block, PLA, provides the polymersomes with pH-sensitivity, due to hydrolisis. The pH-sensitiveness is a delivery strategy that bases on the occurrence of acidic microenvironment in solid tumors when compared to normal tissues.[21,22] Nano, pH-sensitive delivery-systems have already been reported including polymer vesicles, and have proven to be a promising strategy for cancer therapy.[23–26] To our knowledge the combination of this versatile, pH-sensitive mucus-penetrating polymersome systems have not been described. Therefore, by preparing PEG-PLA polymersomes and measuring their mobility in fresh mucus samples, rather than reconstituted ones, we study the polymersomes diffusion in comparison to unprotected particles. We believe that combined mechanisms of mucus-penetration capability and advantages of polymersonal system would enable the use of this nanocarriers to improve treatment options for diseases that involve and affect mucosal surfaces.

CHAPTER 2

From nanotechnology to Polymersomes

1. INTRODUCTION

1.1 Nanotechnology in Drug Delivery

Nanotechnology is a field of study that is decreasing the barriers between biology, chemistry, physics, engineering, and medicine. With growing application in these areas, nanotechnology strength the collaboration between fields in order to reach successful developments/ applications. With that being said and agreed to a consensus, the shift in size from micrometers to hundreds of nanometers has revolutionized the administration methods of medicines, representing a significant technological and medical breakthrough.[27] From the impossibility of intravenous administration of pharmaceutical suspensions to the so-called nanomedicines, nanotherapy, nanotechnology is being crucial to solving several limitations of conventional drug delivery systems, improving, for instance, biodistribution, solubility, bioavailability, activity, and reducing toxicity by directing drugs towards the disease site.[27,28] According to the application, size and surface characteristics, nanoparticles can be tuned to increase circulation time in the bloodstream. Biodistribution of drugs is another critical characteristic to be achieved and studied, especially when dealing with cancer drugs, and local drug delivery for associated mucosal diseases, like bronchitis, asthma and gynecological diseases. For instance, dealing with tumors, one of important property of nanocarriers is the enhanced permeability and retention (EPR) effect, in which they tend to accumulate more in tumor tissues than healthy ones. Such effect happens due to the enhanced requirement on nutrients supply that is achieved by the angiogenic process. In this process, new blood vessels are formed from pre-existing vessels, occurring the development of defective endothelial cell layer, with wide pores. These leads to abnormal fluid and macromolecular transport, including nanocarriers, what would be otherwise restricted.[29] While the EPR effect helps the biodistribution of nanocarriers and drugs inside the cancer tissue, decreasing drug toxicity, alterations of the

biodistribution can increase toxicity in some tissues, being central to the efficacy of pharmaceutical and drugs.[28,30,31] That justifies why studies to find new active targeting mechanism, different materials, or new target ligands are under development.

1.2 Nanocarriers

Since the first report of a polymer-drug conjugate in 1955 by Von Horst Jatzkewitz, a wide variety of nanocarriers have been developed and in the past 30 years, it has been applied to drug delivery systems.[32,33] Using different materials including lipids, polymers and inorganic materials, advances in nanoparticle engineering have been developed. These advances allow the tune of their physicochemical properties and thus studies in their specific applications, opening new opportunities for the development of nanoparticles for diagnosis and treatment of many diseases.[34] Examples of inorganic nanoproducts are carbon nanotubes, quantum dots, gold, silica and magnetic nanoparticles, while organic nanocarriers are polymer-drug conjugates, dendrimers, polymeric particles and capsules, and self-assembly structures. This class of drug delivery systems is represented by micelles, liposomes, polymersomes, which will be emphasized in this thesis.

Around fifty years later, polymer-drug conjugates have been well studied and the potential of polymer-based systems over the others was mainly due to their wide variety regarding nature, properties and composition, ease functionalization and relative simple synthesis methods.[34] There is some knowledge that the use of specific polymers could offer specific characteristics to the nanocarrier. For instance, the addition of low concentrations of polyethylene glycol (PEG) to lipid formulations did not alter vesicle morphology but enhanced the liposome blood circulation/lifetime when compared to conventional liposomes. This strategy originated Doxil® in 1995, first liposomal-based drug formulation approved by the US Food and Drug Administration (FDA), a stealth PEGylated liposome formulation to treat specific tumors that showed improved response rates when compared to the free drug.[33,34]

Self-assembly structures naturally exist and are present in our day-to-day basis, from simple soap bubbles to composite membranes of living cells.[35] All of

these structures are formed by unitary molecules, which in turn, consist of the hydrophobic tail portion and a hydrophilic head group. Micelles are characterized by a hydrophobic central core surrounded by a hydrophilic corona, while liposomes are reservoir-like self-assembly systems.[36,37] Both liposomes and micelles proved to be interesting delivery systems for therapeutic drug delivery and advantages offered by polymers in biomedical application supported the idea of a vesicle-type system composed entirely of polymer, originating polymersomes. These structures are exemplified in Figure 2.

Figure 2 – Schematic illustration of self-assembly delivery systems: micelles; liposomes; polymersomes.

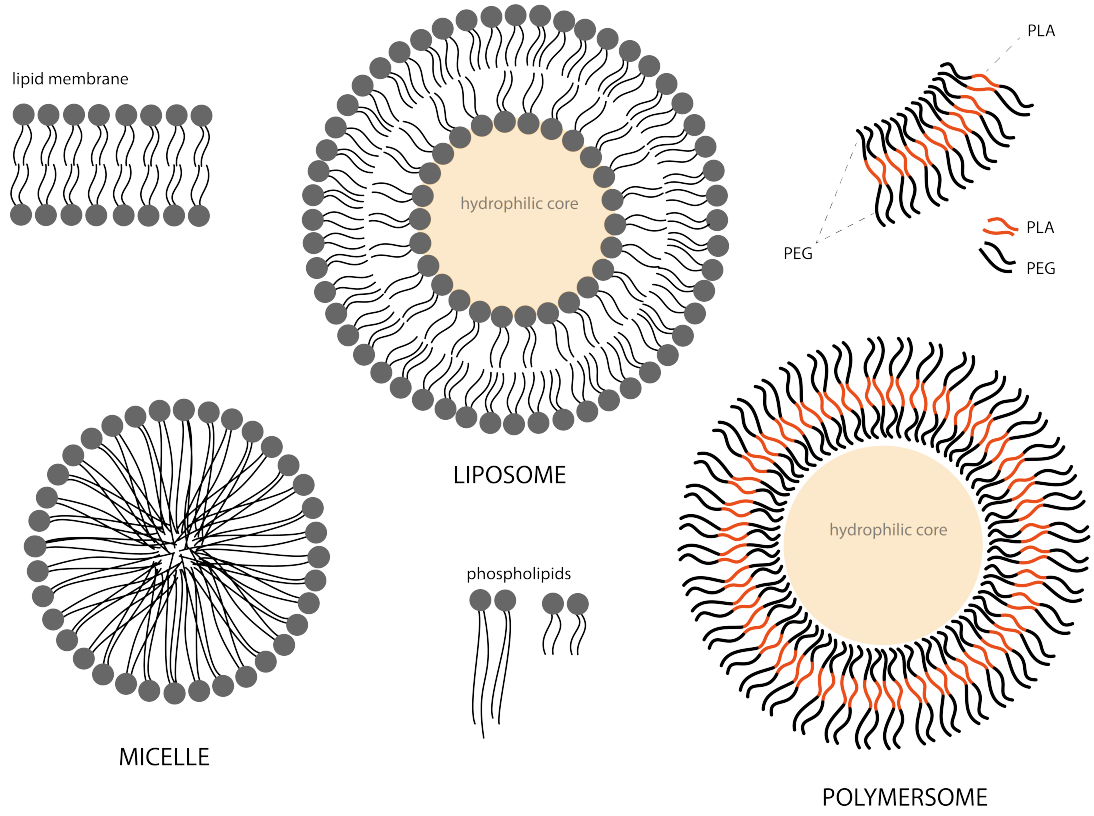

Source: Beatriz N. M. Miranda

1.3 Polymersomes

Polymersomes are self-assembled biomimetic analogs of natural vesicles, made of amphiphilic block copolymers that have been compared to liposomes due

to its similar structure, and also to viral capsids, when it is about available functions and properties.[36,38] Polymersomes should not be mistaken with polymer capsules, that differentiate themselves by the nature of the polymer membrane, which is composed of self-assembled amphiphilic block copolymers in the case of polymersomes.[34,36,37] The hydrophobic blocks of the latter tend to interact in order to minimize direct exposure to water, while the hydrophilic blocks interact with inner and outer aqueous solutions, producing a bilayer membrane, as shown in Figure 2.[34] Comparable to liposomes, polymersomes are biocompatible and allows the encapsulation of both hydrophilic and hydrophobic components, in their aqueous core and synthetic membrane, respectively. Furthermore, its relatively high control of the size and the combination of their chemical and physical properties, enhancing flexibility and stability to those particles, offers advantages over liposomes making them promising vehicles to sustained drug delivery and the active targeting.[34,39] Naturally, over the past two decades studies have been focused on the encapsulation of active substances inside the polymersomes, and the first *in vivo* studies with a drug-loaded polymersome formulation reported was in 2006 by Ahmed *et al.* expanding opportunities for in vivo diagnosis and treatment of many diseases.[38,40–43]

1.4 Block copolymers

A polymeric chain constituted of repetitions a single monomer is referred to as a block. Block copolymers (BCPs) are macromolecules that are formed by the linkage of two or more different polymeric blocks.[35] Different block copolymer architectures have been described. For instance, diblock, triblock and tetrablock copolymers besides grafted and star architectures can be achieved by several synthetic approaches. When hydrophilic and hydrophobic blocks compose the macromolecule it is defined as an amphiphilic block copolymer. Due to the presence of immiscible blocks, these macromolecular structures can microphase separate into a variety of structures with high complexity when in an aqueous solution. They rely on supramolecular forces between their units.[35] Such process is defined as a self-assembling process that can drive the formations of spheres, cylinders, gyroids, lamellae, vesicles, etc.[35]

The concentration of polymer chains in the solution is related to self-assembly since only by reaching the critical aggregation concentrations (CAC) the polymer chains becomes close enough to interact driven by supramolecular forces.[35,39] The self-assembly of its smaller chemical analogs, phospholipids, and surfactants, has been well studied for many decades, and mathematical models have been suggested to describe the morphology of the aggregate. The packing parameter (*p*) uses different characteristics of the hydrophobic and hydrophilic portions to classify preferable morphologies, as shown in Equation 1 and Table 1.

$$p = \frac{v}{a_0 + l_c} \quad (1)$$

where:
v is the volume of the hydrophobic segment;
a_0 is the contact area of the head group;
l_c is the length of the hydrophobic segment.

Table 1 *Packing parameter* (*p*) classification.

Packing parameter	**Morphology**
$p < 1/3$	spheres
$1/3 < p < 1/2$	cylinders
$1/2 < p < 1$	flexible lamellae or vesicles
$p = 1$	planar lamellae

Comparably, the preferred structure such as vesicle, rod-like or micelles is influenced by the aggregate morphology, which in turn depends on the average copolymer molecular shape.[44,45] For copolymers that have the hydrophilic portion, a PEG block, the average molecular shape is related and thus simplified to the hydrophilic fraction ***f***, which is calculated from the fractions mass values according to the homopolymer fusion density and classified as illustrated in Figure 3 (a).[38,45,46]

Besides the molecule architecture, thermodynamic forces also influence the preferred structure to be formed.[44] Hence, an enthalpy contribution is related to interfacial energy between the two blocks according to the solvent, while chain stretching and the conformational liberty of water contributes to an entropic contribution.[47]

Moreover, monomer molecular weight dictates membrane thickness, as shown in Figure 3. The high molecular weights of block copolymer together with low

critical aggregation concentrations and very slow chain exchange dynamics enhance colloidal stability against mechanical shear and osmotic pressure difference.[39,48] Thus, allowing the retention of the payload for longer periods and making polymersomes particularly attractive as vehicles for sustained and controlled release purposes.

Figure 3 – Schematics of block copolymer fractions with respective cryogenic transmission electron microscopy images showing vesicles or worm micelles and spherical micelles. a. morphology dictated by *f*. b. Schematic scaling of polymersome membrane thickness dictated by copolymer molecular weight (MW). PEG, polyethylene glycol.

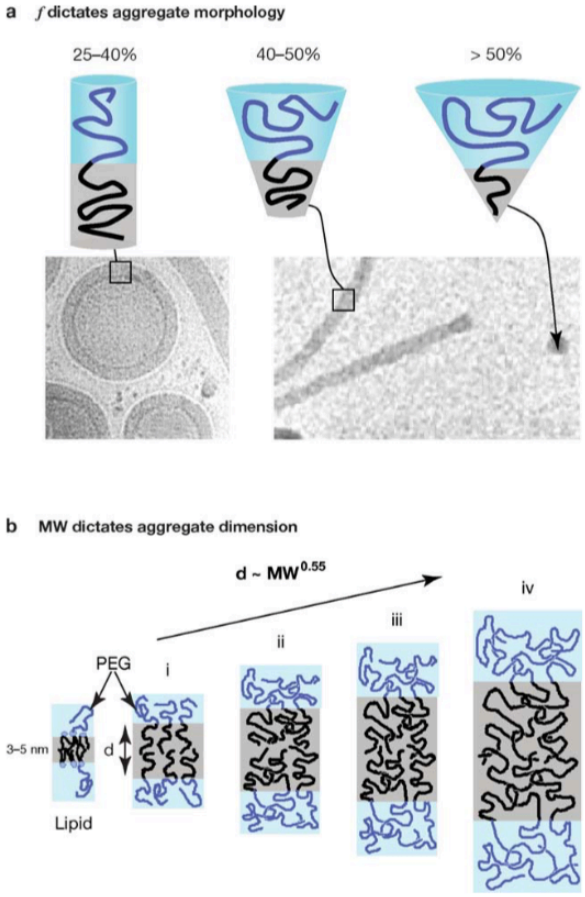

Source: Reprinted with permission from Annual Reviews.[38]

1.5 PEG-PLA Polymersomes

Block copolymers of poly (ethylene-glycol)-b-polylactic acid (PEG-b-PLA) are well established, completely biocompatible and FDA approved.[49] Its combination of properties related to very low toxicity, the PEG-related resistance against antibody

binding and recognition, extending particle circulation times are very promising for pharmaceutical uses. Moreover, biodegradability by hydrolytic degradation enables the production of pH-sensitive polymersomes-like structures. The PLA repeated unit, constituting the hydrophobic part of PEG-PLA copolymer, indeed undergoes degradation rate. Through acid-base catalyzed hydrolyzes of the backbone ester groups,[50] the carbon from the carboxyl group is attacked by a nucleophile (water or hydroxyl ion). In an aqueous base solution, hydroxyl ions are better nucleophiles; in acidic solution, the carbonyl group becomes protonated, facilitating water nucleophilic attack. Temperature shifts have shown also to have a greater effect in PEG-PLA polymersome degradation and consequently, leakage.[41] PEG–PLA vesicles have been described before and their importance as drug-delivery carriers highlighted.[37,40,51,52] Ahmed *et al.* (2006) and Ayen *et al.* (2011) demonstrated the enhanced effect of doxorubicin-loaded (DOX-loaded) polymersomes over free DOX in tumors treatment.[41,53] After injections drug-loaded polymersomes blocked tumor growth and killed cells.[41,53] Ahmed *et al.* (2006) also describe the release difference between bio- and non-degradable polymersomes.[33] Ayen *et al.* (2011) emphasized the effect of solvents, methodology parameters, copolymer concentration, and external energy input on size and dispersity of polymersomes.[53] Consequently, studies related to production techniques are important.

1.6 Production techniques

There are a few strategies that can be employed to nanocarriers production, and the preparation method is chosen according to the material and its intrinsically characteristics. As discussed in previous sections, the average copolymer shape and the phase separation of the two building blocks drive the self-assembly into polymersomes, sustained further by non-covalent forces.[54] Therefore, the copolymers glass transition temperature (Tg) will directly influence the preparation method. If Tg is lower than 25 ^{o}C, the polymersomes can be prepared by direct addition in water. On the other hand, if a higher Tg is the working case, the use of a suitable organic solvent is required to enable chain mobility for the polymers to form the bilayered vesicles.[55] Regarding polymersome formation, if a bigger entity is

assembled before the vesicles, the technique is based on a top-down approach, as what happens in the film rehydration method. On the contrary, if the first morphology assembled by the copolymer unimer is already a vesicle, then it should be classified as a bottom-up approach. Basically, production techniques of polymersomes are, in general, the same for liposome production.[56]

Film rehydration method

To induce the self-assembly of copolymers with higher Tg in aqueous solution generally, the preparation methods can be classified as solvent-free or those that rely on the use of organic solvents. Technically, both groups will require the use of organic solvent, although, for the first one, called film rehydration process, the block copolymer is dissolved in a suitable organic solvent and dried, forming a film, as shown in Figure 4. Only after complete solvent evaporation, hydration is performed. Depending on the system used, different self-assembled morphologies (vesicles, tubes, micelles) can be achieved. Upon hydration, the copolymer film starts to swell and, balance between attractive and repulsive forces yields vesicles[57]; with the advantage of having no organic solvent in the system, which can be mandatory for certain applications.[56]

Figure 4 - Film hydration illustrative protocol.

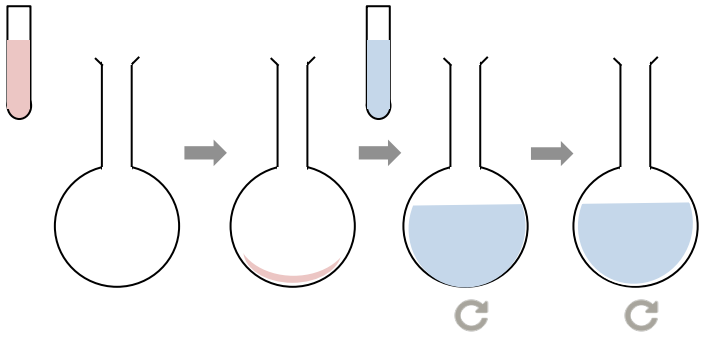

Source: Beatriz N. M. Miranda

Since this method yields polymersomes with a wide size distribution, resizing protocols are frequently applied in attempt to homogenize and decrease the samples average particle size. The decrease of the mean vesicle size and dispersion accomplished by vortexing, freeze-thaw cycles, membrane extrusion and

sonication, as shown in Figure 7.[56] These techniques are often described as a complementary step in the polymersome production methodology. Moreover, factors related to the preparation method such as the length and polydispersity of the individual blocks, solvent composition, temperature, pH, can directly influence the types of self-assemblies produced, size, drug loading, and release.[56,58]

Microfluidic method

Another technique that is based on double emulsion and requires an organic solvent for the production of polymersomes is microfluidics, as shown in Figure 5 and Figure 6.[49,59–61] It is a very consistent and reproducible technique that enables the production of highly monodisperse and complex vesicles, while the spontaneous assembly of the diblock copolymers, typically provide a large size distribution and encapsulation of only small proportions of the cargo.[20]

Figure 5 - Photography and schematic illustration of the microcapillary device for generating double emulsions.

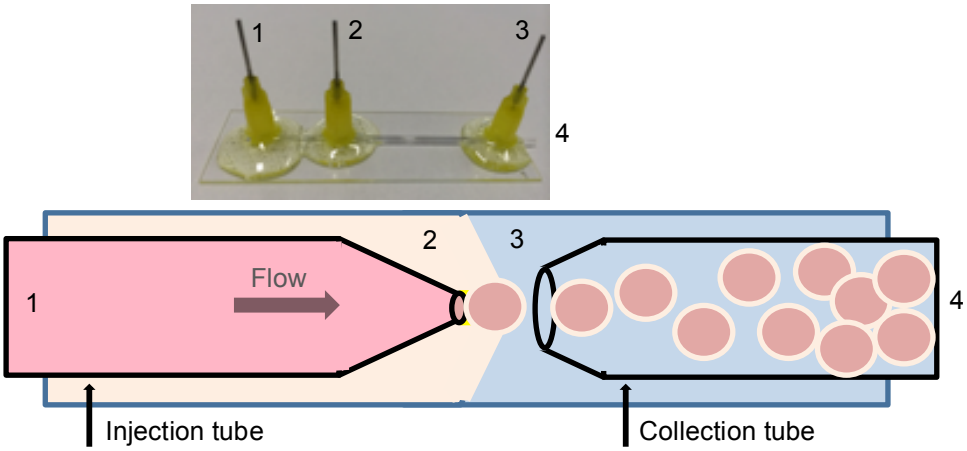

Souce: Beatriz N. M. Miranda , adapted from [20]

Unfortunately, currently available microfluidic methods based on double-emulsion production are based on glass capillary, which limits the size of polymersomes to 50 μm, illustrated in Figure 5. Therefore, it precludes its systemic application as well as other specific applications such as mucus penetration, in which the average pore size range 100-1000 nm, what will be evaluated in this Thesis.[62] For that reason, this production route is being used for developing a

model system for the study of the physical properties of cell membranes, controlled-release techniques and producing multi-compartment polymersomes.[49,59–61,63–65]

Figure 6 - Proposition of polymersome formation after double emulsion wetting and solvent evaporation.

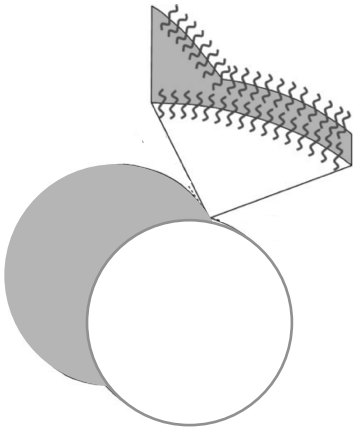

Souce: Adapted from [20]

Figure 7 - Illustrative representation of some commonly used resizing protocols.

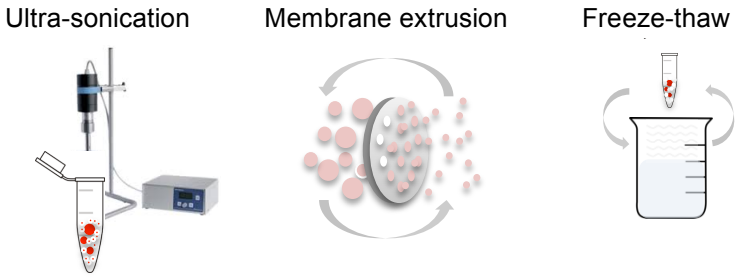

Source: Beatriz N. M. Miranda

1.7 Loading

When the issue is loading, liposomes and polymersomes have a huge advantage over the other carriers, which is the possibility of incorporation of both hydrophobic and hydrophilic molecules. Drug loading methods and efficiency are related to the chemical nature of the drug itself, particularly its polarity.[34] According to the nature of the cargo that is willing to encapsulate, preference should be given to one or another process. For instance, hydrophobic cargo can be dissolved together with the block copolymer in the organic solvent in the nanoprecipitation method. The double emulsion originated in the emulsion-solvent evaporation or

solvent exchange methods is more suitable for loading hydrophilic drugs[66], as long as the cargo is stable in those solvents. Such observation is very important since loading, for instance, proteins, would be inviable by the presence of some organic solvents. Hence, drugs can be loaded by adding them to the reaction mixture during the formation process (top-down approach for drug loading) or by adding them to a previously prepared sample (bottom up). For instance, it is possible to direct hydrophilic drugs encapsulation during polymersome formation or by forcing the encapsulation with the use of salt or pH gradients (pH switch) or by electroporation, to increase loading may also be used.[67] On the other hand, hydrophobic species can be incorporated during the self-assembly process, which can also be added before the film drying; during the formation of w/o/w double emulsions; or by diffusion.[34,39]

1.8 Release Methods

Controlling drug release is the heart of drug delivery systems. As already mentioned before, polymersomes offer the possibility of chemical modification and its combination of physical-chemical characteristics, enabling the tunable release. There are numerous chemical and physical factors that govern this effect according to the methodology used for polymersome preparation; pH, osmotic pressure, temperature, dilution can be used as conditions of the release.[34]

1.9 Characterization techniques

Characterization techniques that enable the study of polymersomes comprise scattering techniques and various microscopies.[56]

1.8.1 Dynamic light scattering (DLS)

As well as its use for the characterization of particles, emulsions or molecules, dispersed or dissolved in a liquid, and in the range of 1–1000 nm,

dynamic light scattering (DLS) is also used for determining the size of polymersomes. Turbidity measurements are promoted using a beam of laser light that passes through the sample solution. By analyzing the intensity fluctuation of the scattered light due to the Brownian motion, the velocity (D_t) of particles or molecules in suspension can be determined and consequently, the particle size measured regarding hydrodynamic radius, using the Stokes-Einstein relationship, shown below in Equation 2.[56,68]

$$D_h = \frac{k_b T}{3\pi\eta D t} \quad (2)$$

where:
D_h is the hydrodynamic diameter;
D_t is the translational diffusion coefficient;
k_B is the Boltzmann's constant;
T is the thermodynamic temperature;
η is the dynamic viscosity.

Other scattering methods such as static light scattering (SLS), X-ray scattering (SAXS) and wide-angle X-ray scattering (WAXS) could also be used, which provide information about colloidal samples structural features.

Zeta Potential

Zeta potential is a measure of the magnitude of the charge that develops at the interface between particles surface and its dispersing liquid. It is a key parameter to analyze the stability of colloidal systems, for example, if it tends to aggregate or not. Therefore, changes in pH or dispersing liquid may also play an important role in particles stability, since their interaction is given by the magnitude of zeta potential and not by their surface charge. When an electrical is applied to the sample, the particles tend to migrate oppositely to its electrostatic charge. The electrophoretic mobility (U_E) is, therefore defined, as the velocity of the particle migration in the field. Using Henry's equation, the zeta potential can be calculated due to its relation to electrophoretic mobility.[69]

$$U_E = \frac{2\varepsilon\zeta f(K\alpha)}{3\,\eta} \quad (3)$$

U_E = electrophoretic mobility
ε = dielectric constant
ζ = zeta potential

f(Kα) = Henry's function, which maximum or minimum values depends on the media polarity, following Smoluchowski or Hückel approximation, and where Kα is the ratio of particle radius to double layer thickness
η = viscosity

Microscopy

According to the sample size and the target analysis, different microscopy techniques can be used to investigate polymersomes' characteristics such as size and morphology. For instance, when dealing with large vesicles, so-called giant unilamellar vesicles (GUVs), optical microscopy technique allows fast, easy and straightforward sample visualization. Sometimes, however, the size, sample characteristics, and analysis demand a more complex technique with a better resolution. Using different light sources, such as photons or electrons, some interesting features emerge as well as some drawbacks.

Among electron microscopy techniques, transmission electron microscopy (TEM) is most frequently used for the study of the morphological details of polymer aggregates in solution. This technique requires drying and staining to enable sample visualization, which can change some sample characteristics such as size. For that reason, cryo-TEM is commonly preferred as it maintains the sample in a natural hydrated state.[56]

Fluorescence microscopy is an interesting technique to visualize tagged molecules and their related dynamic processes. For instance, diffusion, osmolality, kinetic constants, and pH are some of the parameters that can be monitored by independently analyzing the emitted fluorescent light from the brighter excitation light.[56] Among those techniques, confocal fluorescence microscopy is frequently used for GUVs, since enables high *x*, *y* and *z* resolutions, three-dimensional stacks view and precise studies over shell morphology and molecules-membrane interactions.[65]

2. OBJECTIVES

In this chapter, we aim to study the production of polymersomes by microfluidics and by film hydration. A system will be chosen and the relationship among variable methods will be studied. The use of microfluidics technologies

should enable the study of the pH-release kinetics, while smaller sized polymersomes will be produced for further applications. Downstream techniques will also be evaluated as well as encapsulation efficiency.

3. EXPERIMENTAL METHODS

3.1 Materials.

We used the block copolymer $PEG_{5,000}$-b-$PLA_{10,000}$ (Polysciences, cat. 25018) from Polysciences, polyoxyethylene-polyoxypropylene-polyoxyethylene (PEO-PPO-PEO) (Pluronic® L121) and EUDRAGIT® E PO, for polymersome production. As fluorescent probes, we use sulforhodamine-β dye (Sigma-Aldrich) for micro-size polymersomes and for nano-sized: 1,2-dioleoyl-sn-glycero-3-phosphoethanolamine-N-(lissamine rhodamine B sulfonyl) (DHPE-Rh) (Molecular Probes), 1,3,6,8-Pyrenetetrasulfonic acid tetrasodium salt hydrate (PTS), and 2,2,6,6-tetramethyl-4- trimethylammoniumpiperidine-1-oxylIodide (CAT-1). All used solvents were from Sigma-Aldrich.

3.2 Micro-polymersomes

Microfluidic polymersome preparation. Capillary microfluidic devices developed by Kim *et al.* 2011 were used to produce double-emulsion droplets.[70] Using two tapered cylindrical glass capillary tubes (World Precision Instruments, Inc.) with an outer diameter of 1.0 mm that are inserted into a square glass capillary (Atlantic International Technology, Inc.) with an inner diameter of 1.05 mm a flow-focusing configuration is achieved. Typical inner diameters after tapering of circular tubes range from 20 to 40 μm for the injection, and from 100 to 200 μm for the collection tube, tapered by the use of a capillary puller (Sutter Instrument Co. model P-97). The tips of that ~60 μm and ~100 μm tapered capillaries, injection and collection, are treated to become hydrophobic and hydrophilic. For W/O/W double-emulsions the injection tube is treated with n-octadecyl trimethoxysilane (Sigma-Aldrich), while the collection tube is treated with 2-[methoxy(polyethyleneoxy)propyl]trimethoxysilane (Galest, Inc.) and cleaned with purified water (MilliQ System, Millipore). Tapered capillaries are inserted in a square capillary, originating the middle and outer phases injection sections. The inner aqueous phase, 1 wt.% poly(vinyl alcohol) (PVA, Sigma-Aldrich) supplemented with 9 wt.% Dextran (Sigma-Aldrich) and dissolved in ultrapure water (Millipore,

resistivity of 18.2 M Ω cm), is injected through the injection capillary. The oil middle phase is prepared containing 5 mg/mL $PEG_{5,000}$-b-$PLA_{10,000}$ in chloroform:hexane (40:60) and infused between injection and square capillaries, while the aqueous 10 wt% poly(vinyl alcohol) (PVA, Sigma-Aldrich) outer phase is infused between collection and square capillaries. Emulsion droplets are collected in 1× PBS (phosphate-buffered saline; 0.1 M, pH 7.4) and, after the dewetting process, polymersomes are produced and observed by confocal microscopy. The production of double emulsion drops within the microfluidic device which will originate polymersomes was recorded using a 4× objective on an inverted microscope (Leica) equipped with a high-speed camera (Phantom V9).

High-Resolution confocal microscopy of micro-polymersomes. We loaded glass reservoirs with polymersomes and used for high-resolution confocal imaging using a 10× dry objective with a numerical aperture of 0.3 on a confocal microscope (Leica), Z-stacks at 9.8 µm step sizes. Images were processed using ImageJ.

3.3 Nano-polymersomes

PEG-PLA polymersomes preparation by film hydration method. Nano-sized polymersomes were synthesized according to a standard film hydration procedure. Briefly, for the synthesis of PEG(5,000)-b-PLA(10,000), 1-10 mg of the copolymer is added to a round bottle glass tube together with a dye when needed (10 µL of a 0.5 $mg.mL^{-1}$ DHPE-Rh solution in chloroform or 10 µL of a 10 × diluted Vybrant DID Cell® labeling solution in chloroform). This mixture is dried either under N_2 gas flow gently perturbing the fluid surface or by slow rota-evaporation. After evaporation, the copolymer forms a nice, colored layer covering the bottom of the glass tube. At this step, the block copolymer is likely organized, forming a lamellar phase. The film is hydrated by adding 1 mL of PBS 1 × and left overnight at 50 °C under continuous stirring (hydrophilic cargo may be added at this step as well).

Resizing by membrane extrusion. Following hydration, the copolymer-dye/PBS solution with a concentration of 1-10 $mg.mL^{-1}$ is loaded in a glass syringe and

forced the passage through different membranes (Acrodisc 13 mm syringe filter with 0.4 μm and 0.2 μm pore size membrane), with decreasing pore size (mini-extruder from Avanti Polar Lipids) to create polymersomes. The extrusion process is repeated for >11 times to obtain homogenous polymersomes.

Resizing by probe-sonication. After hydration, the whole sample was transferred to an Eppendorff tube and sonicated using probe-sonicator (30 s on, 30 s off for 2.5 min at 20% amplitude under ice bath). After production, polymersomes are stored in a glass vial at 4 °C.

3.4 Purification techniques.

Differential Centrifugation (DC). Polymersome batches were purified by centrifugation and density gradient centrifugation following Robertson's *et. al* description.[71] Briefly, different centrifugation speeds were applied and the reminiscent supernatant was analyzed each time. Fractions were analyzed by DLS and NS-TEM.

Density gradient centrifugation (DGC). 150 μL of polymersome batches was carefully added to a sucrose gradient containing 200 μL of each layer (5, 10, 15, 20 and 25 wt%), and centrifuged at 20,000 RCF for 90 min. Fractions were analyzed by DLS, and NS-TEM.

Size Exclusion Chromatography (SEC). 10 $mg.mL^{-1}$ polymersome sample was produced, concentrated to 10 × using speedvac system and the aqueous suspension was then eluted through a Sephadex G25-column 3,0 g/12 mL. Sample and buffer flow were driven by simple gravity and eluting fractions were collected 20 drops per vial. Collected fractions were analyzed by fluorescence, DLS and NS-TEM when necessary.

3.5 Characterization techniques.

Dynamic Light Scattering (DLS). DLS analyses were carried out using a laser particle analyzer (NanoPlus, Particulate System) using software CONTIN as the calculation method, after 20 × (v/v) dilution in water. DLS measurements were based on 3-5 repetitions of 70 accumulation times. Samples were analyzed at 25 °C with a scattering angle of 165° and at 660 nm HeNe laser based on a dispersant refractive index (RI) of 1.33, a viscosity of 0.89 and a dielectric constant of 78.3. The samples were also characterized for surface charge by determining their ζ-potential using Zeta potential Analyzer (NanoPlus, Particulate System) based on 3 repetitions of 5 accumulation times, 70 cell constant. Cell positions 0.70/0.35/0.00/-0.35/-0.70 at a fixed voltage of 60 V, and a constant current of 51 mA, software Smoluchowski as calculation method and using the same dispersant from size analyses.

Negative Staining Transmission Electron Microscopy (NS-TEM). Polymersomes were prepared as described above and analyzed by conventional transmission electron microscopy using a FEI Tecnai G20 electron microscope (FEI Company, EUA), operating at 200 kV. For conventional TEM imaging, all analyses were carried out with dried samples, using 300 mesh copper grids (Koch Electron Microscopy, São Paulo, Brazil) covered with Formvar (Sigma Aldrich) followed by nanoparticle spotting, negative staining with 2 wt% phosphotungstic acid and proper wash before analysis. The grid preparation is a critical step to enable visualization by TEM, and for that reason, the same protocol was repeated for all samples, diminishing problems related to it.

Gel permeation chromatography (GPC). A Waters GPC system equipped with a Waters Styragel HR1, HR2, HR3 and HR4 gel columns (Waters) and differential refractive index Waters 2414 (sensibility at 32) detector was used to determine the molecular weight of the block-copolymer before and after probe sonication. A calibration curve was performed using polystyrene standards in the range of 370 to

769,000 g.mol^{-1}. THF was used as eluent with a flow rate of 1 mL.min^{-1}. Software Waters Empower 2 was used for data acquisition and analysis.

3.6 Evaluation of drug loading (encapsulation efficiency)

Size Exclusion Chromatography. 10 mg.mL^{-1} polymersome sample was produced in the presence of 0,5 mM 1,3,6,8-Pyrenetetrasulfonic acid tetrasodium salt hydrate (PTS), concentrated to 10 × using speedvac system and the aqueous suspension was then eluted through a Sephadex G25-column (3,0 g/12 mL) to separate PTS-encapsulated polymeric constructs from non-encapsulated PTS. Sample and buffer flow were driven by simple gravity and eluting fractions were collected 20 drops per vial. Loaded PTS was quantified by measurements of its UV fluorescence detection at λ_{ex}=305 nm and λ_{em}=455 nm. Encapsulation efficiency (E.E. %, Equation 4) was calculated as the ratio between the area under the curve of encapsulated PTS over encapsulated and non-encapsulated PTS.

$$EE\% = \frac{\text{Area under the intensity curve of the eluted polymersome fractions}}{\text{Area under the intensity curve of the encapsulated and non-encapsulated PTS fractions}} \times 100 \quad (4)$$

Electron paramagnetic resonance (EPR) Spectroscopy. Sample preparation for EPR analysis: The polymersome was prepared by hydration, as described previously, with a PBS buffer solution containing 1.25 mM of the spin probe 2,2,6,6-tetramethyl-4- trimethylammoniumpiperidine-1-oxyl Iodide (CAT-1). EPR spectra of the probe were acquired at room temperature in a Bruker EMX-200 spectrometer (Bruker, Germany) operating at 9.85 GHz, with a power of 5 mW (16 dB microwave attenuation), modulation amplitude of 1G, sweeping the field of 100 G centered at 3455 G. The gain was adjusted according to the sample concentration. Samples of CAT-1-containing polymersome (180 µL) were placed in flat quartz cells (Wilmad, USA) and the EPR spectra were recorded; 15 µl of 0.05 M ascorbic acid solution was added to react only with non-encapsulated CAT-1. The residual signal was attributed to CAT-1 probe encapsulated into the polymersomes and the volume of the internal aqueous compartments of the polymersomes estimated by the ratio between CAT-1 EPR signal before and after ascorbic acid addition.

4. RESULTS AND DISCUSSION

4.1 Preliminary studies

To test the stability and responsiveness of different pH-responsive polymersomes formulations, we used microfluidic approaches, which produces larger double emulsion drops (~150 μm) but enables an exquisite control of size and provides us information about its behavior under the pH stimulus. Our first system was composed by polyoxyethylene-polyoxypropylene-polyoxyethylene (PEO-PPO-PEO) polymersome membrane (Pluronic® L121) doped with small quantities of pH-sensitive polymers (1-3 wt.% of EUDRAGIT® E PO, a cationic copolymer based on dimethylaminoethyl methacrylate, butyl methacrylate, and methyl methacrylate, sensible to acidic pH) to test stability and pH-responsive test using the microfluidic approach, at a maximum polymer concentration of 20 wt.%. Unfortunately, all the formulations containing the pH-sensitive polymer were unstable as polymersomes, even at neutral pH. Control polymersome sample was produced with 20 wt.% of Pluronic® L121 and we observed that 50% of the cargo was already released by 12 hours of experiment, which may not be sufficient for drug delivery systems. The intensity of sulforhodamine-β present in the core enable precise quantification of the inner content over hours, as shown in Figure 8, and we observed an increase in the size of the double-emulsion drops (Figure 9). This increase in size is related to the presence of pores in the membrane, which enables water inflow into the cores of the vesicles to achieve an osmotic balance.[72] Therefore, the growth of those membrane pores will increasingly release the content and destabilizes the vesicle.[40] In the meantime, Nascimento *et al.* also used the microfluidic approach to produce poloxamers polymersomes and measured the permeability of the Pluronic® membrane to the permeating solutes.[72] Even though they describe their success in producing stable polymersome for more than 10 days, they cannot prevent the release over much less time.[72] Due to the weak hydrophobic nature of the midblock of Pluronic® polymers, polymersomes made of these copolymers are less stable than the ones formed by other copolymers, probably due to shorter membrane width or low hydrophobicity of PPO, what should enhance water permeability.[72] For that reason, we decided to study another

copolymer system, PEG-PLA, in which the midblock is more hydrophobic than PPO, which should increase membrane stability.

Figure 8 – Characterization of Pluronic double emulsions. A. Time evolution of the average fluorescence intensity of the vesicle at the initial average fluorescence intensity measured of the double emulsions for different membrane compositions, at different pH. B. Sample image showing

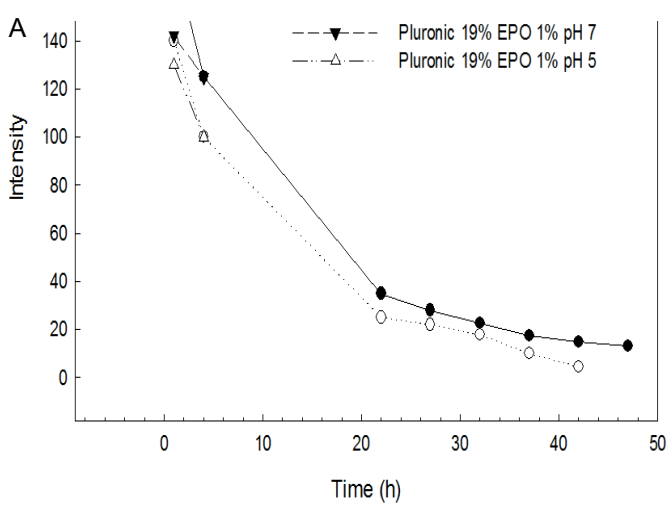

the dewetting process.

Source: Beatriz N. M. Miranda

Figure 9 – Time evolution of the average size of the vesicle at the average initial size measured of the double emulsions for the control sample, at different pH.

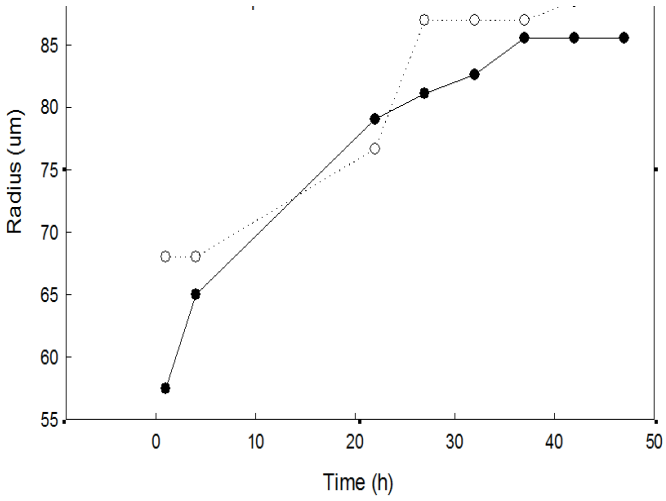

Source: Beatriz N. M. Miranda

4.2 PEG-b-PLA microfluidic polymersomes

Amphiphilic diblock copolymers of poly(ethylene-glycol)-b-polylactic acid (PEG-b-PLA) polymersomes have been described as efficient drug delivery carriers.[40,41] Among various stimuli-responsiveness, the strategy of using the tumor extracellular pH environment (pH_e) as the target is considered more general due to the common occurrence of the acidic microenvironment in solid tumors.[21] The acidic pH-response can be realized by acid-catalyzed hydrolysis of the vesicle-forming amphiphiles containing hydrolytically sensitive hydrophobic blocks, PLA. A relative homogeneous batch of PEG-PLA polymersomes was produced by microfluidics, in the experimental set up as shown in Figure 10.

Figure 10 – Microfluidic production of PEG-PLA polymersomes. a. Schematic illustration and optical microscope image of the capillary microfluidic device for production of double-emulsion drops (scale bar 100 µm). b. Optical and fluorescent image showing polymersomes after the dewetting process. c. Histogram of size and intensity of the polymersome batch after production.

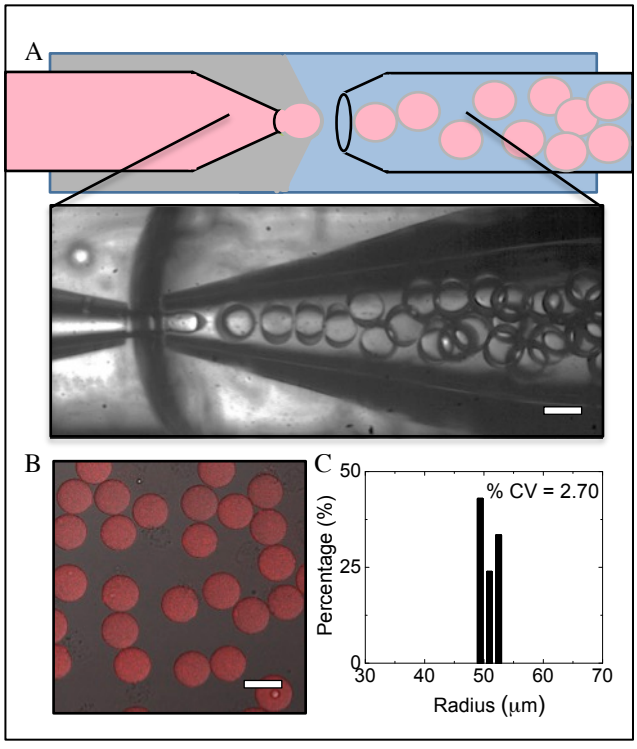

Source: Beatriz N. M. Miranda

By adding drops of a pH 5 buffer the release of sulforhodamine-*β* was detected, as shown in the image sequence of Figure 11, owing to hydrolysis of ester

bonds. pH 5 is close to the one found in endosomes and tumor tissues while blood plasma has a pH of 7.4, showing the possibility of use for such an approach.

Figure 11 – Image sequence of PEG-PLA polymersomes when submitted to a pH change from 7 to 5, 20 μm scale bar. The pH responsiveness can provide a more efficient release of drugs since there is a pH decrease in the mucus layer.

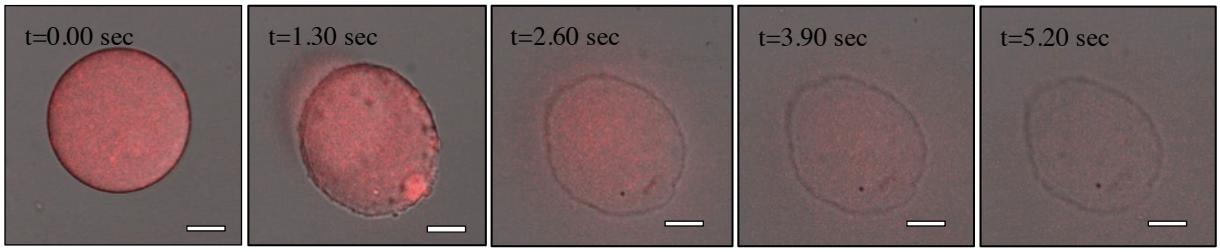

Source: Beatriz N. M. Miranda

Thus, a pH-dependent and slow, sustained release of encapsulated drug from these systems could be achieved, proving the applicability of this system. As polyester, PLA hydrolyzes under acidic and basic conditions, which mechanisms are shown in Figure 12. Such characteristics make it suitable for applications that require biodegradability as well biocompatibility, as controlled drug delivery vehicles.[73,74] The hydrolytic rate was described to be dependent on oligomer's molecular weight, temperature, and pH, and some studies have also purposed kinetic models to simulate the acid hydrolysis.[75–77] Therefore, the polyester undergoes hydrolysis, which produces pores in the membrane, following by final membrane disintegration. Such membrane porosity observation was previously observed by Ahmed and coworker, 2004, which exemplified mechanism is shown in Figure 13.[40] Moreover, as the block-copolymer degrades, it forms acidic components, that should amplify hydrolysis. Further, a pronounced effect of such acidic products over microparticles in comparison to smaller-sized particles was reported by Dune and coworkers[78], therefore in accordance with our observance by confocal microscopy, shown in Figure 11, and anticipating expectance that smaller polymersomes should be more stable.

Figure 12 – Schematic representation of a polyester undergoing hydrolysis. [79]

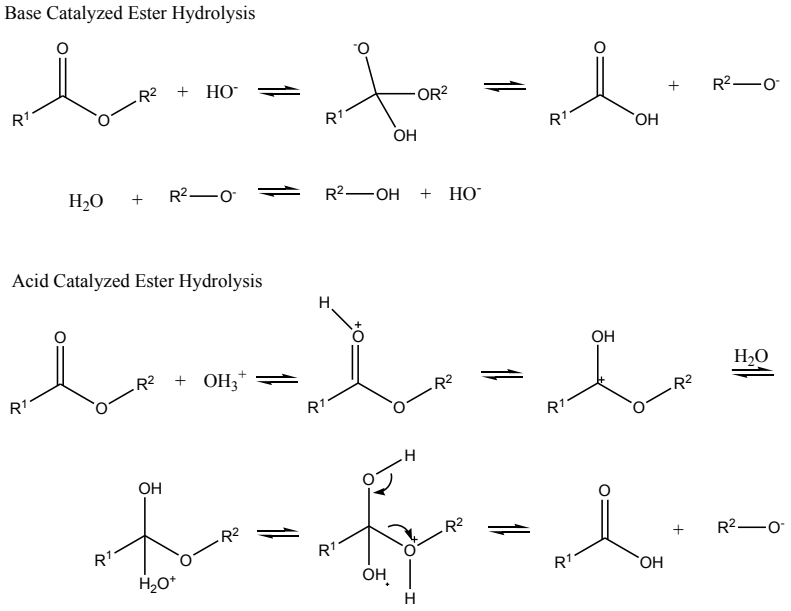

Source: Beatriz N. M. Miranda using ChemDraw Software.

Figure 13 – Polyester trigger of encapsulant release and disintegration of polymersome vesicles. Red chains are degradable polyesters and black chains are inert.

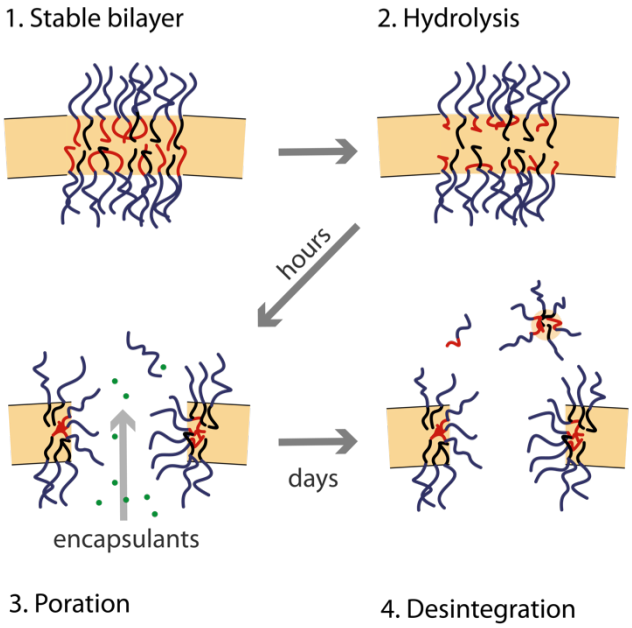

Source: Adapted from Ahmed et. al. Elsevier. [40]

Subsequently, for drug delivery purposes, the production of nanosized polymersomes was evaluated, as follows.

4.3 PEG-b-PLA nanosized polymersomes

The average copolymer molecular shape dictates the aggregate self-assemble morphology, i.e. whether it will form micelles, rods or vesicles.[44,4538] Therefore, for $PEG_{5,000}$-b-$PLA_{10,000}$ with hydrophilic fraction ***f*** of 0.325, vesicles formation should be favorable, hence, aqueous droplets stabilized by polymer membranes, as shown in Table 2 (***f*** 32.5 %; when 25-40 % tends to form vesicles).[38,45,46] These membranes comprise a PLA hydrophobic core and two PEG monolayers that prevent the PLA core from contacting the water. The addition of a PEG corona tends to avoid unspecific interaction with proteins, including mucin fibers, and also should increase circulations times, consequently achieve efficient delivery by topical mucosal or intravenous delivery.

Table 2 $PEG_{5,000}$-b-$PLA_{10,000}$ with hydrophilic fraction ***f*** calculation.

Block	Density	Mass	Volume	*f*
PEG	1,13	5000	4424,778761	0,325
PLA	1,09	10000	9174,311927	

Taking advantage of its self-assemble characteristic, we fabricate nanosized polymersomes by hydration in a PBS solution. Indeed, like liposomes, polymersomes can be produced by film hydration with or without shear, and sized through resizing protocols such as extrusion using polycarbonate membranes with decreasing pore size ranging from 1 μm to 100 nm; this procedure yields polymersomes of approximately 100-200 nm in size, as shown by the DLS data in Table 3. The decrease in the membrane pore size from enhanced homogeneity lowered the polydispersity index (PDI), although its pore size seems not to influence much on the polymersomes size. Moreover, this observation can be explained by a finite distribution of sizes about some mean value. Additionally, PDI values in the range of 0.2 to 0.3 are in accordance to the literature.[53,80] This value displays the width of the fitted Gaussian distribution demonstrating relative size dispersity of the

polymersomes even when different production methods were used for the formation of polymersomes.

Table 3 Size and PDI of film hydrated polymersome samples before and after extrusion with different membrane sizes.

Sample	Size	PDI
Unfiltered	457.4	0.291
200 nm Membrane	198.5	0.263
100 nm Membrane	144.7	0.246

Figure 14 – A. NS-TEM micrographs of PEG-b-PLA polymersomes produced by film hydration followed by extrusion and B. Typical zeta potential graph for PEG-b-PLA polymersome batch.

A

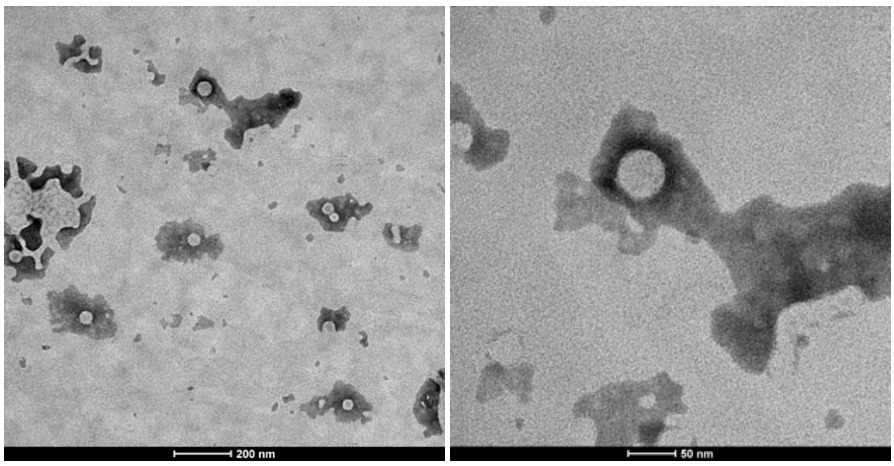

B

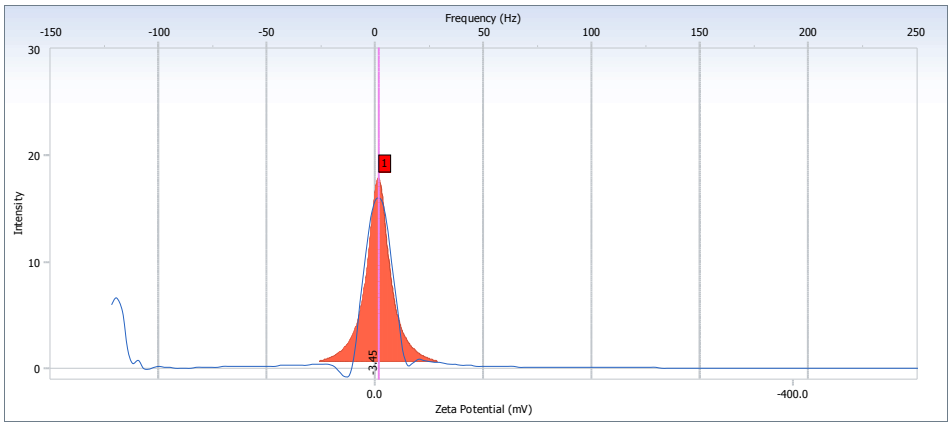

Source: Beatriz N. M. Miranda

Typical sizes obtained for polymersomes range from 50 to 200 nm, larger than those of polymeric micelles, according to the kinetic control variables related to

the manufacturing process.[48] While scattering experiments revealed a size close to 200 nm, the results of TEM analysis revealed a 51.35 ± 12.2 nm size, as shown in Figure 14. The size distribution of the vesicles was calculated from NS-TEM micrographs, using ImageJ Software. Nevertheless, while DLS measures the hydrodynamic radius of the particle, augmenting its size, NS-TEM preparation method requires the use of staining and drying that decreases vesicle size. Moreover, this decrease in NS-TEM can be explained by an osmotic shrinkage due to phosphotungstic acid (PTA), which will have a higher osmotic activity than the buffer in the polymersome lumen due to higher ion concentration. It was previously reported that NS-TEM analyzed polymersomes had diameter values about 20 nm less than for polymersomes analyzed with AFM, Cryo-TEM and FF-TEM (freeze fracture), which is accordance and explains obtained values for polymersome diameter by NS-TEM.[81] A more sophisticated alternative would be the use of cryogenic procedures, what should reduce the error in TEM analysis related to drying or staining.

Furthermore, negative staining using PTA is based on a heavy metal deposition, which provides strong scattering where interacts with the sample. It is a straightforward staining method for polyamides and polyesters since it preferentially interacts with amine and carbonyl groups.[81,82] Therefore, the hydrophobic PLA core of PEG-b-PLA polymersomes is favorably stained than the hydrophilic PEG corona, what provides a bias regarding wall thickness measurement. For instance, 3 nm was the average hydrophobic core thickness of polymersomes calculated by ImageJ using NS-TEM micrographs. However, such information may be biased since the staining agent deposition on copper grids after interaction with the hydrophobic polymersome membrane may lead to the imprecise determination of membrane thickness[83], requiring further combining X-ray studies to precisely determine the bilayer thickness.

Due to the outermost PEG monolayer of the polymersome membrane, the ζ-potential of the polymersomes is slightly negative, which is in agreement with ζ-potential measurements of PEG-coated nanoparticles.[10,16,84,85] Such characteristic is important when mucus-penetrating particles are wanted, once they will not tend to interact with negatively charged mucin fibers, and will be further discussed in Chapter 4.

4.4 PEG-b-PLA nanosized polymersomes production

Unfortunately, one drawback of this preparation technology (regarding BCP chosen for this work) is that such preparation technique is very time-consuming (taking sometimes days for hydration) and difficulty for high throughput. A significant amount of polymer bulk was always observed, making it difficult to quantify the amount of polymer in solution and effective vesicle formation. This may be the reason why there are still no commercially available products based on polymer vesicles.

In order to induce vesicle production, lower hydration times and simplify the resizing process, we, therefore, hypothesize that tip sonication could provide sufficient energy to break and re-form even more mechanically robust nanoparticles such as polymersomes, what may not be achieved as efficiently when using bath ultra-sonicator or membrane extruding.

Self-assembly formation by film hydration was promoted overnight and using Vybrant DID Cell labeling as a dye, one sample was extruded and the other was probe sonicated. As it can be visually noticed in Figure 15 probe sonication did enhance the number of polymeric aggregates in the solution, therefore the energy given to the system should be enough to enhance polymer aggregation and disaggregation. Previous reports that studied sonication-resizing protocol reported the inefficiency of sonication to break the large vesicles probably due to increased rigidity of the membrane and low amount of energy provided by bath sonication in comparison to probe sonication.[86] The DLS analysis for extruded and sonicated samples, shown in Figure 15, and the existence of a large population range supported the need of purification studies.

Figure 15 – Comparison of extrusion and tip sonication polymersome post-formation resizing techniques after film hydration, by (A) DLS and (B) picture using Vybrant DID Cell Labeling solution as a "marker" to track the visual presence of polymer aggregates, where the *contains only hydrated sample while ** was also probe sonicated.

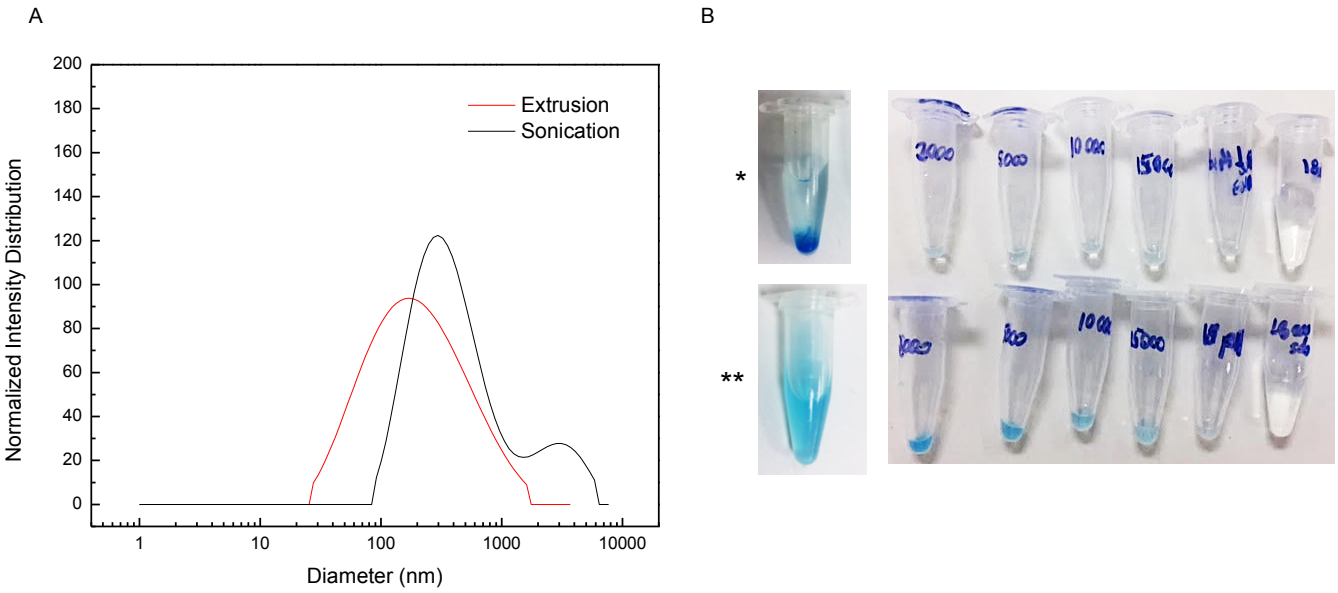

Source: Beatriz N. M. Miranda

4.5 Block copolymer characterization

The chosen protocol for polymersome production tangled film hydration followed by tip ultra-sonication. To assure that the sonication process was not altering the block copolymer (BCP) structure, gel permeation chromatography (GPC) was promoted. While one sample was ultra-sonicated according to a previously described procedure, the other was kept as a control. As shown in Figure 16, the difference in MW of both samples was very modest, from 15192 to 14939, that may not be directly related to the sonication itself. Unfortunately, due to low polymer solubility in water, such an approach using THF was not able to identify weather polymer chains were undergoing hydrolysis. An alternative approach was the analysis of the pH after sonication procedure. This experiment was purposed based on the fact that the hydrolysis of PLA chains forms acidic components, as previously discussed in Section 4.2 (short chain lactic acid oligomers or monomers). Still, using PBS buffer as the aquous solvent, we did not observe the pH difference among sonicated and non-sonicated sample. Such characteristic is very important regarding biodegradability but could have been a challenge upon sonication production procedure.

Figure 16 – GPC chromatograms of (A) PEG-b-PLA BCP in THF and (B) sonicated.

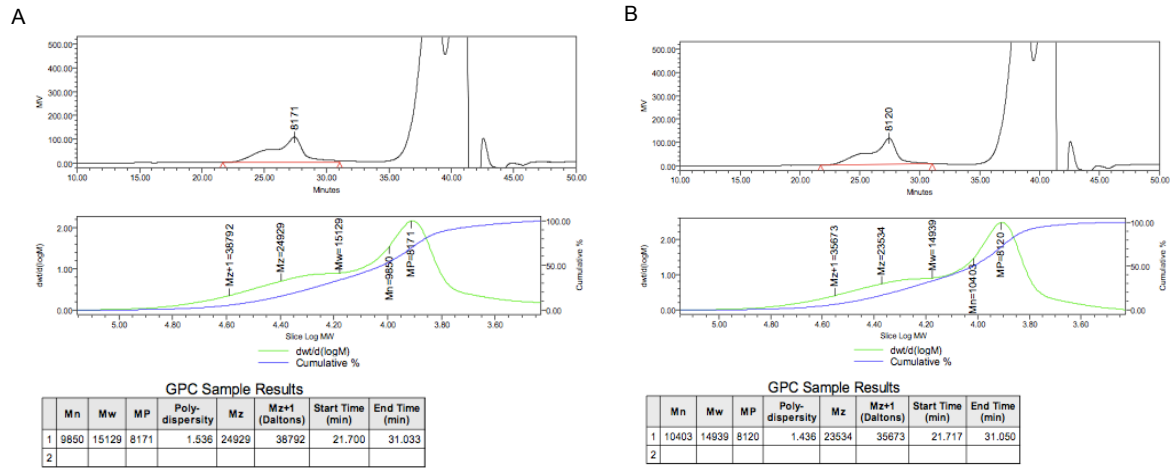

	Mn	Mw	MP	Poly-dispersity	Mz	Mz+1 (Daltons)	Start Time (min)	End Time (min)
1	9850	15129	8171	1.536	24929	38792	21.700	31.033
2								

	Mn	Mw	MP	Poly-dispersity	Mz	Mz+1 (Daltons)	Start Time (min)	End Time (min)
1	10403	14939	8120	1.436	23534	35673	21.717	31.050
2								

Source: Beatriz N. M. Miranda

4.6 PEG-b-PLA polymersomes purification techniques

Figure 17 – Illustrative representation of purification techniques.

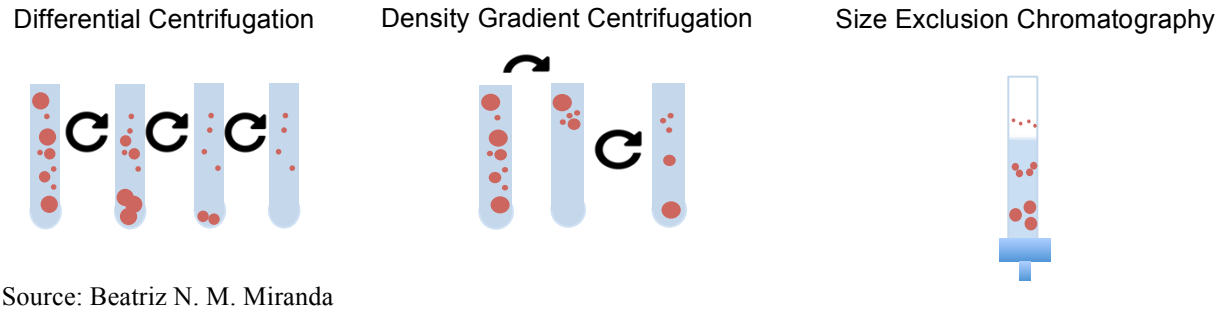

Source: Beatriz N. M. Miranda

Differential Centrifugation (DC)

Regarding all different purification techniques testes for fractioning a mixture by size and density, as shown in Figure 17, centrifugation is one of the most used and well-known.[71] Therefore, in our experiments, polymersomes were formed by film hydration followed by resizing and the supernatants were centrifuged at 2,000; 5,000; 10,000; 15,000 and 18,000 × RCF. Pellets were resuspended in 2 mL PBS solution and analyzed by DLS and NS-TEM, when convenient. Differently than Robertson et al observation for poly(2-(methacryloyloxy) ethyl-phosphorylcholine)-

co-poly(2-(diisopropylamino)ethyl methacrylate) ($PMPC_{25}$-$PDPA_{70}$) polymersome by using this technique, a micelle population was observed by DLS in neither preparations, discarding the need of a previous step for micelle removal.[71] An explanation for this difference may advent from the hydrophobic/hydrophilic interface behaviour characteristic of each BCP. While PMPC-PDPA possesses phosphorylcholine groups of the PMPC that occupies substantial area in comparison to PDPA units, and naturally protects PDPA from water, what most likely induced the formation of micelles.[87] On the contrary, in our PEG-b-PLA copolymer, both hydrophilic and hydrophobic units are modest, and the volume occupied by the ethylene oxide units are not suitable for complete shielding of PLA groups from water. Therefore, in our case, either vesicles or bulk are formed, not being observed the existence of micelles in any batches. DLS analyzes of different size fractions separated by DC of extruded and sonicated samples are shown in Figure 18 and Figure 19, respectively. Such analysis could be promoted only for the lower centrifugation speeds for the extruded sample, probably due to a low amount of polymer vesicles produced by this preparation. The low amount of vesicles in this sample can be due to the low hydration time used - not sufficient for vesicle formation - or due to the rigidity of the polymer membrane, what could influence in the extrusion process. Negative staining NS-TEM micrographs for each sonicated sample fraction after the DC can be seen in Figure 19 C, and DLS average data in Table 4. Even though the method enabled a separation of the sample in more homogeneous size fractions - as previously observed by Robertson et al - micrographs exhibited the not efficient separation by different polymersome shapes.[71] For pharmaceutical purposes, it is important to understand the specific shape of the nanocarrier that is being used, since it can influence cell penetration and release kinetics. For this reason, another strategy for polymersome separation using centrifuge was tested, density gradient centrifugation, based on the possible different polymer/water ratio among each different morphology.

Figure 18 – Film hydration followed by extrusion sample. DLS analysis by (A) intensity (B) correlation coefficients after size separation by centrifugation 2,000; 5,000; 10,000; 15,000 and 18,000 ×RCF pellet after centrifugation and 18,000 ×RCF supernatant.

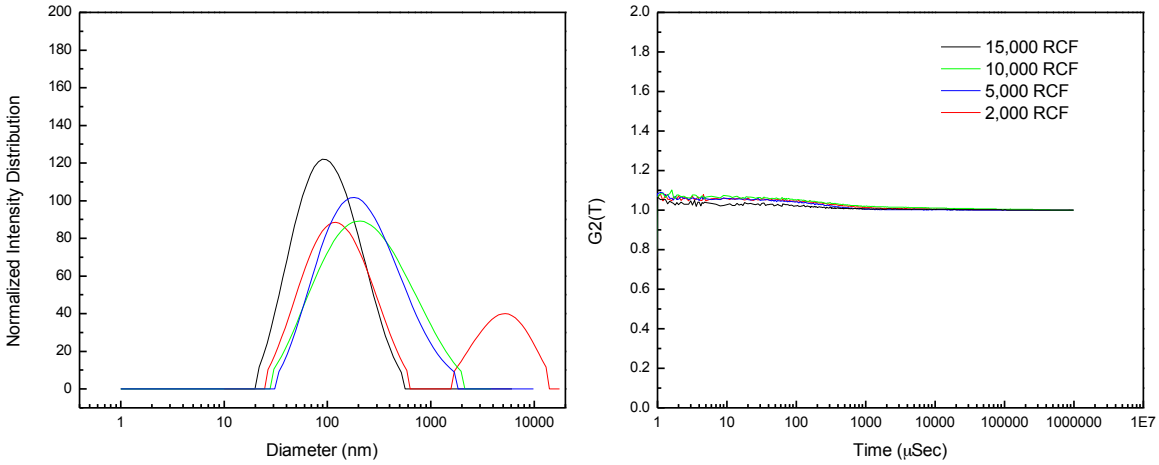

Source: Beatriz N. M. Miranda

Figure 19 – Film hydration followed by sonication sample. DLS analysis by (A) intensity, (B) correlation coefficients, and (C) NS-TEM analysis at 19 K× and 100 K× after size separation by centrifugation 2,000; 5,000; 10,000; 15,000 and 18,000 ×RCF pellet after centrifugation and 18,000 ×RCF supernatant.

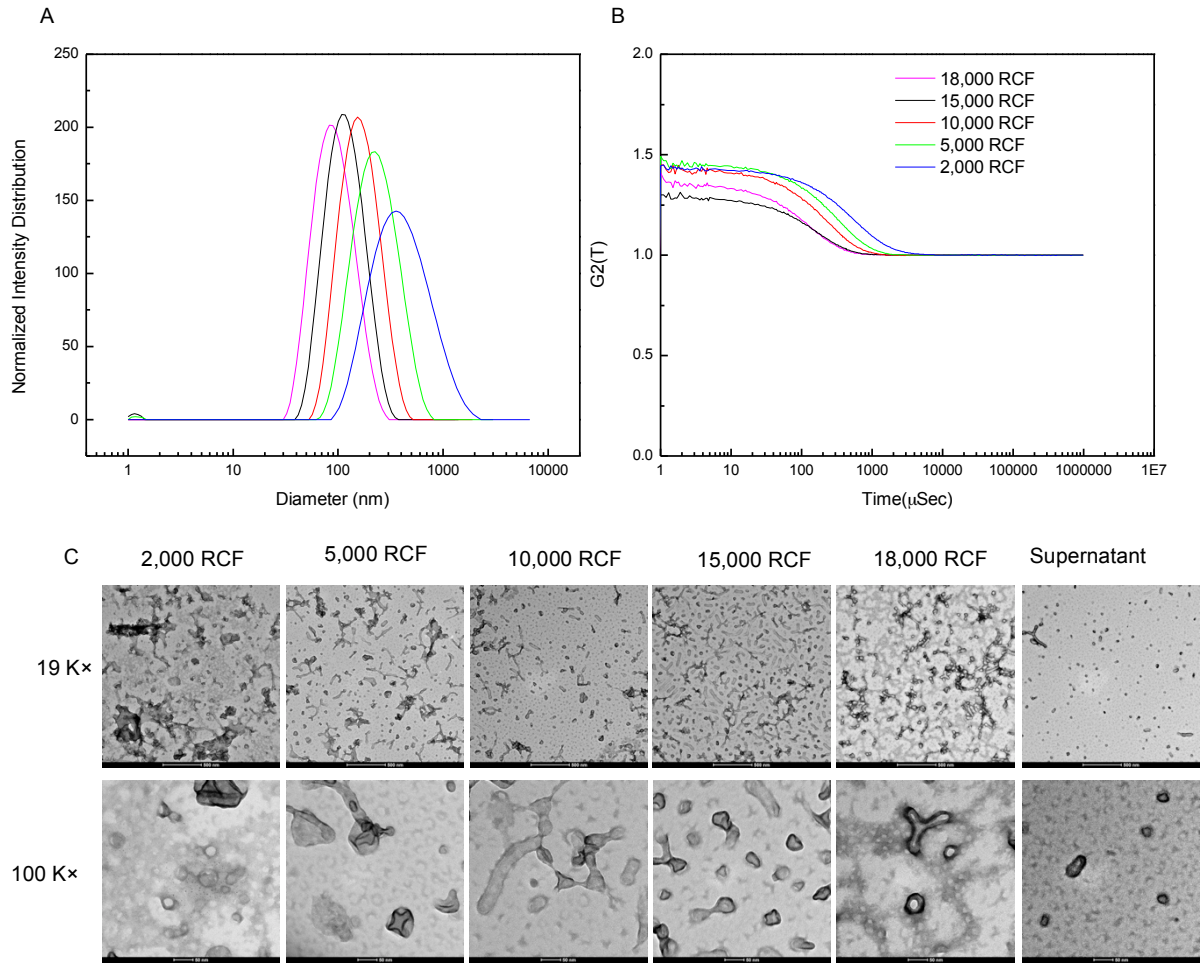

Source: Beatriz N. M. Miranda

Table 4 DLS average data after size separation by centrifugation 2,000; 5,000; 10,000; 15,000 and 18,000 ×RCF pellet after centrifugation and 18,000 ×RCF supernatant.

Item	DLS size intensity (nm)	PDI
2,000 × RCF	365,7	0,242
5,000 × RCF	206,6	0,157
10,000 × RCF	145	0,149
15,000 × RCF	120,9	0,149
18,000 × RCF	107,8	0,129
Reminiscent supernatant	83,4	0,167

Density gradient centrifugation (DGC)

Looking forward to separate polymersomes by shape, DGC separation was promoted. For this experiment, layers containing decreasing amount of sucrose (5%, 10%, 15%, 20% and 25% w/v sucrose in PBS buffer) are carefully and ordered added inside a 1.5 mL Eppendorff tube, forming a discontinuous sucrose density gradient. The polymersome sample is, then, added to the top of this solution and centrifuged for 90 min at 20.000 × RCF. Particle density drives polymersome separation in each layer, therefore its expected that non-spherical constructs have larger polymer/water ratio and therefore, higher density, moving towards the higher sucrose concentration layers on the bottom.[71] Samples suspended in each layer were recovered and analyzed by NS-TEM, and are shown in Figure 20 and Figure 21.

Figure 20 – NS-TEM analysis of film hydration followed by extrusion sample, at 25 K× and 50 K× after size separation by sucrose gradient centrifugation 0-10; 15 and 20% sucrose at 20,000 ×RCF for 90 min.

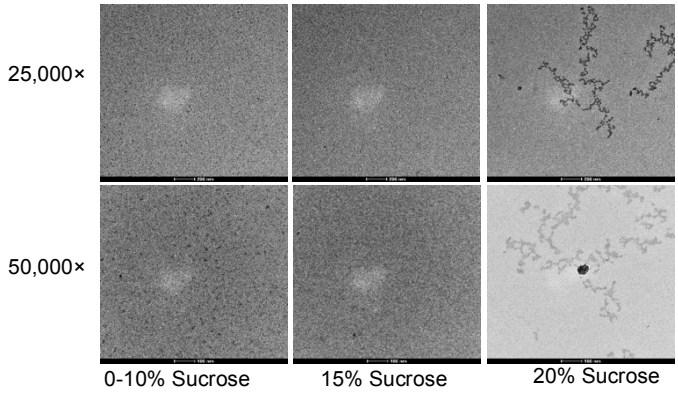

Source: Beatriz N. M. Miranda

Figure 21 – NS-TEM analysis of film hydration followed by sonication sample, at 25 K× and 50 K× after size separation by sucrose gradient centrifugation 0-10; 15 and 20% sucrose at 20,000 ×RCF for 90 min.

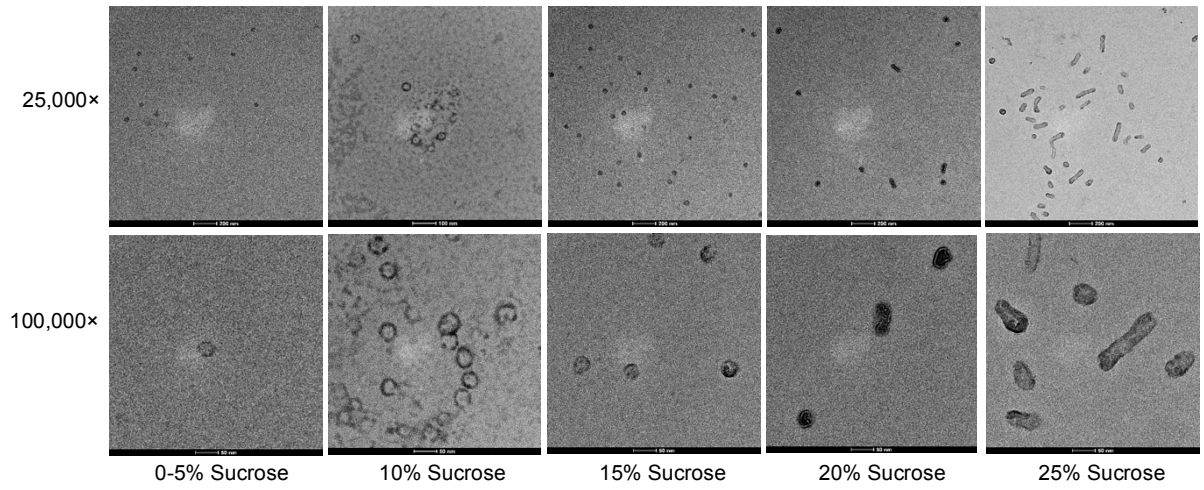

Source: Beatriz N. M. Miranda

The low amount of vesicles in the starting sample previously observed by DLS was unfortunate and probably influenced the inexistence of vesicles by TEM using extrusion as resizing the technique. On the other hand, Figure 21 shows that DGC was a successful technique to separate a heterogeneous polymer aggregate sample into different morphologies. This observance is in accordance to was previously reported by Robertson et al.[71]

Further, the 10 wt.% fractions containing the polymersomes were analyzed again by TEM after a month of production, and the integrity of the vesicles was observed, as it is shown in Figure 22.

Figure 22 – 10 wt.% fraction of the separation by sucrose gradient after a month. A. NS-TEM micrographs at 25 and 50 k×; B. DLS analysis by intensity and correlation coefficient.

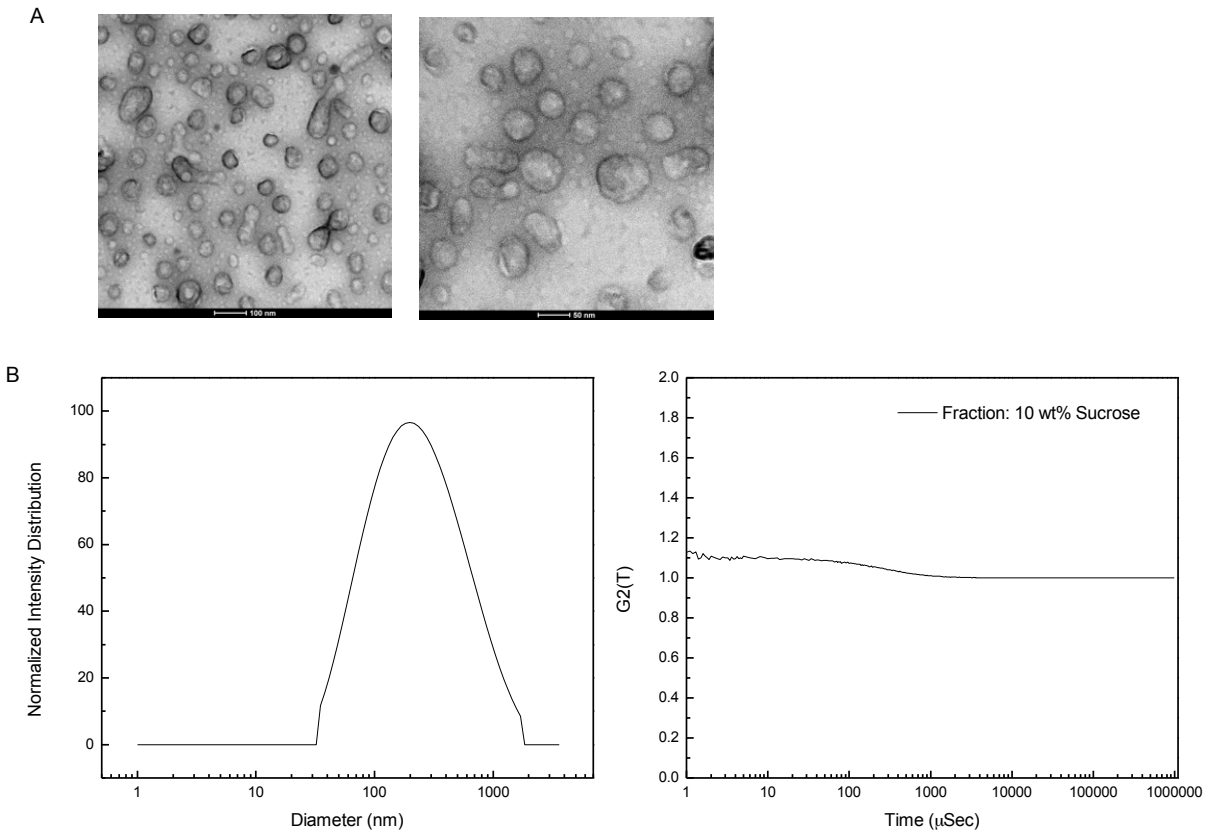

Source: Beatriz N. M. Miranda

Unfortunately, this purification methodology is efficient only for laboratory scale, since it is very time-consuming, dilutes the sample, requires extensive and accurate pipetting steps and may not purify the whole batch all at once. For this reason, we tested size exclusion chromatography.

Size exclusion chromatography (SEC)

Size exclusion chromatography (SEC) was tested assuming that it would provide a more scalable purification and efficient separation of particle morphology as well as free small molecules (what will be discussed later in this report for encapsulation efficiency studies). This technique enables particle separation based on their hydrodynamic volume.[71] The separation is possible due to the specific porosity characteristic of the material used to fill the column, the stationary phase. As the sample passes through the column, smaller molecules tend to penetrate

deep into pores, moving slowly through the column, whereas large molecules flow quickly. Therefore, larger molecules will be eluted sooner than smaller ones. The eluted sample was collected into vials (20 drops/vial) and visual particle existence was observed in 4 separated fractions, and their mean diameter was detected by DLS measurements.

Figure 23 – SEC purification. A. TEM analysis of film hydration followed by sonication sample, SEC elution vial number 10 at 25 and 100 K×, respectively. B. DLS of elution fractions 8-11. C. Chromatograms of PEG-PLA-PTS (pH 7.2), data is representative of at least three experiments, with fluorescence intensity measurement at λ_{Ex} = 355 nm and λ_{Em} = 405 nm. The highlighted area shown in D represents the encapsulated fraction.

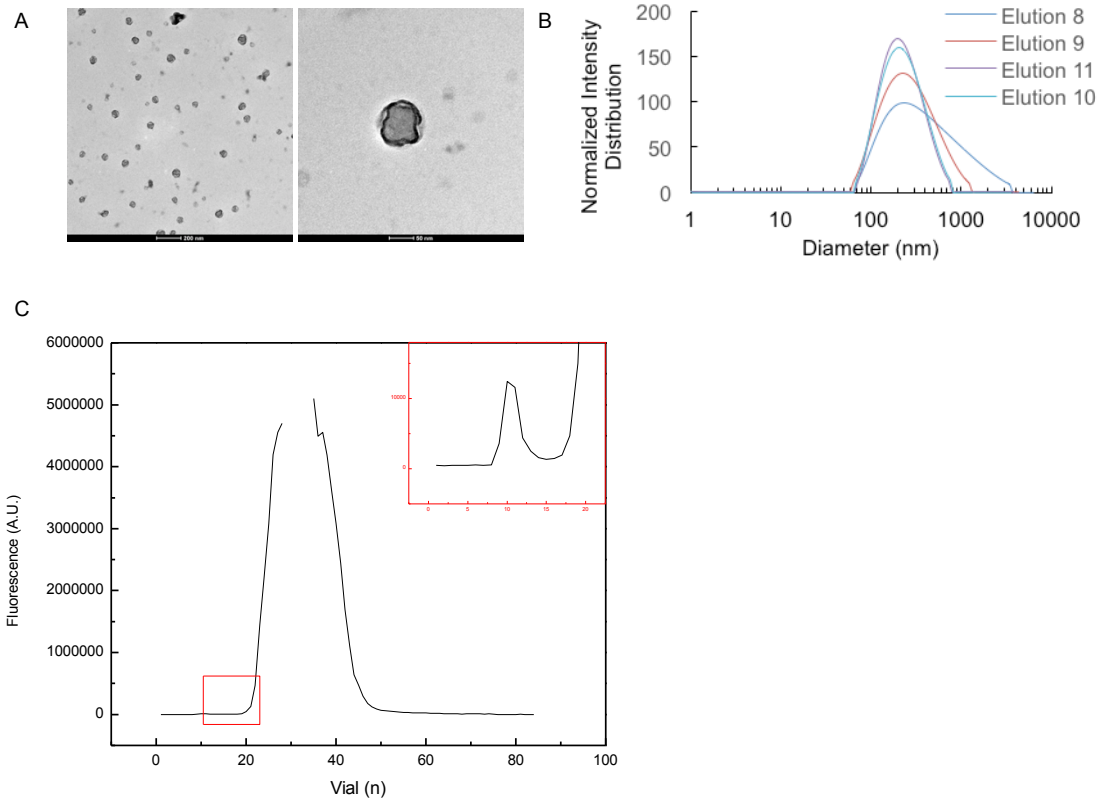

Source: Beatriz N. M. Miranda

The NS-TEM and DLS data are shown in Figure 23, demonstrating effective separation of the polymersomes into different sizes. This observation enables the conclusion that this technique was effective at separating the sample into many discrete monodisperse size fractions, especially in fractions 10 and 11 that revealed a size of 199 nm PDI 0.224 nm, and 202 PDI 0.266, respectively. It can be observed a discrepancy between the vesicles separated by previous methods and

the ones shown in Figure 23. The majority observed previously was intact, as can be seen in Figure 22, however, the ones in Figure 23 appeared ruptured and deflated.[88] This rupture observed in polymersome may be explained by a faster drying due to higher vacuum pressures applied or due the staining agent.[88] The monodispersity of the fractions separated by SEC was improved if compared to the samples purified by the DC technique and similar to those purified by DGC. Even though one may argue that this method is more time consuming and may result in a material loss within the SEC column, the sample morphology was very homogeneous and the purification was less laborious and more efficient for purification since the whole sample was purified all at the same time.

Evaluation of drug loading (encapsulation efficiency)

A key question when using a drug carrier is to understand the loading capacity of the carrier and if the active ingredient affects its stability, especially when dealing with a self-assembled structure.[89] To achieve the information regarding encapsulation efficiency, Men et al [86] reported the encapsulation of hydrophobic dye Nile red and hydrophilic dye FSS and obtained EE% by dialysis followed by freeze-dried under high vacuum. Generally, the encapsulation of hydrophobic actives is more efficient than hydrophilic ones. In fact, hydrophobic loading tends to migrate to the limited organic fraction during membrane formation, hence concentrating it all into polymer aggregates. On the contrary, unless forced penetration, the amount of hydrophilic loading inside vesicles should be relative to its concentration in initial solution.

Here we used SEC protocol to separate and analyze the encapsulation efficiency of PEG-b-PLA polymersomes. As previously shown, we used PTS as a model hydrophilic drug for PEG-b-PLA polymersome carriers, and the chromatogram is shown on Figure 23 C. PTS is a water-soluble fluorescent probe that should mainly remain in the hydrophilic core of polymersomes. For this proposed system, we observe the presence of vesicles in the eluted fractions, by TEM and DLS, although the calculated encapsulation efficiency was 0,04%, calculated according to obtained intensities and Equation 4. This very limited result called our

attention and is in discordance to the literature. It should be said that here we did not take in consideration for the E.E.% calculation the theoretical amount of vesicles formed and therefore its theoretical encapsulation since a relevant amount of bulk was being produced and, tested strategies to calculate the % of loss, including drying and FTIR were not able to provide a reliable information.

Therefore, a new strategy was evaluated, using Electron Paramagnetic Resonance (EPR) spectroscopy, to analyze the protection capacity of drug delivery systems by ascorbic acid reduction assay.

For the purpose of analyzing polymersomes capacity, a spin probe, such as nitroxide spin probe 2,2,6,6-tetramethyl-4-trimethyl- ammoniumpiperidine-1-oxyl-iodide (CAT-1), is encapsulated by the system and EPR signal is recorded, which chemical structure is shown in Figure 24. By adding an especific amount of ascorbic acid, the accessible probes are quickly reduced, leaving detectable signal only for the ones localized in the aqueous phase. Hence, it is possible to differentiate between encapsulated and released CAT-1.[90] As a control, we found that DPPC liposomes (1 $mg.mL^{-1}$) could encapsulate 0.53%. Using the same procedure, 0.36% signal was obtained by analyzing PEG-b-PLA polymersomes sample, as shown in Table 5.

Therefore, EPR spectroscopy was an interesting technique that enabled differentiate between encapsulated and free CAT-1 the reduction depends on how fast pores are created in the shell material.[90] Yet literature reveals that pegylated PLA multilamellar liposomes demonstrated a stronger shell resistance compared to poly(D,L-lactide) PLA nanocapsules, our results indicate that the PEG hindrance was not able to prevent the reallocation of the spin probe.[91] CAT-1 is a positively charged probe, and it was expected that the neutral PEG-charged surface of tested polymersomes would help on retaining the cargo. Moreover, it is well described in the literature the greater stability of the polymersomes shell over their lipid peer. Although, we believe that such stability should not be mistaken with membrane permeability. As Meng[54] reported, a higher release rate was observed for polymers with lower Mw of the whole copolymer, which was purposed to be due to a relatively thinner membrane, and that the lower the glass transition temperature, the thicker the membrane, according to PCL and PDLLA comparison.[54] The hydrophobicity of the PLA chains may also play an important role in membrane permeability, likewise.

For instance, the extra-long alkyl backbone between ester groups of PCL creates a more hydrophobic condition resulting in restricted permeability in comparison to PLA. Ahmed and coworker found that polyethyleneoxide-polyethylethylene (PEO-PEE) polymersomes were 10 times less water permeable than liposomes composed purely of phospholipids with acyl chains, our results indicate that the same does not happen for PEG-b-PLA polymersomes.[52] In other words, we observed that the greater hydrophobicity of the membrane block PEE compared to PLA, as shown in Figure 24, due to the presence of the carbonyl group in this last one, should also play an important role in membrane permeability. The reason may be the fewer bilayer defects in more hydrophobic membranes, what should decrease pores and water-permeation. The relocation of the spin probe in the outer phase due to membrane permeability and diffusion causes changes in the spectra. We observed that after the first data acquisition this dynamical process was enough to decrease the spin signal and therefore, CAT-1 reduction by the ascorbic acid. This observation was further observed in other experiments and will be further discussed in Chapter 3. Still, the opportunity to tune the distinct characteristics of the hydrophobic block conditioned by the BCP structure in polymersomes makes them useful in various applications.

Table 5 EPR results for PEG-b-PLA polymersomes and DPPC liposomes, at 1 mg.mL^{-1}, 5.05 mW.

Sample	Gain	Atenuation	Scans	Average Normalized Integral	StDev		EE(%)
Liposomes	200	16	2	5.777	0.074	0.005366107	
Liposomes + AA	20000	16	4	0.031	0.002		0.53
Polymersomes	200	12	2	5.316	0.047	0.003574116	
Polymersomes + AA	20000	12	6	0.019	0.003		0.35

* AA = ascorbic acid

Figure 24 – PEG, PLA, PCL, PEE, phospholipid, and CAT-1 chemical structures.

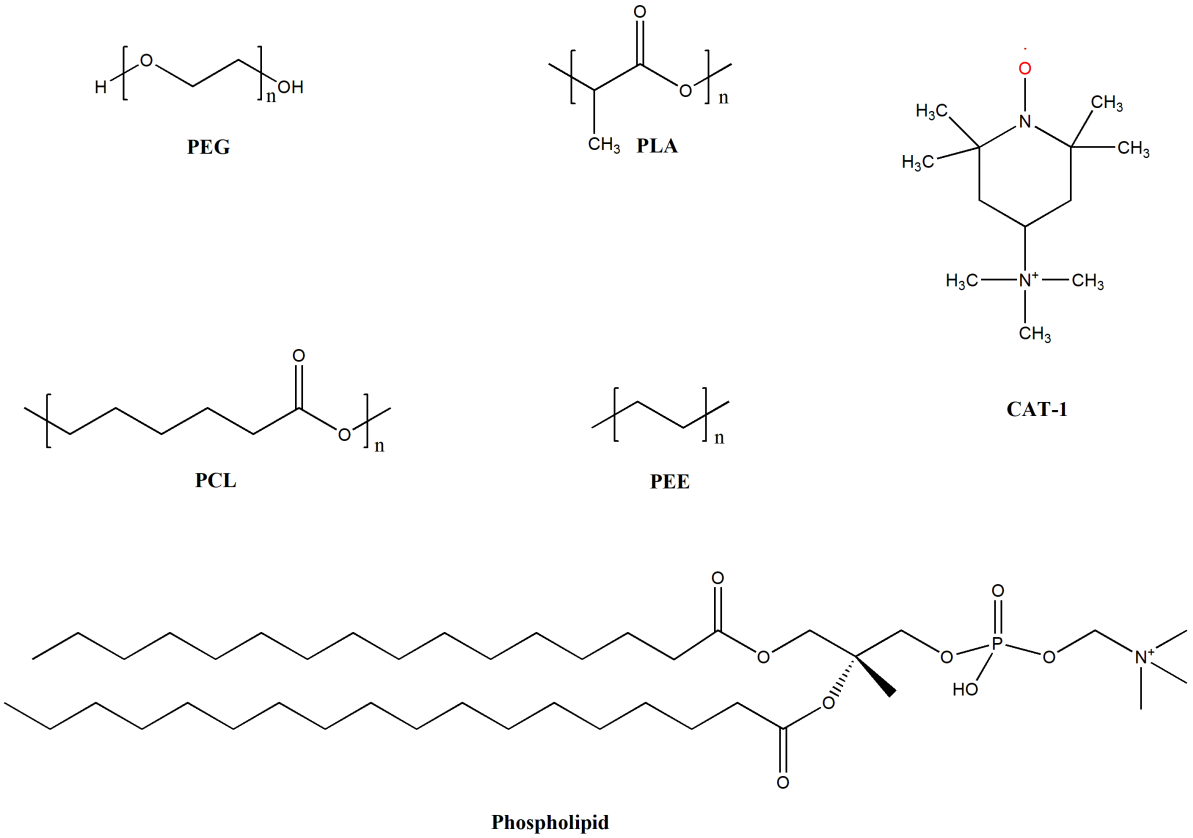

Source: Beatriz N M Miranda using ChemDraw Software.

5. CONCLUSION AND REMARKS

Results from studies with poloxamers systems by microfluidics demonstrated its greater permeability, and therefore less efficient capacity in holding the core content. For that reason, studies using PEG-b-PLA copolymer were followed.

While the capillary microfluidic methodology enables the production of micron-sized polymersomes, film rehydration followed by extrusion or sonication produced nano-sized polymersomes. We use W/O/W double-emulsion drops microfluidic devices to encapsulate a model hydrophilic cargo, which enables the study of the release of material through pH stimulus. The drug release was studied by decreasing the environmental pH from 7.4 to 5 and a rapid release occurred at the acidic condition. The release is driven by the hydrolysis of the ester groups from PLA, which produces pores in the membrane and slowly delivering the inner content, followed by final membrane disintegration. These experiments show the

potential application of such system as an effective nanocarrier to improve the treatment for diseases that involve acidic pH micro-environments, such as solid tumors.

Further, nano-sized PEG-b-PLA polymersomes were successfully synthesized by film hydration and characterized. Different resizing methodologies and purification techniques were studied to elucidate the best method based on aggregate morphology. The achievable size and morphology are relevant characteristics according to the desired application, and as will be described in Chapter 4, to enable mucus penetration, the particles should be smaller than the mucus mesh-size.

Hydrophilic substances could be encapsulated inside these biodegradable polymersomes. Obtained encapsulation efficiency for PTS by SEC was very low compared to the literature (0.04%) EPR studies provided 0.35%, closer to a liposomal control. The decrease in encapsulation may be explained by the less efficient vesicle production using BCP as the membrane structure. Moreover, EPR spectroscopy studies revealed the fast reduction of the spin probe signal, suggesting the formation of pores in the PEG-b-PLA membrane and therefore diffusion of encapsulated cargo. In conclusion, comparing to the literature we believe that the membrane permeation can be adjusted by the tunable copolymer properties, Mw, Tg, and hydrophobicity to polymersome system present advantages as a membrane-controlled reservoir system, besides stability.

CHAPTER 3

Blended PEG-b-PLA Polymersomes and other production strategies

1. INTRODUCTION

Self-assembly can be considered as a fundamental process in the evolutionary course and advent of life. The organization of a disordered system into a specific structure, lowering the antecedent interfacial energy and enabling compartmentalization, granted vital conditions for specific chemical reaction and biological transformations. As well as liposomes, polymersomes are nature-inspired discriminated structures that aim to mimic the selectively permeable barrier characteristics, attractive for current specific applications. Until now we were working on this thesis fundamentally with unitary systems, based on PEG-b-PLA block copolymers. Firstly, yet motivated by the nature transformative process, our system should not take the same amount of time that took the first vesicles to be formed. As our knowledge of this natural phenomenon advances, specific adaptations may be promoted to not only facilitate this process but also advances related to the working materials. Secondly, we understand that in a biological membrane there are having key components of the structure that play a vital role regarding structural integrity as well as the flow of material throughout the membrane, such as proteins, other types of lipids such as sterols, which helps the membrane heterogoneity and the existance of microdomains. In analogy to what happens in the nature, specific combinations of unimers may contribute to membrane formation as well as membrane permeation. For instance, Ahmed and coworkers, 2004, exploited such approach using blends of PEO–PLA in PEO–PBD for polymersomes formation. Studing the role of ester hidrolysis in releasing encapsulant and proposed a mechanism of poration they observed a direct release dependance on the ratio of PEG–PLA.[40]

Hydrophobic triblock copolymers, such as poloxamers, are non-oionic molecules comprising of a central hydrophobic block of poly(propylene oxide), PPO, enclosed by two hydrophilic PEG chains, which tradenames are Pluronic® and

Synperonic®, as shown in Figure 25. This class of polymer is well known as vehicles for drug delivery and theranostic related applications, and its key attribute related to the incorporation into cellular membranes, preferentially to cancer cells, have been extensively studied.[92] Due to its very hydrophilic membrane, bilayer membranes are less stable than those made of highly hydrophobic copolymers, still, vesicles were produced by using Pluronic® L121 (PEO_5-PPO_{68}-PEO_5) by its direct dissolution in water under vigorous stirring.[93,94] Therefore, the design of a PEG-b-PLA system containing Pluronic® L121 as an adjuvant should lead to an increase in efficiency of aggregate formation, decreasing bulk and consequently, polymer loss.

Figure 25 – The chemical structure of Poloxamers.

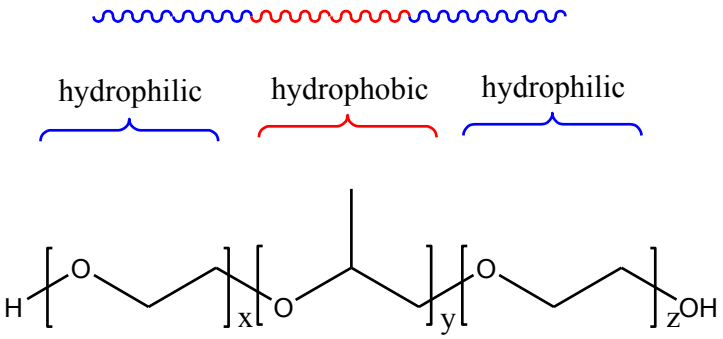

Source: Beatriz N. M. Miranda, using ChemDraw Softare.

Solupus®, BASF, is a polyvinyl caprolactam–polyvinyl acetate–polyethylene glycol graft copolymer (PCL-PVAc-PEG) that was developed for solid dispersions, is also capable of solubilizing poorly soluble drugs in aqueous media.[95] Due to its low critical micellar concentration (CMC, 7.6 mg.L), very stable micellar dispersions are formed in aqueous media that can be used as effective drug carriers to improve bioavailability of drugs.[96] Moreover, as an amphiphilic excipient it should stabilize nanosuspensions by reducing the surface energy of the particles, and therefore, preventing agglomeration.[96] The chemical structure of Solupus is shown in (Figure 26) and its polyethylene glycol (PEG) backbone suggests its possible application for trans-mucosal delivery. Therefore, the use of this BCP as adjuvant for PEG-b-PLA polymersome formation, increasing vesicles in solution and encapsulation efficiency may be evaluated.

Figure 26 – The chemical structure of Soluplus®.

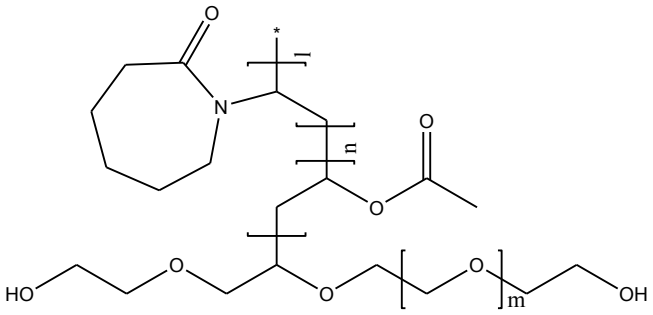

Source: Adapted from Elsevier, using ChemDraw Software.[96]

The use of polymersome system for the drug delivery and treatment of diseases possesses tremendous potential, yet to our knowledge, clinical applications of these therapeutic agents were not described. Considering the literature claimed advantages over liposomes, polymersomes promises enhanced stability, represents longer circulation times, target delivery of both, hydrophobic and hydrophilic cargo. Therefore, efforts should be made to support advances in this technology to achieve the market and help save peoples lifes. In special, the lack of efficient and safe delivery systems for hydrophilic drugs remains a critical factor. By tuning the characteristics of the polymersome membrane composition, its physical properties should also be modified, and hopefully optimize production methods towards high throughput as well as encasulation and delivery performances.

Another strategy that was here briefly exploited was the use of low energy production methods. For such technology make to maket, production methodology should be scalable, which is an issue when high energy methods such as sonication, membrane extrusion, vortexing, stirring, and high-performance dispersing are needed to decrease vesicle size and increase homogeneity..

For preparative methods based on the use of organic solvents, a general method is the solvent displacement, in which generally involves the sequential solubilization in organic solvent and water, and therefore, double emulsion generation. In this approach, single entities of the polymers are not yet organized in a bigger structure, therefore is classified as a bottom-up approach for vesicle

formation. The solvent order as well as the nature of the organic solvent and its removal technique may vary, but the copolymer self-assembly is driven by phase separation, and therefore the interfacial tension between the hydrophobic block and water and the hydrophilic bloc and the water-soluble organic solvent. A disadvantage of this technique is that the mixing of organic solvent with water followed by a solvent evaporation process does not always warrant a solvent-free condition.[34,56] Further developments related to type of solvent used, polymer concentration, injection speed and order of polymer hydration should drive the evolution of other more methodologies, enabling fine tuning of the size and size distribution of the resulting polymersomes.[54] A good example of this development is the microfluidic method, which relies on the solvent dewetting proccess for polymersome formation, as further described.

Figure 27 - Method based on water-soluble organic solvents.

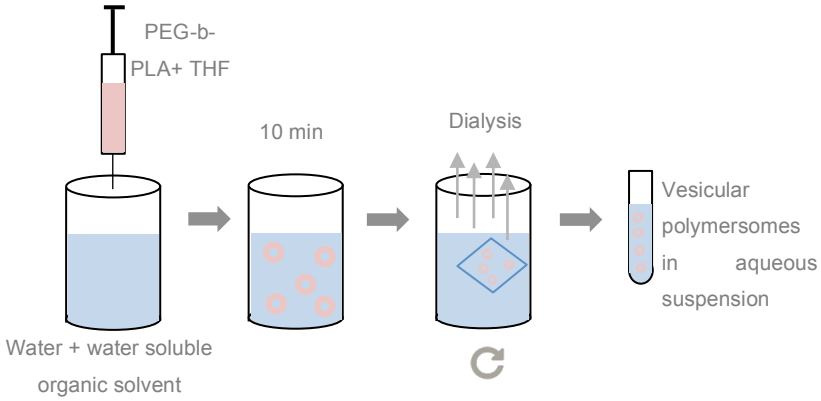

Source: Beatriz N. M. Miranda.

2. OBJECTIVES

Finding a way to decrease bulk formation during polymersome production and hence improve vesicle production efficiency was the main goal of this study. Therefore a set of approaches was evaluated, from a different production method to the formation of blends of Pluroni L121 and Soloplus in PEG-b-PLA polymersomes.

3. EXPERIMENTAL METHODS

3.1 Materials.

We used the block copolymer $PEG_{5,000}$-b-$PLA_{10,000}$ (Polysciences, cat. 25018), polyoxyethylene-polyoxypropylene-polyoxyethylene (PEO-PPO-PEO) (Pluronic® L121) and Soluplus® (polyvinyl caprolactam–polyvinyl acetate–polyethylene glycol graft copolymer, PCL-PVAc-PEG) from BASF, for polymersome production. As fluorescent and spectroscopic probes, we use 1,3,6,8-Pyrenetetrasulfonic acid tetrasodium salt hydrate (PTS), and 2,2,6,6-tetramethyl-4-trimethylammoniumpiperidine-1-oxyllodide (CAT-1), respectivelly. All used solvents were from Sigma-Aldrich.

3.2 Polymersome preparation.

In general, two approaches were considered. For the first one, film hydration method was emplyed as previously described, and the use of adjuvants in the polymersome formation was analyzed. In a typical experiment, a binary mixture of PEG-b-PLA and an adjuvant (Soluplus®, Pluronic® L121; 8:2, total copolymer concentration of 10 $mg.mL^{-1}$) in chloroform is dried under gently N_2 flow. After complete drying, PBS 1×is added and samples are left at 50 ^{o}C under continuous stiring. Polymersomes were characterized by DLS and NS-TEM, and encapsulation efficiency experiments including SEC and EPR spectroscopy were promoted in specific samples. To enable such characterization, PTS for SEC, whereas spin probe CAT-q, for EPR spectroscopy were dissolved in the aqueous phase, incorporated during polymersome preparation. For the second approach, polymersomes were prepared by addapting the optimized procedure described by Meng, 2003.[54] Basically, PEG-b-PLA block copolymers are first dissolved in THF (100 μL, 10 mg) and was quickly injected into an aqueous phase (5 mL) containing a mixture containing water and 8.00 v.% ethyl acetate or water and 4.25 v.% benzyl alcohol (referred to as EA/water and BA/water, respectively) using a syringe or a pipette, without stirring. After approximately 10 min without agitation, the mixture was gently inverted twice. Samples were dialyzed against PBS buffer. The dispersions were characterized by DLS. An indication of the yield of the

polymersomes was obtained from the count rate and size as determined with dynamic light scattering measurements (DLS).

3.3 Characterization techniques

Dinamic Light Scattering (DLS). DLS analyses were carried out using a laser particle analyzer (NanoPlus, Particulate System) using software CONTIN as calculation method, after 20 × (v/v) dilution in water. DLS measurements were based on 3-5 repetitions of 70 accumulation times. Samples were analyzed at 25 °C with a scattering angle of 165° and at 660 nm HeNe laser based on a dispersant refractive index (RI) of 1.33, a viscosity of 0.89 and a dielectric constant of 78.3. The samples were also characterized for surface charge by determining their ζ-potential using Zeta potential Analyzer (NanoPlus, Particulate System) based on 3 repetitions of 5 accumulation times, 70 cell constant. Cell positions 0.70/0.35/0.00/-0.35/-0.70 at a fixed voltage of 60 V, and a constant current of 51 mA, software Smoluchowski as calculation method and using the same dispersant from size analyses.

Negative Staining Transmission Electron Microscopy (NS-TEM). Polymersomes were prepared as described above and analyzed by conventional transmission electron microscopy using a FEI Tecnai G20 electron microscope (FEI Company, EUA), operating at 200 kV. For conventional TEM imaging all analyses were carried out with dried samples, using 300 mesh copper grids (Koch Electron Microscopy, São Paulo, Brazil) covered with Formvar (Sigma Aldrich) followed by nanoparticle spotting, negative staining with 2 wt% phosphotungstic acid and proper wash before analysis. The grid preparation is a critical step to enable visualization by TEM, and for that reason, the same protocol was repeated for all samples, diminishing problems related to it.

Size Exclusion Chromatography. 10 $mg.mL^{-1}$ polymersome sample was produced in the presence of 0,5 mM 1,3,6,8-Pyrenetetrasulfonic acid tetrasodium salt hydrate (PTS), concentrated to 10 × using speedvac system and the aqueous suspension was then eluted through a Sephadex G25-column (3,0 g/12 mL) to separate PTS-

encapsulated polymeric contructs from non-encapsulated PTS. Sample and buffer flow were driven by simple gravity and eluting fractions were collected 20 drops per vial. Loaded PTS was quantified by measurements of its UV fluorescence detection at λ_{ex}=305 and λ_{em}=455. Encapsulation efficiency (E.E. %) was calculated as the ratio between the area under the curve of encapsulated PTS over encapsulated and non-encapsulated PTS.

Electron paramagnetic resonance (EPR) Spectroscopy. Sample preparation for EPR analysis: The polymersome was prepared by hydration, as described previously, with a PBS buffer solution containing 1.25 mM of the spin probe 2,2,6,6-tetramethyl-4- trimethylammoniumpiperidine-1-oxyl Iodide (CAT-1). EPR spectra of the probe were acquired at room temperature in a Bruker EMX-200 spectrometer (Bruker, Germany) operating at 9.85 GHz, with a power of 5 mW (16 dB microwave attenuation), modulation amplitude of 1G, sweeping the field of 100 G centered at 3455 G. The gain was adjusted according to the sample concentration. Samples of CAT-1-containing polymersome (180 µL) were placed in flat quartz cells (Wilmad, USA) and the EPR spectra were recorded; 15 µl of 0.05 M ascorbic acid solution was added to react only with non-encapsulated CAT-1. The residual signal was attributed to CAT-1 probe encapsulated into the polymersomes and the volume of the internal aqueous compartments of the polymersomes estimated by the ratio between CAT-1 EPR signal before and after ascorbic acid addition.

4. RESULTS AND DISCUSSION

4.1 Polymersome formation methods

One of the strategies herein tested was the ability of adjuvants to help the efficiency of polymersome formation, and therefore decrease bulk accumulation. Because Pluronic® L121 has a lower Tg and polymersome formation may be promoted by direct polymer dissolution, by applying small quantities of this triblock copolymer together with the PEG-b-PLA, polymersome formation should be forced, leading to an increase in the number of vesicles and decrease in bulk formation,

which membrane structure is proposed in Figure 30 A. The same trend is therefore expected for the Soloplus-doped preparation.

Figure 28 – Production methodologies data

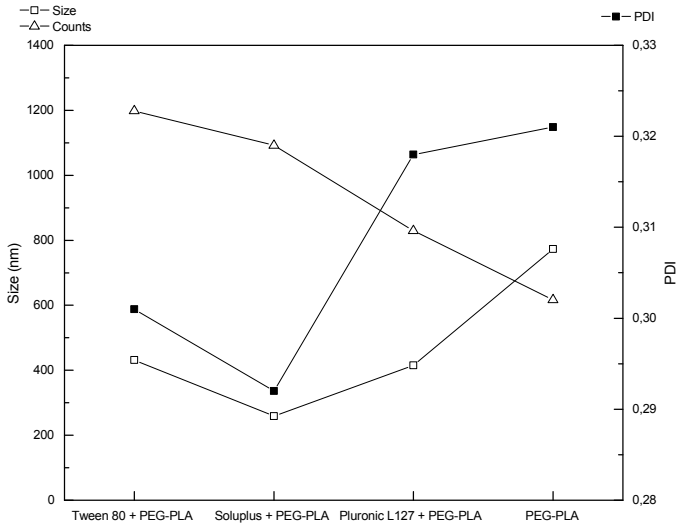

Source: Beatriz N. M. Miranda

Despite the significant variations in size for PEG-b-PLA formulations to the ones that was previously obtained using a round botton flask, the final amount of polymer vesicles was higher for both dopped formulations in comparison to the sole PEG-b-PLA batch, as shown in Figure 28. Regarding PEG-b-PLA production, this result indicates that experimental conditions such as difference in the form of substrate used for film drying may play an important role in the hydration proccess and vesicle formation. Still, we understood that added adjuvants were indeed affecting the formation proccess.

Hence, it is hypothesised that greater encapsulation efficiency for hydrophilic cargo would be achieved by using PEG-PLA/Soloplus® polymersomes which vesicle formation is considerably more efficient. Therefore, a new preparation of PEG-b-PLA/Soloplus® polymersomes was promoted, this time using a conventional round bottom flask at otherwise identical conditions. The particles in the turbid dispersions have a size of 216.7 nm and a PDI of 0.22. NS-TEM images are

consistent with DLS measurements and reveal a vesicular structure for the particles, as shown in Figure 29.

Figure 29 – PEG-b-PLA polymersomes blend with Soluplus® (80:20). A. NS-TEM micrographies at 25 k×, and B. DLS data of purely Soloplus® sample versus blended PEG-b-PLA/Soluplus®, by intensity and correlation coefficients.

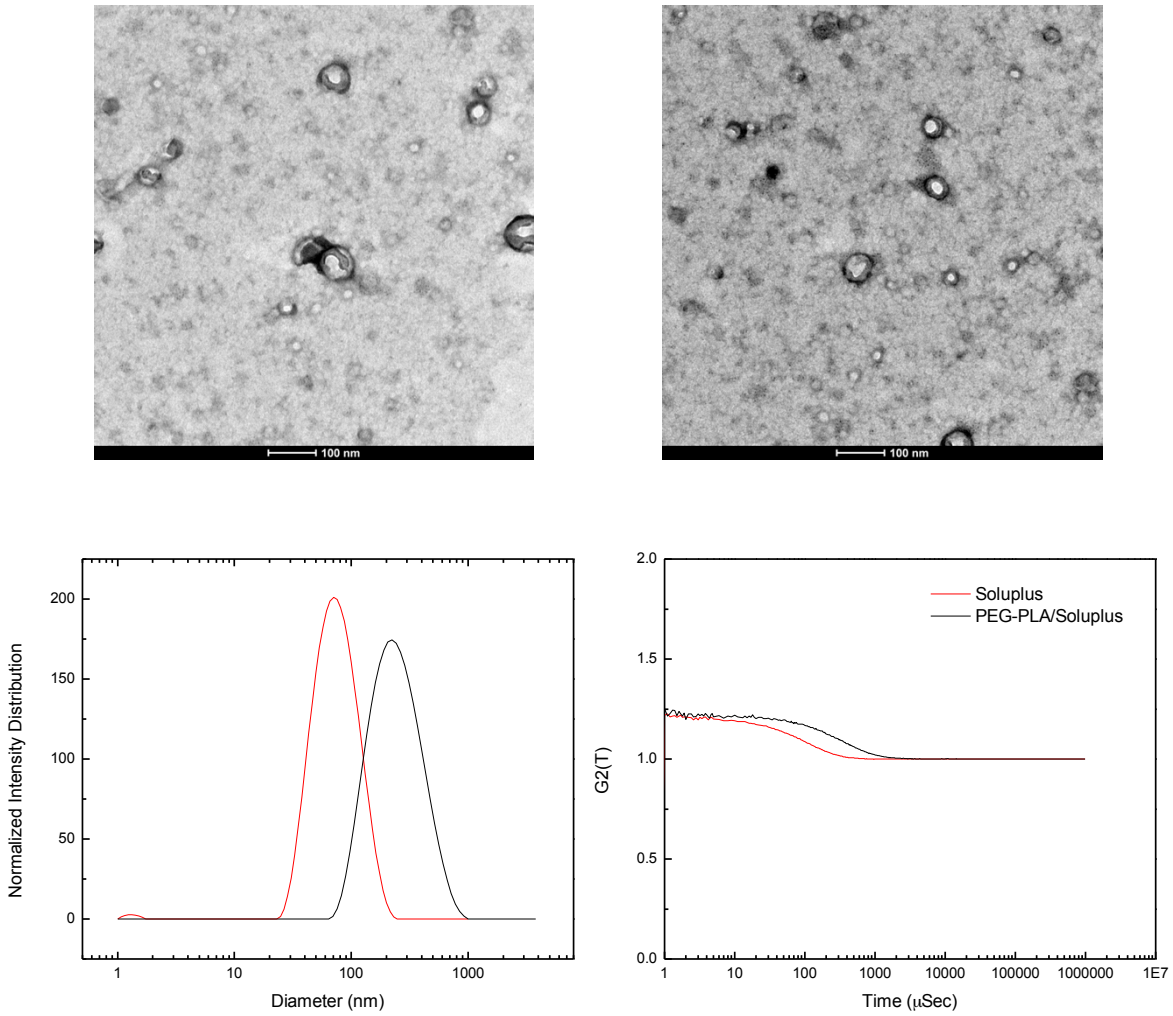

Source: Beatriz N. M. Miranda

By analyzing the smaller size of only Soloplus® formulation obtained by DLS, represented in Figure 29, and comparing our NS-TEM data of blended polymersomes to the literature-reported Soloplus® micelles, we antecipated that vesicles morphology were formed combining both copolymers. Therefore, we undestand that Soluplus® was stable integrated into the PEG-b-PLA membrane, which structure is purposed in Figure 30 B. Notably, no bulk formation was observed for this preparation, which also suggests effectiveness of Soloplus as an

adjuvant. Moreover, the stained polyester walls of the particles in Figure 29 can be clearly distinguished from the nonstained hydrophilic center, indicating that PLA is not in the interior, and therefore, a vesicle structure is obtained. Comparing Soloplus® to PEG-b-PLA/Soloplus® formulations an increase in particle size is observed, from 67.2 nm PDI 0.13 to 216.7 nm PDI 0.22, respectively.

Figure 30 – Proposed arrangement of the structure of a membrane composed by a mixture of A. Pluronic® L121 and B. Soloplus® with PEG-PLA. In blue, hydrophilic PEG blocks, while in red, hydrophobic PPO and PCL-PVAc groups

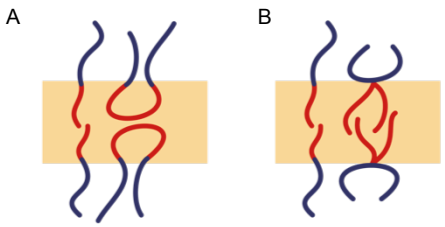

Source: Beatriz N. M. Miranda

Figure 31 – PTS chromatogram usinf PEG-PLA/Soloplus formulation.

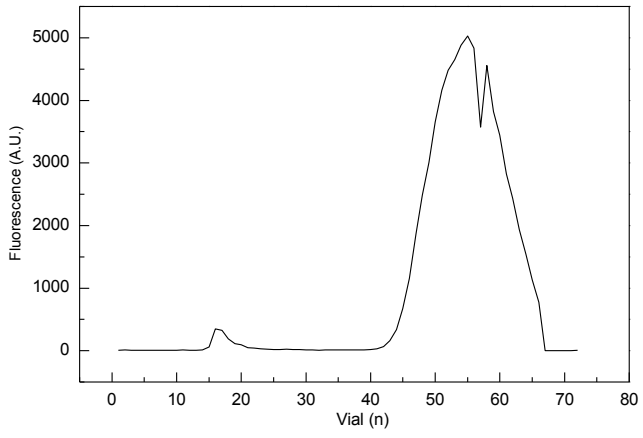

Source: Beatriz N. M. Miranda

Further, greater encapsulation efficiency was obtained using Soluplus dopped formulations, as shown in the chromatogram from Figure 31. Since a hydrophilic sample cargo (PTS) was used, the vesicle morphology is once again revealed enhanced encapsulation efficiency over pure PEG-b-PLA polymersomes, increasing encapsulation efficiency from 0.04% as described in previous chapter to

1.8%. It should be said that here, the encapsulation efficiency (E.E. %) is calculated based on the total amount of cargo in solution and the encapsulated fraction, not discussing the theoretical encapsulation based on the amount of particles in solution. Such kind of calculation may lead to a biased result, since a number of assumptions and/or rounding values have to be made. Notably, our blended polymersomes improved 45 times the encapsulation of a hydrophilic cargo.

Another strategy that was also evaluated for the purpose of analyzing polymersomes capacity was EPR spectroscopy, based on the spin probe reduction procedure by ascorbic acid. As shown in the first column of Figure 32, CAT-1 is encapsulated by the system and EPR signal is recorded. After adding ascorbic acid, the unecapsulated probes are quickly reduced, decreasing aquired signal and therefore leaving detectable signal only for the encapsulated ones. Although, when this experiment was promoted with pure PEG-b-PLA sample (Figure 32 first line), no sign was detected in none of the reads after arcorbic acid adition. Hence, it is presumable that no vesicles were formed, or that the polymersome's membrane is permeable to the tested probe. As previously described, the hydrolysis in the esther PLA chains may lead to pores in the polymersome membrane, which progressively swells and eventually experience disassemble, as shown in Figure 13.[40] Surprinsingly, when the same analysis is promoted to the 8:2 blended PEG-PLA/Soluplus® polymersome sample (see second line of data in Figure 32), the integration of first aquisition reveals a 3% volume of the internal aqueous compartments. Although, this signal decreases and, in a matter of less than a minute, when the second data aquisition is promoted, no more signals from CAT-1 are detected, as shown in Figure 32. The explanation of such observation may still be related to the poration based on PLA hydrolysis. Also, the vynil acetate groups from Soluplus® chains may undergo transesterification triggered by the carboxilic acids formed after PLA hydrolysis. It is noteworthy, blended polymersomes were able to sustain the cargo for longer than the pure sample, in agreement with previous report Ahmed and coworkers, 2004 that observed a direct release dependance on the ratio of PEG–PLA in the membrane composition.[40]

To gain further insight into the complete loss of membrane integrity due to hydrolysis, dynamic light scattering (DLS) was used to monitor vesicle population before and after pH reduction during EPR experiments. Particle size was slighly

affected from pH 7.2 to pH 3, when a increase from 124.3 nm PDI 0.265 to 137.1 nm PDI 0.260 was observed, indicating swelling due to water permation. Still, regarding structure, the acidic sample displayed a considerable amount of particles, suggesting that polymersome membrane was intact. Therefore, we hypothesize that instead of solely due to vesicle desintegration; the decrease in spectroscopic signal can be explained by the porosity of the polymersome membrane.

Figure 32 – EPR spectra of CAT-1 probe in environments with: 1. PEG-b-PLA and 2. PEG-b-PLA/Soluplus polymersomes; A. before and B, C. after ascorbic acid addition. C represents the second data aquisition after ascobic acid addition.

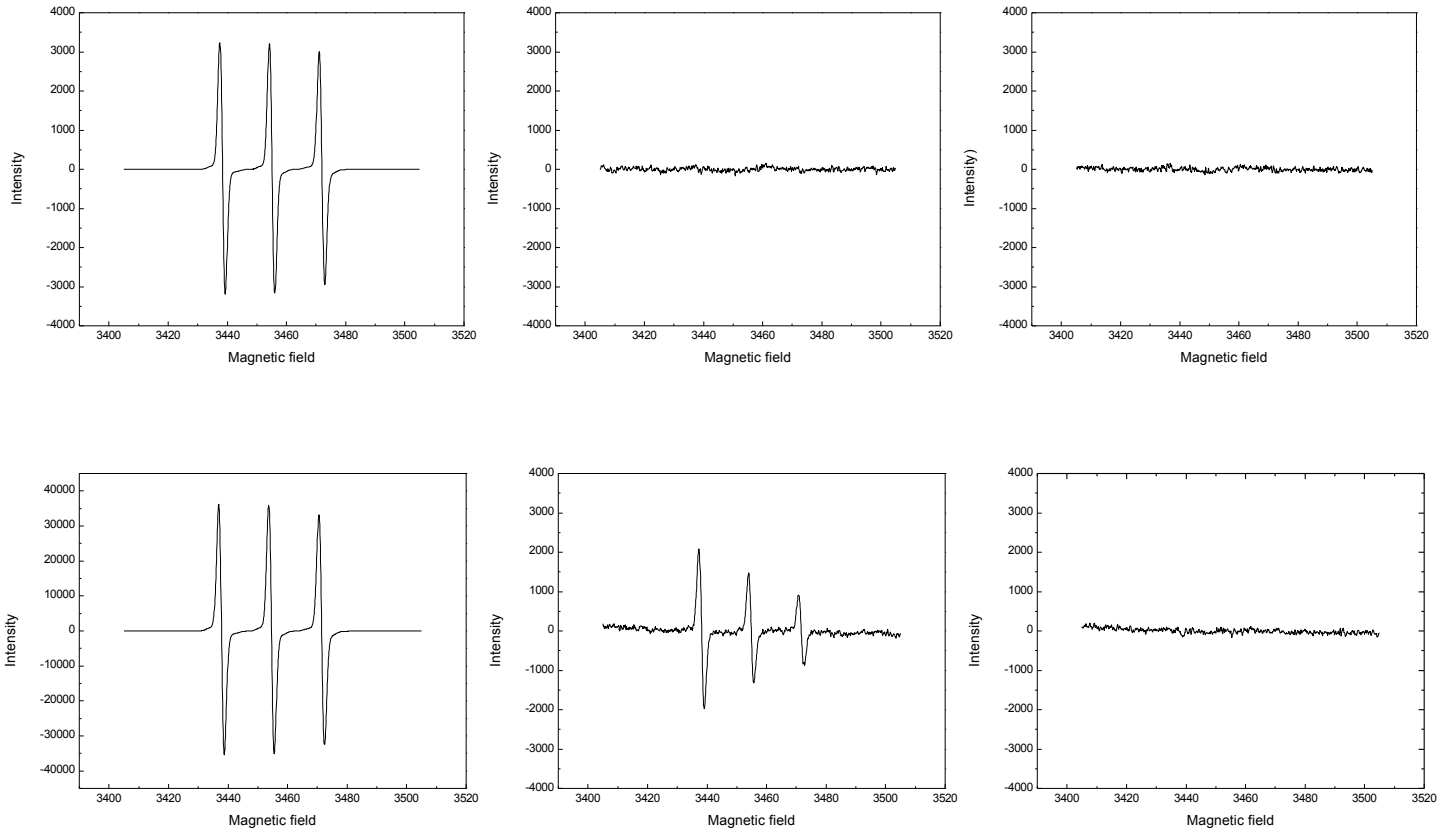

Source: Beatriz N. M. Miranda

Moreover, zeta potential values decreased from pH 7.2 to pH 3, with values of -9.81 to -14.46 mV. Surface potential decrease at pH 3, due to the protonation of the carboxilic acid groups present on PLA with a pKa value is around 3.84, therefore increasing the magnitude of the charge around particles' surface.

Figure 33 – DLS analysis of PEG-PLA/Soluplus® blended polymersmes by (A) intensity, (B) corelogram, before and after pH decrease.

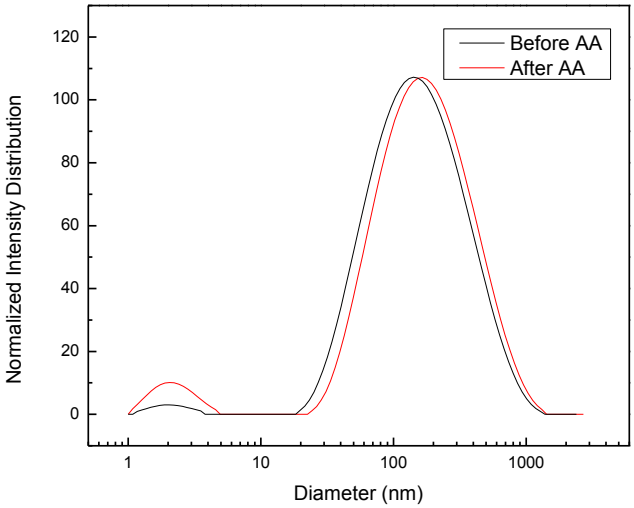

Source: Beatriz N. M. Miranda

4.2 Different production method

As previously discussed, there are different ways in producing polymersomes. One relevant disadvantage regarding film hydration for PEG-b-PLA polymersome formation is that due to its higher Tg and therefore rigidit of the membrane, a substantial amount of polymer remains insoluble, as large polymer aggregates, which inviabilizes its large-scale production required for comercial use. For this reason, new production strategies based on previous work from Meng, 2003, were tested, illustrated in Figure 27.[54]

THF was chosen as preffered solvent according to previously advantages observed by Meng, 2003, over dimethylformamide, dimethyl sulfoxide, and acetone.[53] The first relevant outcome of the use of water miscible organic solvents and an aqueous phase in this specified condition was the nonexistance of precipitates in all preparations. This observance may be explianed by the favourable dissolution of the BCPs and its solubility parameter of THF, which lowers interfacial tension.[54] Moreover, the presence of water-soluble organic solvents decreases the rate of THF dissolution in water, allowing the polymer chains to

organize and contributing to the system to achieve equilibrium and therefore, form polymersomes. The great presence of water contribute to the PEG block chain solubility, while the hydrophobic block tends to locate itself within the organic solvents, leaving the BCP chains on the surface of the organic droplets, inducing layers arrangement. Therefore, solely the interfacial turbulence and spontaneous emulsification, leads the self-organization of the membrane blocks, not requiring external source of high energy.

Figure 34 – Comparison of Meng's production methodology based on the use of water-soluble organic solvents and film hydration followed by sonication.

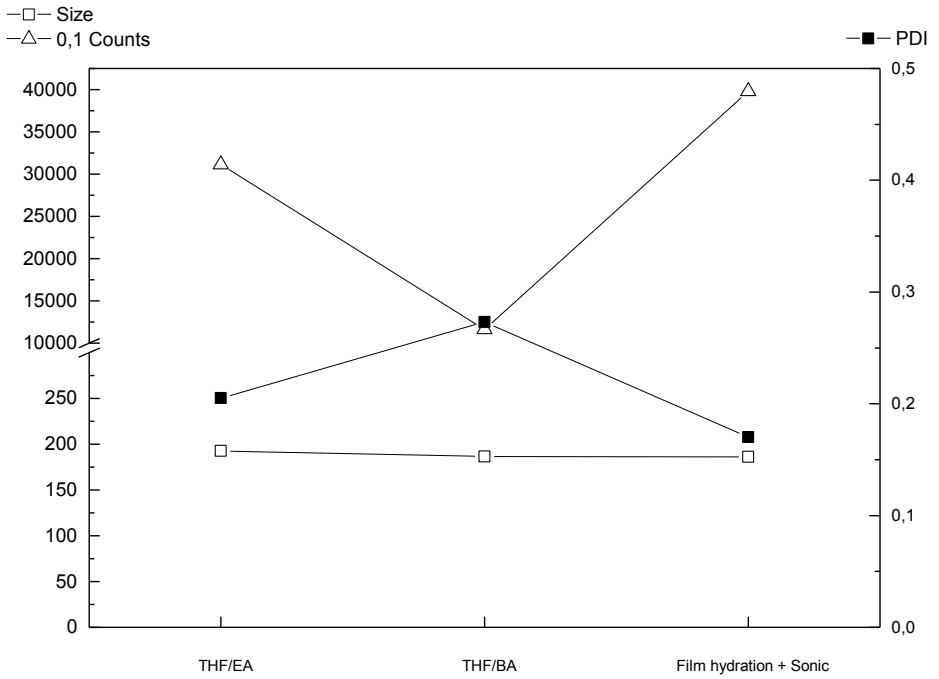

Source: Beatriz N. M. Miranda

In both preparations (EA/water and BA/water) bulk aggregate formation was discreetto almost nothing, in comparison to film hydration followed by ultra-sonication. Remarkably, for the EA/water polymersome dispersions more homogeneous size was observed, with PDI smaller than 0.2, and grater intensity counts, very similar to the one obtained by film hydration, as shown in DLS data presented in

Figure 34. BA/water batch originated fewer particles in solution (according to CPS data) and more micelles as well as bulk was created in comparison to the formulation that used EA instead. Further experiments should be promoted to

confirm the vesicle aggregate morphology as well as encapsulation efficiency. Still, it is noteworthy to mention that, these preliminary results related to water miscible solvent for the production of polymersomes have already demonstrated its value related to scale up opportunities.

5. CONCLUSION AND REMARKS

This chapter demonstrates the production of blended polymersomes by mixing a binary compostition of copolymers before the film formation process. The vesicular structure of both samples was confirmed by TEM measurement. For the Soluplus® system, encapsulation efficiency was measured by SEC and EPR spectroscopy, which revealed that the blended polymersome system could be considered as a better membrane-controlled reservoir system then pure PEG-b-PLA polymersomes. The arrangements of the blended membrane structure is proposed and based on the relocation of the spin probe and changes in the recorded spectra in comparison to the pure membrane sample. Our results are in accordance to the literature and therefore, the release can be adjusted by the copolymer composition. This result also suggests that encapsulation efficiency may be further improved by taking in consideration the increased polymersomes number in solution, and further experiments are ongoing to assess this issue.

Since colloidal systems undergo dilution, changes in equilibrium causes a relocation of the cargo, especially for in vivo applications after administration. Therefore, further studies related to the dynamical process of probe reallocation from inside to outside the capsules may be promoted to monitor its distribution kinetics. Moreover, further experiments the fine tune of the membrane properties, such as % composition of the shell material may be evaluated. The spin probes inside blended polymersomes were protected to a higher degree than the ones incorporated into PEG-b-PLA ones. In conclusion, this study provides information about the preparation of PEG-b-PLA polymersomes as well as blended ones. Furthermore, these biodegradable blended polymersomes may have a potential for biomedical applications e.g. as mucus penetrating drug carriers. Although, there is

a need for the deeper understanding of the appropriate downstream techniques as well as determine the extension of the hydrolysis and membrane permeability.

Following these observations, another preparation method for PEG-b-PLA polymersomes was evaluated, using water miscible solvents in aqueous media, as a matter to decrease external energy input during preparation, anticipating scale-up opportunities. Despite the limited characterization results, of only DLS, polymersomes in the desired size range (100-200 nm) was obtained, with homogeneous population characterized by narrow size distribution, specially using the EA/water system. Therefore, further experiments should be performed in attempt to confirm the vesicle morphology as well as encapsulation efficiency evaluation.

Finally, increasing the efficiency of polymersome production, higher encapsulation capability, combined with a straightforward production procedure should increase the chances of polymersome-based products achieve the market. Moreover, low cytotoxicity due to effective PEG charge shielding are key for its application in the field of drug and gene delivery. Those trends in size, structure and properties are fundamental characteristics or mucus penetration, what will be covered in Chapter 5.

CHAPTER 4

Structure and Function of Mucus

1. INTRODUCTION

Mucus is a biological gel that protects most surfaces of our body that are directly exposed to the external environment like airways, mouth, eyelids, ears and genital tract and also those that otherwise are indirectly exposed, such as stomach and gastrointestinal (GI) tract.[12,62,97] Regarding protection, mucosal surfaces do its job by physically trapping and chemically interacting with pathogens and particulates that, together with its immune and clearance functions, inhibits inflammation and infection.[98]

1.1 Mucus composition

Like any other viscoelastic material, mucus exhibits characteristics from both viscous liquid and elastic solids, which is directly related to mucus composition. The water percentage varies according to its organ or region of action and the individual's health condition, varying from 98% for a healthy airway mucus and 92% or less for a cystic fibrosis state.[99] The rest of its composition includes a dense network of mucin fibers, which contain highly glycosylated segments interspersed by hydrophobic, lipid-coated domains, besides nucleic acids, lipids, salts, proteins, antibodies, cells and cellular debris.[12,19] The glycoprotein is the main component and the reason why mucus presents viscoelastic properties.[6]

1.2 Mucin

Mucins are high molecular weight (0.5 to 20 MDa), heavily glycosylated filamentous extracellular proteins that are mainly produced by specialized epithelial cells.[6,100] Over 20 MUC genes have been deposited in GenBank and its tissue specificity gives an idea of the complexity of the protective mucosal barrier.[100,101]

Mucin can be classified in secreted or membrane-bound, and according to this classification, its terminal epitopes will show different characteristics.

Figure 35 – The domain structures of gel-forming and transmembrane intestinal mucins. The figure illustrates the domain structures of the gel-forming mucins and the transmembrane mucins that are normally expressed in the small intestine. The proline, threonine, and serine (PTS) domains become heavily O-glycosylated to form the mucin domains. These are rod-like and extended, looking like a bottle brush. The non-PTS parts of the gel-forming mucins are rich in cysteine amino acids and form compact structures. AMOP; adhesion-associated domain; C8, conserved 8 cysteines domain; CK, cysteine knot domain; NIDO, nidogen domain; Signal Seq, signal sequence domain; SEA, sea urchin sperm protein, enterokinase, and agrin domain; TIL, trypsin inhibitor-like cysteine rich domain; TM, transmembrane domain; VWC, Von Willebrand factor type C domain; VWD, Von Willebrand factor type D domain

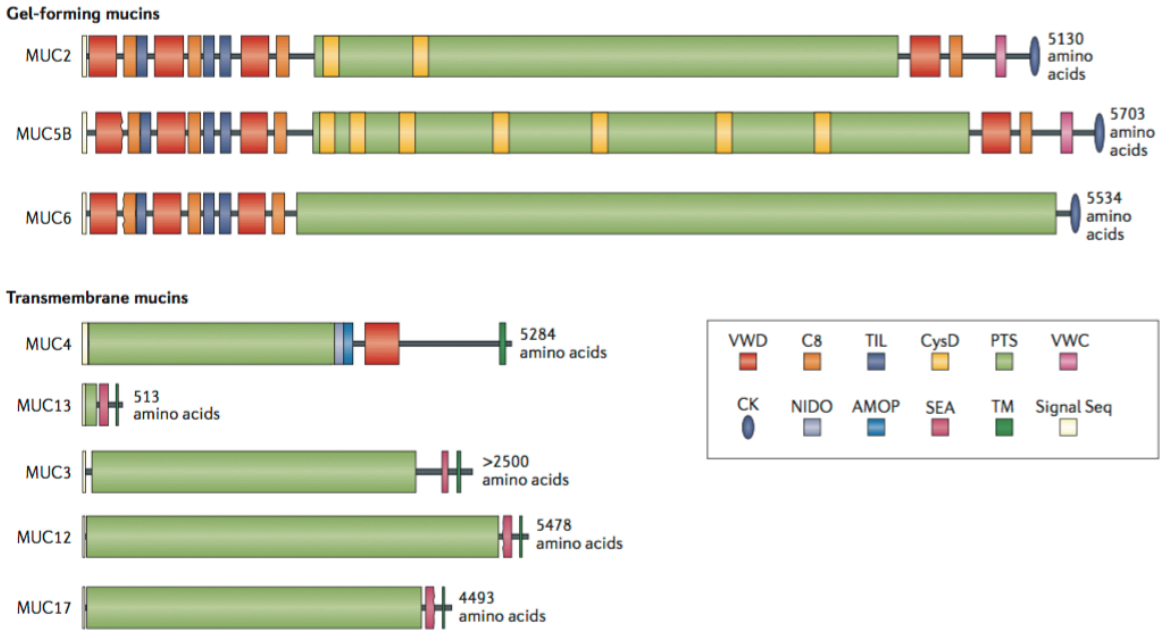

Source: Johansson and Hansson, 2016.Reprinted with permission from Nature Publishing Group.[109]

Generally, human mucin genes show tandem repeats, with a peptide sequence rich in serine (Ser), thirozine (Thr), and proline (Pro) in its the core (STP sequence). O-linked oligosaccharides produce branches what confers a more rigid conformation since its linked to the hydroxyl side chains of serine and threonine, with a signal peptide sequence at N-terminus.[6,100,102,103] In the secreted forms, this STP sequence is repeated along the core, forming the majority of the backbone and is linked mainly by regions with amino acid that codifies globular proteins, von Willebrand factor B, C, and D and by Cys. The later forms disulfide bonds and enables dimerization and subsequent polymerization characterizing the gel-forming mucins, as shown in Figure 35.[6,100,102,104] Among secreted mucins, MUC2, MUC5AC, and MUC5B are the major gel-forming mucins expressed at most

mucosal surfaces.[105–107] On the other hand, membrane-associated mucins do not form gels, are monomeric, and have typical properties of membrane glycoproteins, with membrane peptide domains, like MUC3, MUC12, and MUC17.[100] Another group of soluble mucins has been described to undergo autoproteolytic reaction, which was yet/until this moment only observed for MUC1.[108]

While originally mucins were considered to have the unique function of protecting and lubricating the epithelial surfaces, over the past two decades studies have shown other essential functions of mucus and its different mucins, such as growth and integrity of epithelial tissues, carcinogenesis, and metastasis. Moreover, mucus is also associated to many disease processes such as, which makes them an important focus for localized drug delivery.[6]

1.3 Mucus rheology

To better understand the mucus properties and relationship to diseases it is also important to study the relationship regarding its chemical composition and physical behavior. Mucus viscoelasticity is related to many different physiological processes regulating its ability to function as a lubricant, selective barrier, and the body's first line of defense against infection. For instance, when a person is suffering from severe bronchitis or cystic fibrosis (CF), the mucus becomes too thick; patients experience great difficulty in breathing due to inefficient mucus clearance.[12] Mucus in normal concentrations have 1.5–2.5% of dry weight while CF-like mucus have 6.5% of dry weight.[13] The accumulation of mucus results in bacterial overgrowth that triggers the inflammatory effect and production of more gel-forming mucin as a protective barrier, crating a vicious-cycle. On the other hand, during the time of ovulation and bacterial vaginosis infection, woman cervical mucus becomes significantly less viscous than in those with normal flora. While in humans it helps sperm swim through this mucus favoring fecundation, it also may be responsible for the increased risk of infection by HIV and other sexual transmitted diseases.[12] Thus mucus viscoelasticity is also related to the motility of many types of external agents such bacteria or nanocarriers. Equally important to the mucin concentration the ionic environment can also regulate mucus hydration and hence viscoelasticity.[13] Indeed, many other factors contribute to regulation of mucus

viscoelasticity, and are carefully balanced according to the necessity of our body; these factors include secreted lipids, pH, ions, and external agents such as bacteria and non-mucin glycoproteins.

Mucus samples are frequently characterized by ts bulk rheology in special by two physical properties which are the loss (G") and the storage modulus (G').[12]

2. OBJECTIVES

In this chapter we were willing to understand some chemical and physical properties of the mucus sample that will be used in the following experiments. We analyzed the pH, % dry weight and macro-rheology of porcine intestine mucus. Then, this mucus sample was used for the study of mucus penetration by particle tracking experiments, using control particles and polymersomes, which will be discussed in Chapter 5.

3. EXPERIMENTAL METHODS

Mucus sample preparation. Porcine intestine mucus was provided by the Katharina Ribbeck's Lab at MIT. Samples were separated in small aliquots to be used as needed, frozen in liquid nitrogen and stored at −80 °C.

Mucus characterization. A pH paper was used to measure the mucus pH. To determine the relative solid content, we dried crude mucus at 65 ^{o}C until constant weight was reached and the weight of dried mucus was divided by the weight of crude mucus.

Macrorheological methods. Mucus sample was unfrozen under water bath and subjected to centrifugation (2000 rpm) at room temperature for 2 min to remove the bubbles. To minimize the evaporation effect, the sample container outside was filled with water, making sure that would not contact the sample in the interior. All rheological tests were performed using a stress-controlled Physica MCR 501 rheometer (Anthon Paar, USA) with an adapted 25-mm cone-plate geometry (cone angle 1^{o}) at 25 ^{o}C, with small grips to prevent sliding. After loading each skin mucus

on the rheometer, the program used was: pre-shear 10 s with oscillation of 1 rad/s ω at 25 ^{o}C followed by 10 points per decade, 1% Y and 1 rad/s ω oscillation. Having the program ready, we promoted dilutions of pig intestine mucus sample in increments of 50% of water to achieve a wt.% concentration closer to diseased and healthy states, and those samples were analyzed in the same conditions.

4. RESULTS AND DISCUSSION

To understand the properties of the mucus samples we were dealing with and understand its behavior, we promoted sequential experiments with fresh porcine intestine mucus (INT) sample. Animal mucus models are slightly different than human mucus, although this later may sometimes not be readily available, making animal mucus models helpful.[12] Porcine intestine mucus has neutral pH, and presents 15 wt.% of dry weight, meaning that this sample was already dehydrated if compared to mucus from individual healthy state (1.5–2.5 wt.%), even more dehydrated than a diseased state (6.5 wt.%), either due to the samples characteristics or due to its sample handling. It is composed of water, lipids, DNA, salts, antibodies and other proteins, including mucins, and acts as a viscoelastic fluid. Because of protein degradation, temperature change, and other factors that influence mucus mesh and its rheological properties, we used each sample only once, all from the same source.

We were interested initially in observing possible abnormalities that could be caused by factors such as concentration, ethanol presence, blood, or drugs. We first studied the rheology of native porcine intestine mucus in different dilutions (or hydration states). We used 20% 500 kDa Dextran solution as a control to stabilize and prepare measurements (data not shown). Having the program in the rheometer ready, dilutions of PIM sample were promoted in increments of 50% of water and analyzed under the same conditions.

Increasing sheer rates are applied in the sample while the plate rotates, and the resulting force on the cone is continuously measured, as shown in Figure 36. As the shear stress increases, the mucus samples become thinner. The viscosity of the fluid decreases with shear rates, and increasing the amount of water in the mucus

sample (from 100% fresh sample mucus down to 12.5% diluted sample) decreased the viscosity as well, since the water viscosity at 25 °C is 0.89 mPa s^{-1}.

Figure 36 – Viscosity profile of porcine intestine mucus in different hydration states, as measured by a cone-plate rheometer at room temperature, 25°C. The steady state viscosity of porcine intestine mucus at shear rates 0.1 - 100 rad/s.

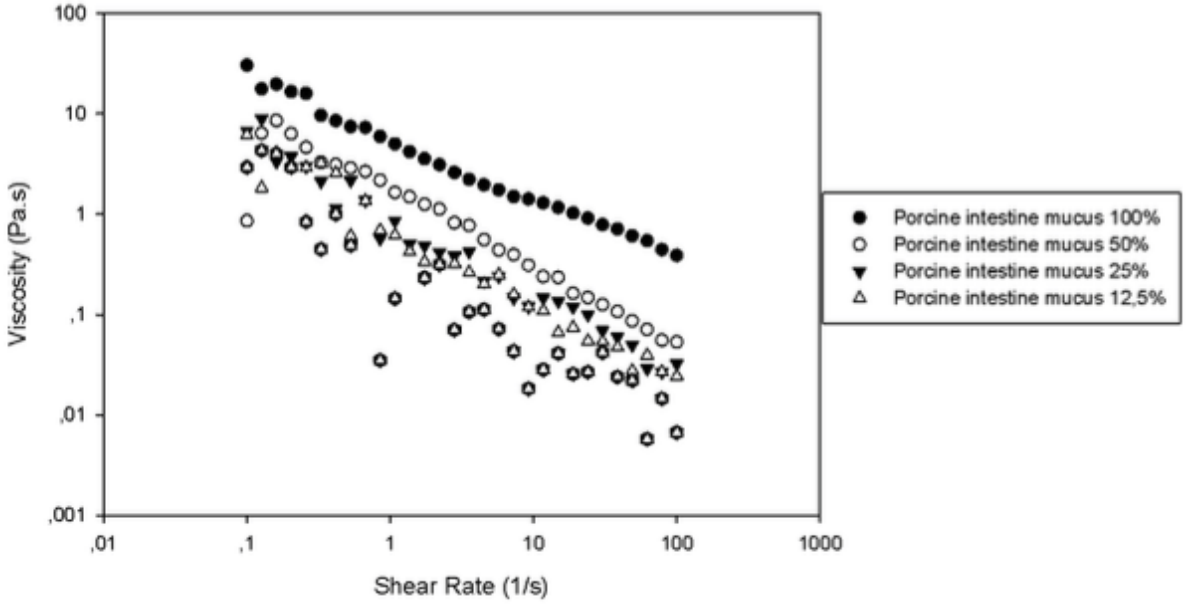

Source: Beatriz N. M. Miranda

These rheological measurements, including viscosity and elasticity are important to understand the consistency of mucus, and its characteristics as pseudoplastic.[12] As already mentioned, the value of 15 wt.% of dry weight is about 10x higher than the healthy state and about 2.3 x higher than a cystic fibrosis state, in which the mucus becomes very concentrated. For that reason we wanted to analyze the rheological properties of this sample in accordance to healthy and disease state, where 100% represents the crude sample, 15 dry wt.%; 12,5% represents a healthy state, 1.875 dry wt.%; and the 50% represents a disease state, 7.5 dry wt.%. Those properties should vary as a function of shear stress, time and length scale of shearing.[12] For the measured range we observed a linear response to viscosity with shear rate, data that is clear for the more concentrated samples (100 and 50%) but becomes harder to measure with increasing water concentration. The increase in water makes the sample even more heterogeneous, since mucin fibers tend to stick together. That may lead to sliding between the

cope-plate what may interfere causing erroneous measurements. Even though, our results are in agreement with the literature that describes a slope of the viscosity vs. shear rate for mucus within the range of −1 to −0.5, with an average of −0.85.[12] Moreover, physiological shear rates are close to 10 s^{-1}, the measured viscosity of the PIM was 1 Pa.s (9806.65 cP) for the original sample and close to 0.1 Pa.s (980.67 cP) for the most diluted one. These results are in accordance to the literature as a viscosity of ~1000 cP is expected for physiological shear rates.[110]

The Storage Modulus (G') increased with the frequency applied, although at higher frequencies all the samples demonstrated a decrease in the tendency for the gel to recover its original shape following stress-induced deformation which occurred with more intensity for the more diluted the sample was. The higher the frequency, less time the molecules have to reorganize its networks, occurring the decrease in the storage ability. On the contrary, the Loss Modulus (G'') drastically increases in higher frequencies, showing the tendency to flow, observed at lower shear rates for diluted samples, as shown in Figure 37**Error! Reference source not found.**. For that reason we wanted to analyze. The dynamic viscoelastic properties of mucus are closely regulated biochemically and the regulation of these various constituents is complex and highly interdependent. For instance, Dawson and co-worker, 2003, as well as Sanders and co-workers did not observe changes in macro-viscoelasticity of the mucus after short term freezing storage when compared to fresh samples.[111,112] For that reason, handling procedures could drastically interfere mucus rheological properties, so we wanted to ensure that our procedures were carefully manage and we were obtaining results similar to what was already in the literature. Our goal was to use the porcine intestine mucus sample for later studies by MPT and analyze the mucus penetration of polymersome system. The use of real mucus sample was chosen since reconstitution of mucus leads to different viscoelastic properties what will also influence the particle-mucus interaction. Moreover, the study of the overall macroscopic viscoelasticity of the porcine intestine mucus using a sensitive strain-controlled cone and plate rheometer will allow further studies related to the comparison with the novel characterization of the micro-rheological properties of mucus by MPT.

Figure 37 – Macro-rheology of porcine intestine mucus. The frequency-dependent Loss and Storage Modulus of diluted mucus samples were recorded at constant strain amplitude of 1%.

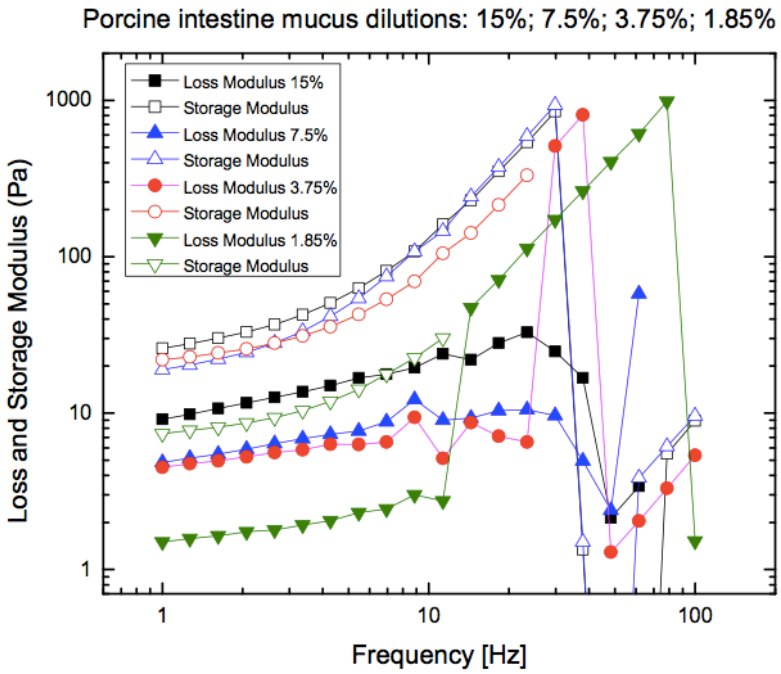

Source: Beatriz N. M. Miranda

5. CONCLUSION AND REMARKS

We studied the bulk rheological properties of mucus in different dilutions. This experiment was promoted to study the properties of both, diseased and healthy state, according to the dry weight percentage of raw sample. Rheological characterization is critical for the understanding of mucus physiology, disease pathology, and development of drug-delivery systems for use at mucosal surfaces. These results may be used as control for the comparison with further results obtained from micro-rheological experiments. Moreover, these results may be used as a parameter for the diffusion coefficient calculation by MPT and NTA analysis, as described in the next chapter.

CHAPTER 5

Mucus penetrating polymersomes: concept and development

1. INTRODUCTION

The primary goal of nanomedicine, the application of nanotechnology for medical purposes, is to improve clinical outcomes.[113] Drug delivery application is vast, and may play direct effect over patients suffering from mucosal-related diseases such as cystic fibrosis (CF), chronic obstructive pulmonary disorder (COPD), bronchitis, lung and cervical cancers, sexually transmitted diseases, and more. For instance, in cystic fibrosis, occurs production of abnormal mucus that is excessively thick and sticky, which leads to blockages within the lungs and airways, and to reach diseased cell layer the drug delivery system has to overcome the dense and protective mucosal barrier. To this end, nanoparticles are especially prepared to reduce mucosal interaction and, therefore, enhance drug distribution and improve therapeutic efficacy.[113] Therefore, the development of mucus-penetrating drug delivery system is an unmet need. Recent years have witnessed remaekable growth of research in nanomedicine, as demonstrated by the growing number of publications in the area over the past 25 years, in Figure 38, nourishing optimism related to nanotechnology application in disease treatment and diagnosis.

Figure 38 – Graphical timeline showing publications containing nanomedicine term.

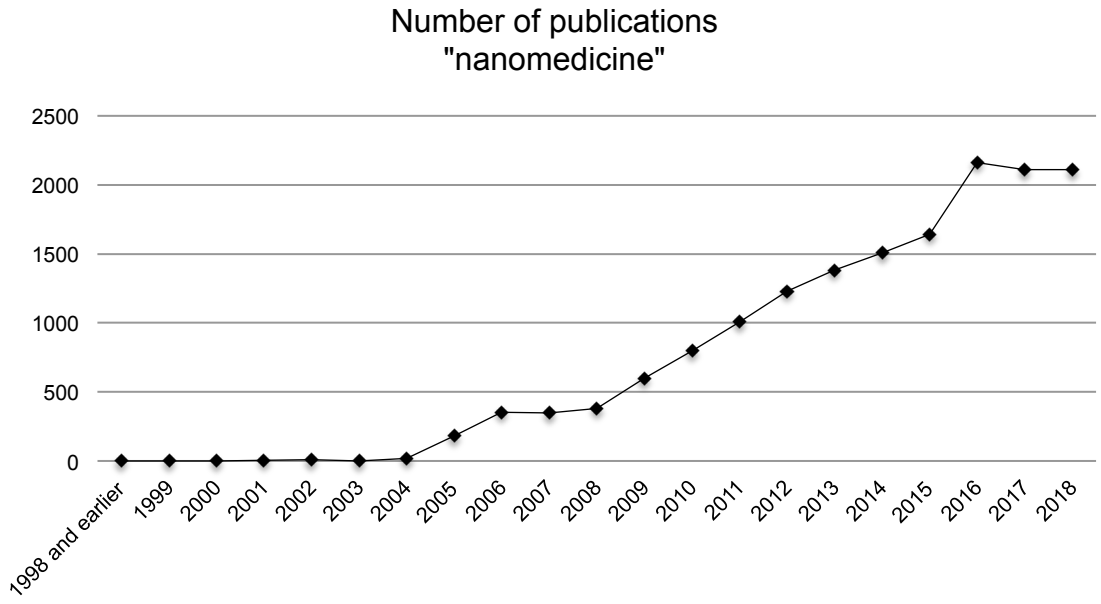

Source: Data from the ScienceDirect base.

1.1 Mucus Penetrating Particles

As previously discussed in Chapter 4, mucus is a very complex matrix that protects the human body, but also poses a barrier for drug delivery. Fortunately, there are strategies that aims to overcome this barrier, and they play an important role in mucosal drug delivery, drug development and nanoparticle development processes.[114] One strategy to reduce drug adherence to mucus though non-covalent interactions (that include electrostatics: ionic interactions and hydrogen-bonding and hydrophobic interactions) is to take advantage of agents that are capable of disrupting the mesh-like structure of mucus. Another strategy, regarding drug development is the chemical conjugation of drugs with such agents, or other molecules that may enhance drug resistance to mucosal enzymes, or even its conjugation to specific molecules that may decrease the mucoadhesion, and therefore, help the achievement of longer retention times and better prophylactic and therapeutic treatments.[115]

Further, improvements on nanoparticle design also play an important role in sustained, triggered and controlled drug release, cargo protection from enzymatic degradation, modulations on intracellular trafficking, and mucosal clearance.[84] Similarly to free drugs and foreign particulates, the primary challenge in conventional nanoparticle drug delivery systems is therefore the mucus trapping via steric and/or adhesive interactions. To overcome this natural barrier, nanoparticles must be small enough to avoid steric hindrance and have a neutral hydrophilic surface to avoid adhesion.[116,117] Thus, reported strategies focus on the development of particles smaller than mucosal mesh-pore size (i.e. smaller than ~200 nm) to undergo diffusional transport and by altering their surfaces in various ways (such as with muco-inert material[10,16,84]; photolytic enzymes[118] and other strategies[119]). Due to its protective and clearance function, mucus is continuously secreted and renewed; therefore, nanoparticles coverage with inert surface chemistries is usually preferred over mucolytic-related modifications.

In that direction, some studies have suggested the use polyethylene glycol (PEG)[10,16,84] and N-(2-hydroxypropyl) methacrylamide copolymer (pHPMA) derivatives[120]. Due to its biocompatibility and versatility, PEG coating attracted more attention and a greater amount of studies.[10,16,18,116,121,122] PEG is a inert polymer that have shown promissing results when applied in nanoparticles surface to increase mucus-penetration. For instance, it was reported that the dense coating with low-molecular-weight PEG [10,16,84] are both required for minimizing mucin-nanoparticle adhesive interactions, and therefore achieve rapid mucus penetration. This was proposed on the basis that greater steric obstruction apperceived by the PEG chains increases in high densely coatings, as shown in Figure 39.[10,16] Furthermore, higher PEG coatings molecular weights (10 kDa) can lead to an increase in mucoadhesion due to intermolecular interactions, such as hydrogen bonding, between PEG chains and mucins.[16] Taking advantage of this, Lai et al (2007) demonstrated that even large 200- to 500-nm nanoparticles, if properly coated, could penetrate through cervicovaginal (CV) human mucus.[84] However, even though the majority of mucosal barriers are much similar to each other, CV mucus is one of the most hydrated ones, and it also varies not only according to the person but also the fertile cycle, what may explain the larger particles diffusivity and, therefore, effective mucus-mesh size.

Figure 39 – Schematic illustrating the effect of nanoparticle PEG surface density on transport behavior in mucus showing that nanoparticles with low density PEG coatings adhered to mucus (blue mesh) allowing the access of mucin molecules to nanoparticle core, whereas nanoparticles with high PEG surface density rapidly diffused through the open spaces in mucus ex vivo (particle trajectory depicted in green) by preventing the mucin adsorption. Low (light blue), inter- mediate (blue), and high molecular weight (red) mucin molecules are depicted in the middle row.

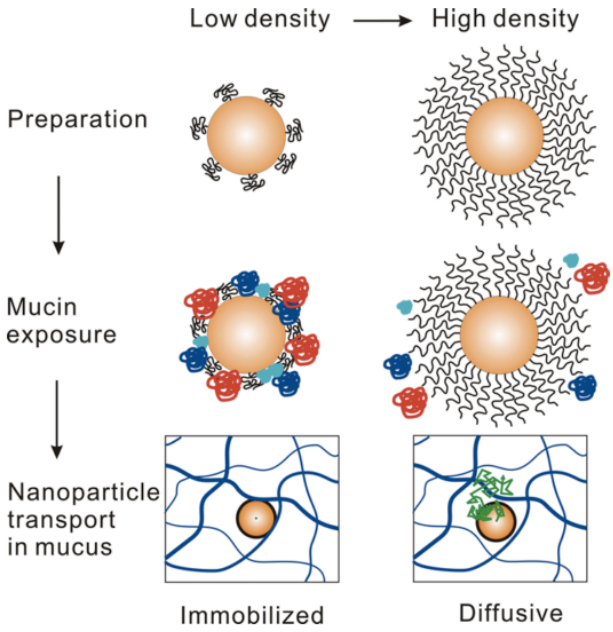

Source: Reprinted with permission from (ACS Nano 9, 9, 9217-9227). Copyright (2015) American Chemical Society. [10]

1.2 Multiple Particle Tracking

As previously described in Chapter 4, mucus rheology can be achieved by conventional rheological experiments. Although, when studying the interaction between foreign particles and/or pathogens in the mucus, the macro-rheological characterization becomes inadequate. For that reason, the term micro-rheology is defined as the characterization of the viscoelasticity that is encountered by micro- and nanoscale entities.[12] Mucus samples comprise a nanoscopically heterogeneous environment and micro-rheological studies enables the local characterization of its mechanical properties that are, however hidden during bulk rheological analyzes.

Specifically, for drug and gene delivery applications, the diffusive behavior of particles through biological barriers, reaching target sites, are generally the focus.[123] Therefore, in the process of diffusion, the existing gradient that drives the

movement of molecules or particles from a region of high concentration a region of low concentration, is a as a result of random motion of the molecules or atoms. Such process enables, for instance, the nanoparticle trespassing through mucosal barriers, and increases the system entropy by bringing the system closer to equilibrium. The diffusion coefficient (*D*) measures how efficiently a material can diffuse through another material. In this case, it is a measure of particle diffusion through a specific solvent, or media. For instance, in water, typical diffusion coefficients are in the range of 10^{-10} to 10^{-9} $m^2.s^{-1}$, around 4 times slower than typical diffusion in the gas phase. In a viscous fluid such as biological barriers, it should be even slower, since particle should encounters even greater resistance. The Stokes-Einstein equation, Equation 5, states that the diffusion coefficient (D) is proportional to the temperature (T) and inversely proportional to the viscosity of the solvent (η) and the particle radius (r).

Stokes-Einstein equation:

$$D = \frac{kT}{6\pi\eta a} \quad (5)$$

where,
k is the Boltzmann constant
T is the temperature
η is the viscosity of the fluid
a is the radius of the particles

Although, biological barriers are very complex systems, and diffusive effect on these environments are not fully known, efforts have been made to mimic and predict the complexity of these environments. Strategies such as using freshly excised samples or a vertical diffusion chamber system[112] have been described in order to predict whether a therapeutic will traverse the barrier effectively and what are the factors related to physical and chemical characteristics that may enhance their diffusivity.[124] In another approach, Li et al. studied the acid diffusion though a mucosal barrier in a microfluidic system, which may be used as a platform tool for studying interactions such as mucus-drug.[125] An interesting review on purposed methods until 2015 is reviewed by Grießinger et al., as shown in Table 6.[124]

Table 6 Comparison of presented methods and techniques among each other (I.S. – particle-mucus interaction studies; P.S. –particle permeation studies; D.S. particle diffusion studies)

	I.S. via particle size and zeta potential measurement	I.S. via rheological measurement	QCM-D method	SANS method	P.S. via Transwell–Snapwell system	P.S. via Transwell diffusion system	D.S. via rotating tube	MPT method	Diffusion NMR method
Used technique within this review	Particle–mucus interaction study	Particle–mucus interaction study	Particle–mucus interaction study	Particle–mucus interaction study	Particle permeation study	Particle permeation study	Particle diffusion study	Particle diffusion study	Particle diffusion study
Mainframe required	No	Yes: rheometer	Yes: weighing device	Yes: diffractometer	No	No	No	Yes: fluorescence video microscope	Yes: NMR spectrometer
Additional apparatus required	No	No	No	Yes: particle sizer	Yes: fluorometer	Yes: fluorometer	Yes: fluorometer	No	No
Labeling of particles required	No	No	No	No	Yes	Yes	Yes	Yes	No
Experimental time	Long	Long	Medium		Long	Long	Long	Short	
Kind of measurement					Static	Static	Static	Dynamic	Dynamic
Required sample amount	High	High	High		High	Low	Low	Low	

Source: Reprinted with permission Grießinger et al.[124]

One interesting example is Multiple Particle Tracking (MPT) method. This versatile technique, developed by Valentine et al. uses fluorescent micron-sized particles and high-speed, high resolution video microscopy to simultaneously track particles undergoing Brownian motion in inhomogeneous materials.[126] Taking advantage of an image processing software its possible to analyze individual or a group of particle trajectories, it is possible to analyze the diffusivity and quantify the mechanical properties of micro-scale environments.[127] Therefore, understanding particles behavior in a given environment enables the comprehension of the mechanics of the microenvironments that those particles explore, i.e., if are undergoing Brownian motion or if are hindered.[126]

The diffusive particles should undergo a sequence of discrete steps of fixed length, yet random motion in direction, the well-known Random-Walk model. [110] The time-average over *t* and/or an ensemble-average over several particle trajectories can be calculated, and is defined as the Mean Square Displacement, <MSD>, displaying the dynamics of the particles are been tracked in the medium used.

$$< MSD > = \langle \Delta x^2(\tau) \rangle = \langle (x(\tau) - x_0)^2 \rangle = \langle [x(t_0 + \tau) - x(t_f - \tau)]^2 \rangle \quad (6)$$

where,
x is the particle position
t_0, initial time of the trajectory
t_f, final duration of the trajectory
τ is lag time

For a viscous fluid:

$$< MSD > = q_i D \tau \quad (7)$$

<MSD> = is the mean distance from the starting point that a molecule will have diffused in time, t
q_i = numerical constant which depends on dimensionality: q_i = 2, 4, or 6, for 1, 2, or 3 dimensional diffusion
D is the diffusion coefficient (usually in $cm^2\ s^{-1}$)
τ = lag time

Therefore:

$$< MSD\ (\tau) > =\ 2\ dD\tau^{\alpha} \quad (8)$$

where,

d is the dimensionality of the track
D is the diffusion coefficient
α is the extent of impediment, and tends to 1 when particles are diffusing by Brownian motion, and to 0 as the extent of obstruction increases.[18,110,128]

Then, MPT studies enables the study of micro-rheology by measuring deviations from thermally-driven Brownian diffusion of probes in the sample.[12] Moreover, with this technique it is possible to develop predictive models for nanomedicine development. Aiming the development of mucus penetrating particles, they must efficiently overcome the mucus barrier to avoid rapid clearance. Multiple particle tracking studies for mucosal drug delivery issues have been extensively investigated by Hanes group[18,19,111,129–132], from The Johns Hopkins University, and some of their findings, specially the ones regarding PEG coating are previously discussed in this Chapter.[10,16,18,116,121,122] The basic principles of particle tracking and state-of-the-art applications have been highlighted by the same group[131], including a more recent review.[123]

Here, we sought to investigate the ability of PEGylated polymersomes to diffuse through a mucus sample in comparison to PS particles, frequently used as a control parameter. To check the data obtained by MPT, we compared the results with the data obtained by the comercial Nano Particle Tracking System (NTA, Malvern). We performed our studies minimally altered ex vivo porcine intestine mucus (PIM), using multiple particle tracking. To detect changes in particle permeation, freshly obtained and minimally altered ex vivo porcine esophagus tissue was used for permeation studies using Franz cell, and tissues containing nanoparticles were analyzed by confocal microscopy. Further, to investigate the ability of foreign particles (control and polymersomes) to be inhaled and used as a local drug delivery to lung diseases, we promoted in vivo biodistribution studies,

providing another assessment of permeation ability of polymersomes. An enhanced mucus penetration should facilitate uniform distribution and prolonged holding of drug carriers at mucosal surfaces, diminishing its clearance and leading to improved pharmacokinetics and therapeutic efficacy.[133]

2. OBJECTIVES

In this chapter we aim study the ability of polymersomes to penetrate though mucus. First, in vitro Multiple Particle Tracking experiments demonstrate the greater hindrance observed for conventional PS particles, used as a control parameter. Same comparison was promoted using NTA analysis system to confirm previous results. Using a Franz cell, ex-vivo experiments were promoted using porcine esophagus tissue, and the tendency of particle permeation though the mucosa was analyzed by confocal microscopy. Then, nanoparticles mice lung permeation followed by pulmonary administration and biodistribution was also observed by confocal microscopy, similar to what was reported for particle distribution in the mouse colorectum[134], vagina[3,135], and brain tissue[136].

3. EXPERIMENTAL METHODS

Polymersome preparation. Polymersomes were prepared by film hydration following the procedure described in Chapter 2. Briefly, PEG-b-PLA was dissolved in chloroform and dried under N_2 flow. Then, the polymer solution was hydrated with PBS solution, left overnight at 50 ^{o}C under continuous stirring, followed by resizing protocol. In order to allow particles detection during the diffusion studies 0.25 mol% of rhodamine was used during the preparation.

Intestinal mucus collection and purification. Porcine small intestinal mucus was collected and debris removed following a protocol developed by the research group of Prof. Katrina Ribbeck, MIT. Thereafter, the clean intestinal mucus was stored at -80 ^{o}C until further use.

High-resolution confocal microscopy study of polymersomes in mucus. Using grease, square sections were mounted on a glass slide, for delimiting the mucus sample and used for high-resolution confocal imaging. A Leica SP5 confocal microscope with 63× 1.4 APO oil immersion objective equipped with a HeNe laser (λ = 633 nm) as an excitation source for the DHPE-Rh was used to obtain image sequences at zoom 10. Images sequences were processed using ImageJ and MatLab. For Multiple Particle Tracking (MPT) we adapted the MatLab version of Maria Kilfoil's Group tracking code. We conducted our tests using a control parameter established by 0.2 μm FluoroSpheres carboxylate-modified microspheres (PS-COOH, Invitrogen).

Nanoparticle tracking analysis (NTA) Briefly, samples were diluted in 10× in PBS 1× or mucin-water 1.5 wt.% (Sigma Aldrich) mixture and introduced to an NTA system NS300 (Malvern, UK) equipped with a CCD camera through a syringe continuously injected using a NanoSight syringe pump. The syringe pump flowed at approximately 50 $\mu L.h^{-1}$. The chamber temperature was maintained at 37 °C. Data was captured in continuous flow mode, at 24.98 fps, and were collected 5 videos of 120 s for each sample. Analysis was promoted using NTA Build 3.1.45 and 0.69 cP for water viscosity and 1000 cP for reconstructed mucin, which is the value at physiological shear rates. The concentration, size distribution and diffusion coefficient of particles were calculated using manufacture's software according to the collected tracking data. The system was flushed with filtered deionized water between runs to prevent cross contamination.

Permeation Experiments. Esophagus tissues were obtained from a local slaughterhouse (Frigorífico Raja Ltda, Carapicuíba, Brazil). Esophagus preparation was adapted from a method described the litherature.[137] Briefly esophagus was cut longitudinally, carefully to not alter the internal mucosa. The mucosa was separated from the muscular layer by cutting the loose connective fibers with a scalpel, separated in square samples of 2.5 cm^2 and kept frozen at 80 ^oC until use.[137] Six Franz cells were used. The internal side of the esophagus tissue was mounted upwards in the diffusion cell. The donor and receptor compartment were

filled with PBS buffer - exact same amount in each cell - and the cells were allowed to stabilize for 15 min in a water bath at 37 °C. The experiment was initiated by replacing the buffer in the donor compartment with 0.5 mL of a polymersome and PS-COOH particle solution. The receiver compartment volume was 7.0 mL. Diffusion experiments were conducted for 1 h.

Mice lung biodistribution in vivo. To investigate the lung biodistribution of PEG-b-PLA polymersomes and compare them to PS particles, 30 μL samples were intranasal injected, having standadized fluorecence intensities. All the experiments were performed with the approval of the Institute of Biomedical Sciences Ethics Committee, from University of São Paulo, (CEUA-ICB/USP), under the protocol number 70/2017. After 2 hours of treatment, euthanasia was performed and lungs were excised, frozen and analyzed.

*Cryo-microtome, histological assessment and confocal microscopy***.** Samples immersed, immediately after excision, in Neg-50™ Frozen Section Medium (Thermo Scientific). NEG-tissue blocks were cut to 15-50 μm thickness using a microtome (Thermo Scientific™ HM525 NX Cryostat) and stained with Fast Panoptic LB Kit (Centerlab), for conventional microscope observation. The isolated epithelia and lung were also examined without staining to assure the presence of tested particles in the sample and by light microscopy. High-resolution confocal imaging was promoted using a 5 and 10× dry objective on a confocal microscope (Leica), using 480 nm laser intensity. Images were processed using ImageJ.

4. RESULTS AND DISCUSSION

The existing PEG corona in PEG-b-PLA polymersomes tends to avoid unspecific interaction with proteins, including mucin fibers, and also should increase circulations times, consequently achieve efficient delivery by topical mucosal or intravenous delivery. Figure 40 schematically illustrates the polymersome structure, which should be diffusive by nature, with enhanced mucus-penetration capability by lowering their interaction with the mucus. Therefore, due to the presence of the

outermost PEG monolayer of these polymersomes, we hypothesize that their mucus-penetration capability is improved if compared to non-coated particles. We fabricate these polymersomes by hydration in a PBS solution, as previously described in Chapter 2. Generally, PS-COOH nanoparticles were used as a model system to study the effect of self assembled PEG hindered surface.

Figure 40 – Polymersome structure, containing the PEG corona that was formed during self-assmble process.

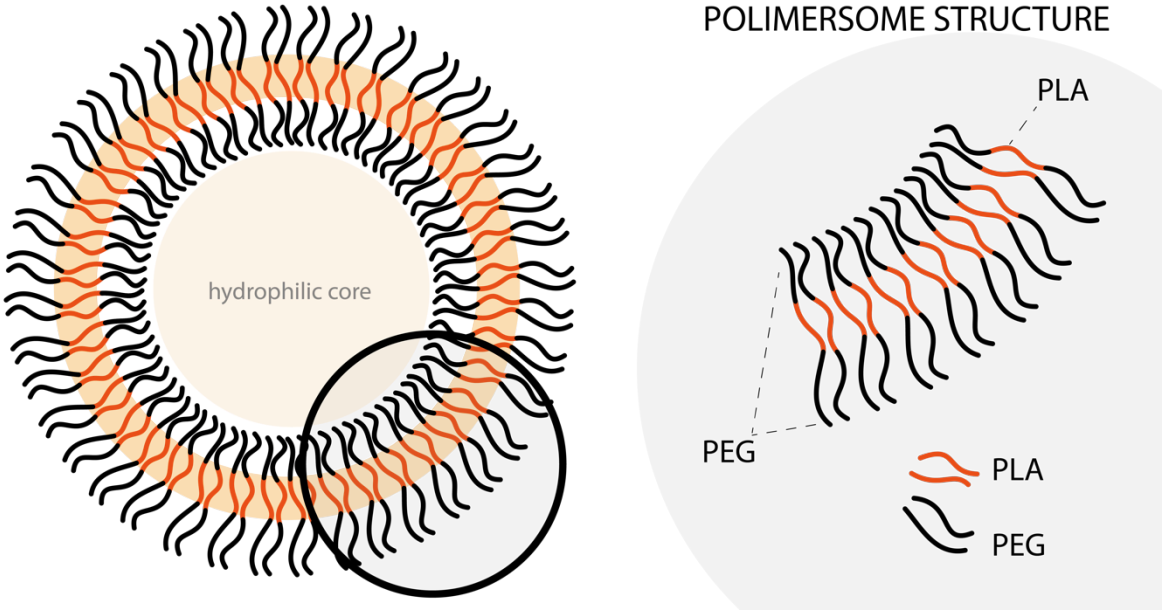

Source: Beatriz N. M. Miranda

4.1 Polymersome Transport in Porcine Intestine Mucus ex Vivo

We used multiple particle tracking (MPT) to observe the transport dynamics of fluorescently labeled polymersomes and particles in undiluted PIM. 500 nm PS nanoparticles were completely immobilized in PIM (data not shown). A sample observation windown for polymersomes and particles in PIM is shown in (Figure 41). We track the motion of PEG-b-PLA polymersomes in 15 wt.% untreated porcine intestine mucus using a resonant confocal fluorescence microscope. For this experiment, the PEG-PLA polymersome membrane is fluorescently labeled with 0.25 mol% of rhodamine 1,2-dihexadecanoyl-*sn*-glycero-3-phosphoethanolamine. As a matter of comparison, we tracked the motion of fluorescent uncoated particles of approximately the same size as the polymersomes, in untreated porcine intestine

mucus, as shown in Figure 41. By analyzing a sequence of these images, we observe that particles remained highly constrained (Figure 42) when comparing their trajectories to the polymersomes (5 kDa PEG), which exhibited increased diffusivity in mucus. This is likely due to the interactions between uncoated particles and untreated mucus. The presence of PEG corona in the surface of the polymersome hinders the interaction with mucin, which is expected to facilitate mucus permeation. From these trajectories, we calculate the ensembeled mean-square displacement, MSD, of polymersomes and particles. Interpreting the data leads to the observation that at long time scales the profile of the MSD traces are descendent and the explanation is that at that point, as shown in Figure 43, the data is biased due to slight convection of the solutions, which is difficult to prevent for low viscosity fluids. For that reason it is frequently used a period smaller than 1 s to analyse this kind of data, avoiding artifacts that arise from statistical limitations. It can be observed that the MSD of both the polymersomes and the particles increases linearly with time, indicating that they are diffusing though the mucus sample. The rapid transport of polymersomes was also reflected by the slight higher slope, α, when α=1 represents unconstrained Brownian transport, whereas increased obstruction to particle movement is reflected by a decrease in α. Still, for both particles and polymersomes, α was very close to 1, indicating more diffusive particles then hindered. Sample videos can be analyzed in the supporting information. The momentanely decrease in intensity of some particles, or their disapearance and sudden appearance can be explained by their trajectory as they move in and out of the plane of focus. The use of a second camera horizontaly orientated to the sample would enable tracking over all 3 directions, but unfortunatelly was not possible during the aquisition time. Therefore, adaptations to the tracking parameters were made, in order to accuratelly track particles using the MPT software. It has to be said that these parameters still need little refining, but we observed the heterogeneity of the mucus, which is reflected in the transport of individual particles, by plotting <MSD> for 7 different aquisition spots for each sample group, particles and polymersomes.

Further, by plotting the distribution of the logarithms of individual particle effective diffusivities (D_{eff}) at τ =1s, as shown in Figure 44, we can observe that the majority of the polymersomes exhibited Deff values greater than 0 $\mu m^2/s$, while the

same cannot be said for PS nanoparticles. Therefore, the self-assemble production methodology related to polymersome production enables not only the high densely coating by PEG chain but also presents the advantage of not requiring a coating step, still demonstrated mucus-penetration capability, as antecipated.

The distributions are not Gaussian, which is expected since mucus is a heterogeneous gel, but exhibit a tail at low values of D_{eff}; however, this tail is more pronounced in the case of particles, as expected from their constrained trajectories. Moreover, $\log_{10}$ Deff for polymersomes is bigger than for particles. Using the Student t test, we further determined that the mean of $\log_{10}D_{eff}$ of PEG-PLA polymersome is significantly different than the mean of $\log_{10}D_{eff}$ of particles, $p<0.05$. Further thoughts and discussion should be focused on the ratio of the average diffusion coefficient of each nanoparticle type in water compared to in mucus (Dw/Dm) when both particle and polymersomes should show a decrease in their diffusivity when in the mucus environment.

Figure 41 – Typical single frame Laser scanning micrograph of multiple tracking experiments for (a) polymersomes (b) 200 nm PS nanoparticles in mucus.

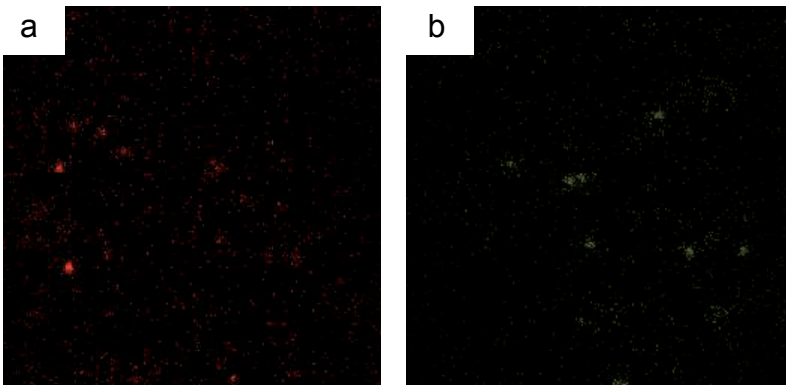

Source: Beatriz N. M. Miranda

Figure 42 – Particles and polymersomes random *x* and *y* trajectories over a period of 3.9 seconds. Scale in µm.

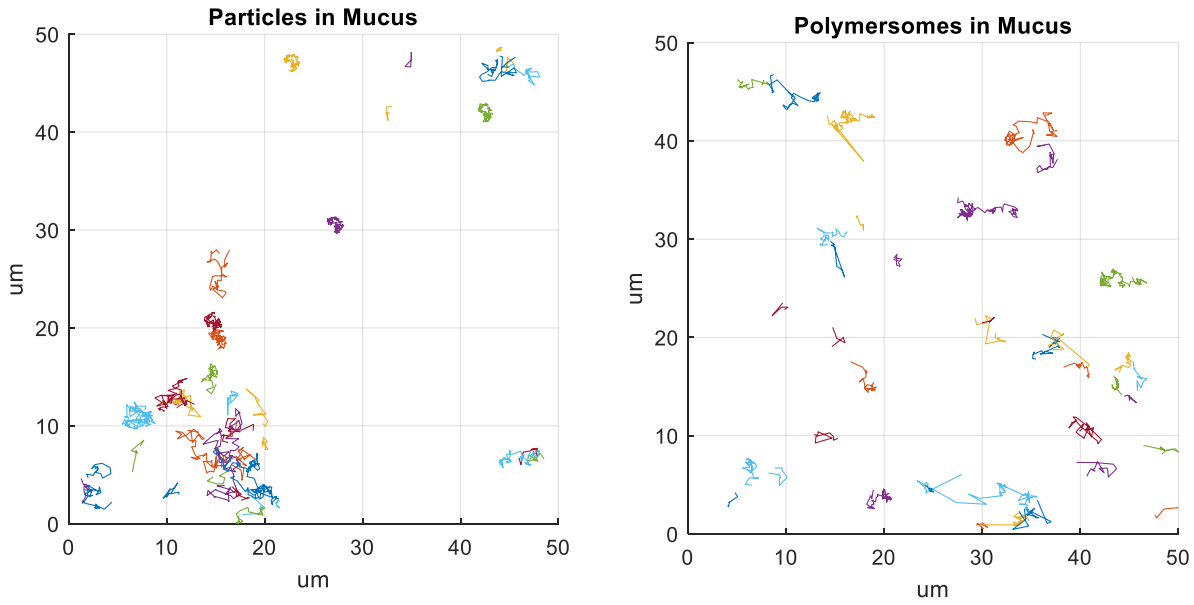

Source: Beatriz N. M. Miranda

Figure 43 – Transport rates of 200 nm uncoated PS-COOH particles (red) and 160 ~200 nm PEG-PLA polymersomes (blue) in porcine intestine mucus. a. Ensemble-averaged mean square displacements (<MSD>) as a function of time scale.

a

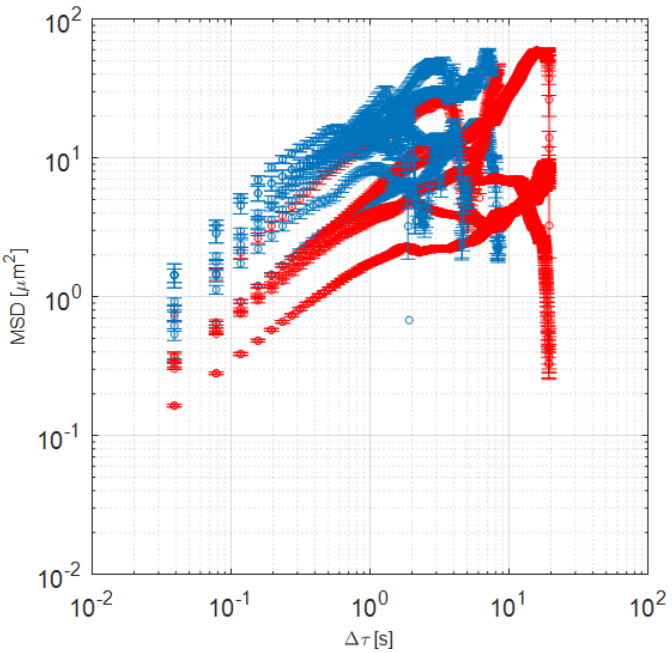

Source: Beatriz N. M. Miranda

Figure 44 - Tracking individual beads is possible to analyze the diffusion coefficient of each one. *t*=1.

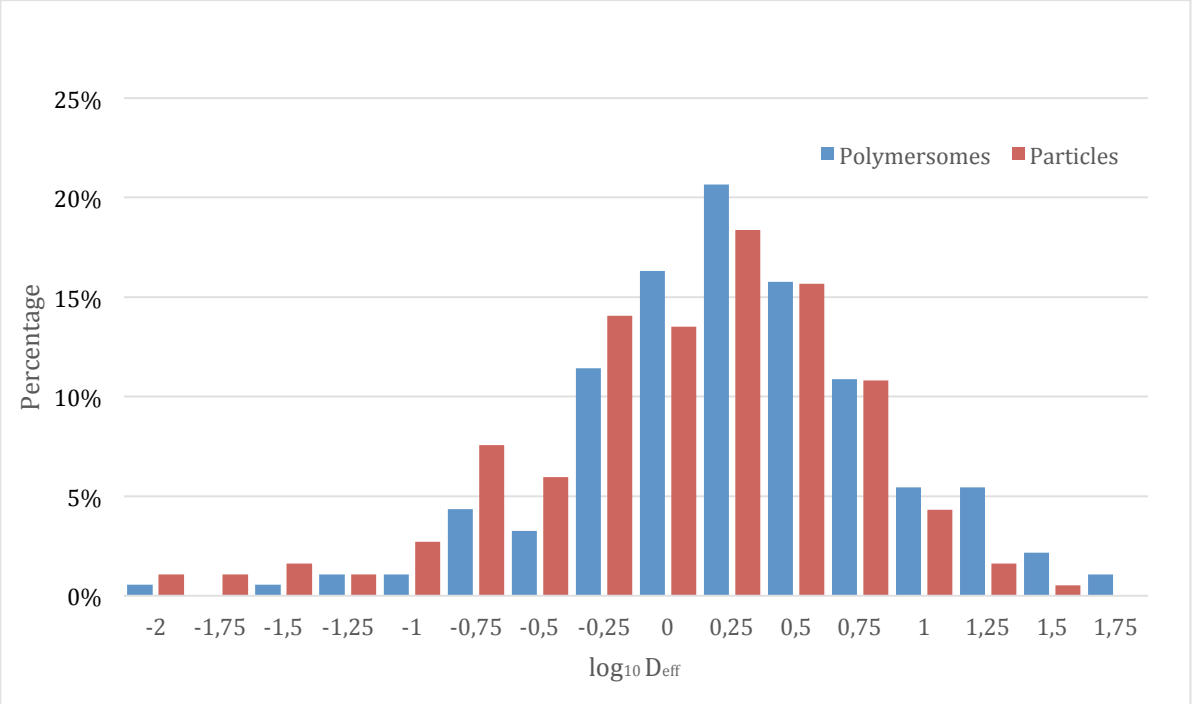

Source: Beatriz N. M. Miranda

4.2 Nanoparticle tracking analysis (NTA)

As forehead mentioned, PEGylated surfaces are typically used to decrease protein adsorption from human plasma, as in the case of the well-known PEGylated liposomes, but it as well has a characteristic repealing effect as muco-inert particle surface. Since we previously used the MPT to estimate the diffusivity of polymersomes over particles, NTA analysis was performed to compare the data and different techniques. NTA provides particle size distribution as well as diffusion coefficient in both media tested, as shown in Table 7. Reconstructed mucin was used here instead of real mucus sample, due to limitations in sample obtention. Still, polymersomes were 2.3 faster than PS-COOH particles.

Our findings are in accordance with the trend reported by Lai and co-workers[84]: uncoated PS particles diffuse slower (D_m/D_w) 0.0010), but diffusion is 2.4 × improved for polymersomes, with PEGylated surface (D_m/D_w) 0.0024). We understand our data reveals slightly higher values for PS-COOH than the ones from the literature, although we believe that slight changes in the experiment settings,

from the mucosal sample used, to the tracking parameters and techniques may incur in some discrepancy in the data. An increase in D_m/D_w was also observed for PEGylated poly(lactic-co-glycolic)acid (PLGA) nanoparticles by Cu and coworker, 2008, using human cervical mucus.[122] At the same time, we expected that polymersome data would be similar to PS-PEG 200 nm particles, analyzing D_m/D_w, which were 2 orders of magnitude smaller. Instead, if we use the diffusion coefficient obtained for PS-COOH particles and polymersomes in PBS buffer, D, instead of D_w, we observed an improved value for both, PS particles (D_m/D) 0.62, but specially for polymersomes (D_m/D) 1.4). Since we were willing to investigate and potentially improve the transport of drugs across the mucus barrier, we understand that the PEGylated surface of the polymersome does help to improve its quantitative transport rates in comparison to uncoated nanoparticles. To discuss weather polymersomes have increased mucus penetration over PEG-coated nanoparticles, other particles should be used instead in further experiments. Moreover, for such analysis, the PEG-coating and surface coverage should also be an important characteristic to be precisely determined, what will be not be accessed here.

Table 7 Characterization of uncoated PS nanoparticles and PEG-b-PLA polymersomes by NTA, and ratios of the ensemble average diffusion coefficients (D) in water (D_w) compared to in reconstituted mucin (D_m).

Sample	Media	Viscosity (cP)	Size (nm)	Valid Tracks	D	D_m/D_w	D_m/D
	PBS	0.69	245.2 ± 2.7	2206	2.71E-12		
PS-COOH	Mucin	1000*	299 ± 1.5	7674	1.69E-15	1.01 E−3	6.22E−1
	PBS	0.69	325.3 ± 22.8	4001	2.80E-12		
Polymersomes	Mucin	1000*	208.1 ± 21.6	5771	3.92E-15	2.4E−3	1.4
PS-COOH[§]			216.6 ± 4.5			4.2 E−4	
PS-PEG[§]			232.3 ± 6.8			1.6 E−1	

D and D_m values are given by NTA software, in PBS and mucus. D_w is calculated from the Stokes-Einstein equation.
*at shear rates of 10 s^{-1} mimicking physiological shear rates
[§]data from Lai et al. 2007[84]

This study demonstrates that PEGylated polymersomes can readily penetrate to mucus. As discussed in Chapter 2, another major advantage of polymersomes over particles is that they should be able to encapsulate both, hydrophilic and hydrophobic payloads within their innermost water cores and membrane, besides having superior colloidal stability over its lipid peer.[48] Here we

compared the obtained data from MTP and NTA and observed that in both cases polymersomes are less contrained than particles, demonstrating its ability to permeate though mucosal surfaces. This type of information can allow researchers to develop new kinds of trans-mucosal carriers, based on polymersomes. Therefore, as mucus penetration carrier, polymersomes represent a promising candidate for drug delivery.

4.3 Polymersome Transport in Porcine Esophagus Mucosae ex Vivo

In that context, to investigate the permeation of polymersomes in mucosa and compare to PS control particles and previous experimental *in vitro* data from particle tracking experiments, permeation studies using Porcine Esophagus Mucosae (PEM, Figure 45 A) was promoted, in Franz cell apparatus (Figure 45 B). For that, polymersomes and PS particles left in contact for 1h with the mucosae. Samples were frozen and prepared and cryo-cutted for confocal microscopy visualization.

Interestingly, the stratified-aquamous epithelium, E in Figure 45 E was the area the most of PS Particles were found, in D, indicating the accumulation of such nanoparticle in the epithelium. Therefore, we observed non-uniform distribution such particles, which appeared more condensed. On the other hand, there was not a specific area were polymersomes were found, from stratified-aquamous epithelium to the connective tissue, demonstrating improved distribution over conventional PS particles on PEM. Even though the fluorescence intensity of this sample was lower (DPPC-rhodamine was used, while PS particles are commercially available one and do not specify the amount of dye used), this nanocontruct was distinctly found indicating that its permeation though PEM was favorable and therefore, probably faster than tested particles. Despite those important observations suggesting that the outer PEG layer was sufficiently shielded to avoid mucoadhesion in vivo, further comparison of PEG-b-PLA polymersomes and PEG-coated PS particles, with known surface shield, must be promoted to eliminate doubt regarding PEG surface coverage and compare to existing literature data. Still, these findings led to our hypothesis that polymersomes could be interesting carriers for trans-mucosal drug delivery.

Figure 45 – *Ex-vivo* experiment using PEM. (A) PEM sample preparation; (B) Franz-cell apparatus; (C) Optical microscopy of PEM, E, stratified-aquamous epithelium; B, basal lamina; CT, connective tissue; P, papillae. Confocal microcopy of PS particles permeation (D) and Polymersome permeation in PEM.

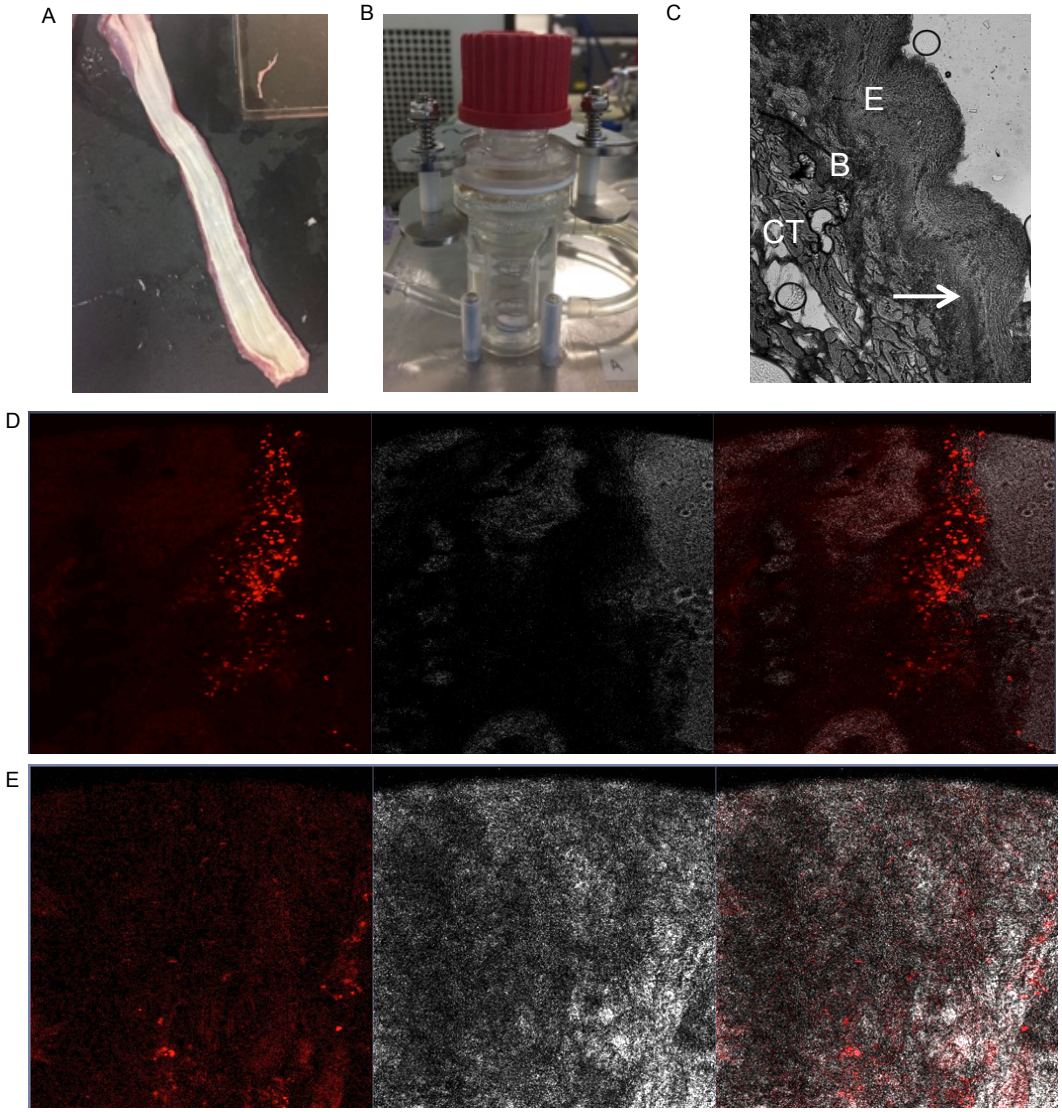

Source: Beatriz N. M. Miranda

4.4 Polymersome biodistribution

We finally investigated whether the improved distribution profile of MPPs would lead to improved particle permeation in mice by intranasal treatment. To further explore the distribution of control uncoated PS particles and polymersomes, samples were. Remarkably, the results demonstrated that polymersome sample was evenly present in the lungs sections at 2 h post-injection (Figure 46), in agreement with previous permeation results. In contrast, it was found that lower

amount fluorescent particles were present in the excised lung tissue at 2 h post-injection, indicating that these particles were likely trapped before reaching the lungs. Therefore, it is reasonable to assume that polymersomes should become interest approach for local lung drug delivery system. Despite those important observations, further semi-quantification analysis of the fluorescence should still be performed, as well as thinners histological sections.

Figure 46 – In vivo distribution of Polymersomes and PS-NP formulations in mice lung. Photomicrographs show localization of fluorescent (red) in sections of bronchioles and alveolar ducts. Negative sample was used to remove backgoud noize. The images reported in the figure are representative of 2 slides per animal, containing at least 3 sections (2 animals per group), scale 50 μm.

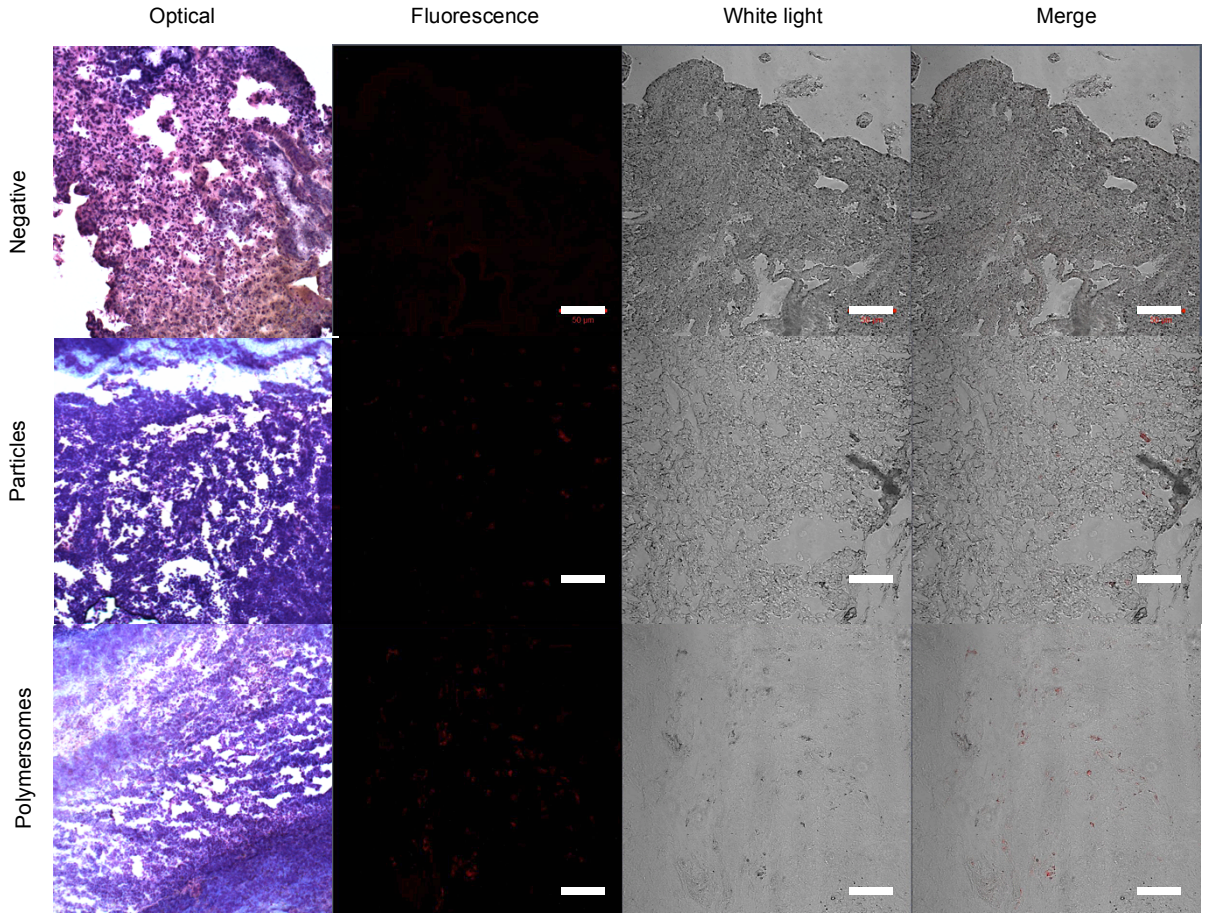

Source: Beatriz N. M. Miranda

5. CONCLUSION AND REMARKS

Multiple Particle Tracking experiments revealed greater diffusivity of PEG-PLA polymersome over particles. A prominent advantage of this platform over

mucus-penetrating nanoparticles is its weaker interaction with the mucus mesh, which imparted by the highly dense PEG outer layer of the polymersome membrane. Another main benefit comes from the hollow structure of the polymersomes; unlike solid particles, these contain an aqueous core that can be loaded with hydrophilic cargo, while hydrophobic molecules can be loaded within the embrane. Furthermore, the cargo can be controllably released using an external trigger. In particular, the PLA core of these polymersomes is designed to respond to acidic pH environments, such as solid tumors. These advantages, their biocompatibility and their ease of fabrication make them excellent candidates for clinical management of different diseases, including cancers. Further enhancement of this platform including drug loading and active delivery will further overcome challenges encountered for the trans-mucus drug delivery, enabling locally administration, decreasing side effects and enhancing drug effectiveness.

Mucosal entrapment greatly contributes to the difficulty in locally delivering drugs by nanotechnological approaches. Studies have shown previously that high densely coating nanoparticle surface with PEG shields and diminishes biding interactions, which may be also correlated with mucus permeation capability driven by Brownian motion. To effectively minimize mucin binding regardless of the need of coating process and of the drug, combining the advantageous properties of polymersomes, we took advantage of the self-assemble property of polymersomes and its mucus-permeation capability was determined by MPT studies. PS particles were more inclined to mucus interaction likely due to their non-hindered surface. More studies analysing the possible interference of a cargo in the polymeromes mucus permeation capability are still needed. Still, considering obtained results, the PEGylated surface of polymersomes and size were important to achieve mucus permeation. Moreover, the ability of polymersome to permeate though freshly excised mucosal tissue was further analyzed by confocal microscopy and confirmed the enhanced penetration of polymersomes over PS conventional particles. The enhanced mucus penetration observed for polymersomes should facilitate prolonged retention of the drug in the target area and a more uniform distribution at mucosal surfaces, leading to improved pharmacokinetics and therapeutic efficacy.[133] Therefore, this platform offers an ease of fabrication, core-shell robust platform for mucosal drug delivery.

CHAPTER 6

PEGylated polymersomes as a model system for mucus penetrating Drug Delivery: Doxorubicin encapsulation, release, in vitro and preliminary in vivo studies

1. INTRODUCTION

The use of nanotechnology in medicine for therapeutic drug delivery and the development of treatments for a variety of diseases and disorders. Such developments made emerge the Nanoterapeutics field of study. Since it's beginning it have played an important role in drug delivery, showing many potential benefits through passive and active targeting, increased solubility/bioavailability, and novel therapies. Still, efforts should be made in order to attend preclinical characterization, since the variety of materials, their unique surface properties, reactivity, and the task of tracking the individual components of multicomponent, multifunctional nanoparticle therapeutics in in vivo studies are very complicated.[31] Meanwhile, regarding the cancer research, such strategies have shown appreciable improvements in achieving therapeutic dosing via targeted therapies (and therefore higher efficacy), decrease in drug toxicity, enabled sustained-release drug profiles (helping patient compliance and therefore results) and efflux or degradation protection (diminishing the amount of drug and therefore side effects). One of the standard drug used for cancer research is Doxorubicin (DOX), an effective chemotherapeutic for many types of tumors. The DOX molecule is both amphiphilic and amphoteric, since the quinone derivative part (anthraquinone) of the molecule is highly lipophilic, while the sugar part is hydrophilic, as shown in Figure 47. This is reason why the salt DOX hydrochloride version of the drug is frequently commercialized, having increased aqueous solubility - when the amino group of the sugar is protonated.[138] DOX specific anti-tumor activity mechanism is not completelly resolved, but what is known is that it interfeers with the function of DNA, and that it comes along with severe cardiotoxicity, limiting dosing regimens.

Figure 47 – Doxorubicin chemical structure.

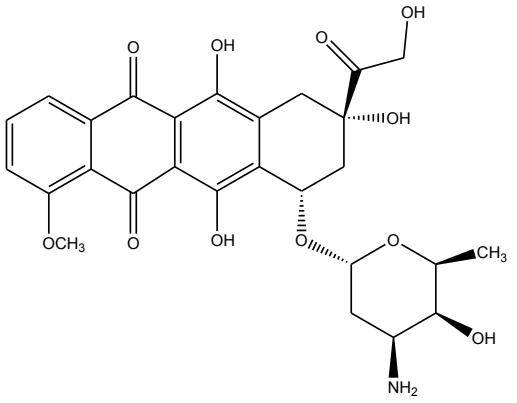

Source: Beatriz N. M. Miranda using ChemDraw Software.

In attempt to reduce cardiotoxicity and make DOX more tumor specific, several strategies have been reported related to DOX encapsulation, including drug-polymer complexes, dendrimers, polymeric micelles, nanoemulsions, nanoparticles, liposomes and more recently, polymersomes as well.[138,139] And the number of DOX-related publications is still growing. Such strategies have shown important results related to drug delivery reduced side effects, longer circulation times, enhancement of drug concentrations in the tumor and improved pharmacokinetics profiles of the drug.[138] Important features of the drug encapsulation in the PEGylated liposomal system enabeled the introdution of Doxil® in the market, which was the first FDA-approved nano-drug formulation. Following this trend, other similar formulations were also approved, such as Myocet® (non-pegylated form), and Caelyx®, and the list is growing.

As previously discussed in previous chapters, polymersomes have shown advantages over liposomes, but no equivalent polymersomal formulation is available in the market. Efforts of many laboratories and study groups have been focused on developing DOX-polymersomes allowing the benefitial characteristics of polymersomes associated with tumor control provided by DOX. Some of these reports are described in Table 8.

Finally, the high DOX toxicity, limitation of terapeutical concentrations together with the ability to engineer particle-based technologies that can cross mucosal barriers for improved efficacy and localy delivery drugs to the lungs has

motivated this work, specially for the treatment of lung cancers. Moreover, such approach could also help diminishis mucositis, which is one of DOX side effects besides decreasing DOX degradation at physiological pH.

Table 8 Literature overview of polymersome formulations for DOX delivery.

BCP	Preparation Method	Size (nm)	PDI	DOX EE (wt.%)	DOX LC (wt.%)	Cancer Type	Ref.
PBLG-b-HYA	nano-precipitation	220	0.06	50	12	rat breast cancer model	[140]
PEG-PCL	double emulsion method	175 ~208		84.3	19.7	right rear flank area of female Balb/c mice leg?	[141]
mPEG-PLGA	pH-gradient method	120–140		91.25 ± 4.27	7.3 ± 0.34	mouse breast cancer model	[142]
PEG-S-S-PLA	solvent-exchange method DOX-loading: pH gradient	P4 157 P5 209 25 nm to 700 nm		Passive 13 ± 4 Active: gradient method DOX 27±7		Cancer cells only	[55]
PEG-PTTMA-PAA	solvent exchange	112.1, 86.4, to 63.9 nm Dox loaded bigger 105.7 - 254.1	0.15-0.21 dox 0.13 - 0.28	62.5- 88.8	3.75-15.9	HeLa cells	[143]
PBLG-b-HYA	nanoprecipitation	220; 86-99	0.08		12; -	Ehrlich ascites tumor-bearing BalB/c mice	[144, 145]
2-hydroxy-4-(methacryloyloxy) benzophenone (BMA)	pH swich	72-120					[146]
(PEG)3-PLA	nanoprecipitation	2-10 μm and 50-250 nm		51.7± 2.3	10.9±0.49	DMBA-Induced Mammary Carcinoma Rat Model	[53139]
PCL-PEG	Film hydration	100-200					[147]
PTMC-b-PGA	nanoprecipitation	131 pH 7.4 147 pH 10.5	0.24 pH 7.4 0.4 pH 10.5	23 pH 7.4 47 pH 10.5			[148]
PEPs	solvent exchange - dyalisis	53.21- 243.35		~52.92-97.47%	8.82-16.23 %	breast cancer - mice	[149]
PEG-PLA + PEG-PBD	film hydration DOX-loading: pH-gradient	sized down to ~100					[150]
(PTMC-b-PGA)	nanoprecipitation pH 10.5	100-400		47.5-74	9-12		[151]
PEG-PLA and PEG-PCL	film rehydration DOX is loaded by pH-gradient						[41]
PEG-P(TMC-DTC) and cNGQ-PEG-P(TMC-DTC)	solvent exchange method.	105 118 DOX	0.10-0.15	64.3-80.3	7.3-12.2	A549 human lung cancer cells	[152]
PCL_{8000}-PEG_{8000}-PCL_{8000}	film rehydration	208.1 ± 3.5	0.278 ± 0.013	14.55 ± 1.61 DOX	3.49 ± 0.21 DOX		[153]
p(THP-HEMA)-b-p-(DMAEMA)	Nanoprecipitation	~30-40nm and aggregates 300 nm		30.7	1.5	L929 cells	[154]
PEG-PLGA	Film hydration DOX-loading:pH gradient	115±0.6	0.172	96%±3.5		Mice colon adenocarcinoma C26 in BALB/c mice	[155]

poly(γ-benzyl l-glutamate)-b-hyaluronan (PBLG-b-HYA)
hyaluronan-block- poly(γ-benzyl glutamate) copolymers PBLG-b-HYA

2. OBJECTIVES

In this chapter we aim to investigate the functionality and drug delivery capability of mucus-penetrating polymersomes formulations and explore their anti-tumor efficacy. In parallel, in vitro cytotoxicity tests with whole sample. Such experiments were promoted in order to confirm in vitro results and demonstrate the enhanced ability of polymersomes to be used as mucus penetrating nano-carrier for disease treatment.

3. EXPERIMENTAL METHODS

3.1 **Materials.**

We used the block copolymer PEG5,000-b-PLA10,000 (Polysciences, cat. 25018), DPPC (1,2-dihexadecanoyl-sn-glycero-3-phosphoethanolamine, Avanti Polar Lipids), for polymersome production. All used solvents were aquired from Sigma, unless otherwise stated.

3.2 PEG-PLA polymersomes preparation by film hydration method.

Nano-sized polymersomes were synthesized according to a standard film hydration procedure. Briefly, for the synthesis of PEG(5,000)-b-PLA(10,000), 1-10 mg of the copolymer is added to a round bottle glass tube together with a dye when needed (10 µL of a 0.5 $mg.mL^{-1}$ DHPE-Rh solution in chloroform). This mixture is dried either under N_2 gas flow gently perturbing the fluid surface or by slow rota-evaporation. After evaporation, the copolymer forms a nice, colored layer covering the bottom of the glass tube. At this step, the block copolymer is likely organized forming a lamellar phase. The film is hydrated by adding 1 mL of PBS 1 × and left overnight at 50 °C under continuous stirring. Same procedure was performed for DPPC-liposomal formulation production. DOX-loaded samples were prepared by adding DOX during the hydration step, during vesicle assembly.

Resizing by probe-sonication. After hydration, the whole sample was transferred to an eppendorff tube and sonicated using probe-sonicator (30 s on, 30 s off for 2.5 min at 20% amplitude under ice bath). After production, polymersomes are stored in a glass vial at 4 °C.

3.3 Characterization techniques.

Dinamic Light Scattering (DLS). DLS analyses were carried out using a laser particle analyzer (NanoPlus, Particulate System) using software CONTIN as calculation method, after 20 × (v/v) dilution in water. DLS measurements were based on 3-5 repetitions of 70 accumulation times. Samples were analyzed at 25 °C with a scattering angle of 165° and at 660 nm HeNe laser based on a dispersant refractive index (RI) of 1.33, a viscosity of 0.89 and a dielectric constant of 78.3. The samples were also characterized for surface charge by determining their ζ-potential using Zeta potential Analyzer (NanoPlus, Particulate System) based on 3 repetitions of 5 accumulation times, 70 cell constant. Cell positions 0.70/0.35/0.00/-0.35/-0.70 at a fixed voltage of 60 V, and a constant current of 51 mA, software Smoluchowski as calculation method and using the same dispersant from size analyses.

Negative Staining Transmission Electron Microscopy (NS-TEM). Polymersomes were prepared as described above and analyzed by conventional transmission electron microscopy using a FEI Tecnai G20 electron microscope (FEI Company, EUA), operating at 200 kV. For conventional TEM imaging all analyses were carried out with dried samples, using 300 mesh copper grids (Koch Electron Microscopy, São Paulo, Brazil) covered with Formvar (Sigma Aldrich) followed by nanoparticle spotting, negative staining with 2 wt% phosphotungstic acid and proper wash before analysis. The grid preparation is a critical step to enable visualization by TEM, and for that reason, the same protocol was repeated for all samples, diminishing problems related to it.

DOX in vitro release. The amount of drug released from xxx using dialysis. Briefly, the absorbance of DOX in the solution was determined using the UV–Vis

spectrophotometer at 480 nm, and DOX content was calculated using the calibration line of DOX in PBS (pH 7.4).
The amount of drug encapsulated was calculated from the measurement of the residual drug inside and outside the dialysis bag.

Differential Scanning Calorimetry (DSC) analysis. Possible drug-polymer interaction(s) and the physical changes that may be occurred in the samples can be studied using the thermal analysis. DSC analysis was carried out on pure drug, drug-polymer bulk and pure polymer, using a equipment model DSC 822e/700 (Mettler Toledo). Samples were heated at a rate of 10 $^{o}C.min^{-1}$ and the data were recorded from 20 ^{o}C to 150 ^{o}C.

3.4 Biological acessment

Cell line and culture conditions. B16-F10 murine melanoma cells were routinely cultured in complete DMEN medium containing 10 % (V/V) fetal bovine serum. All experiments were performed using the cells within 3 successive passages. The cells were seeded into 75 cm^2 culture flask (106 cell per flask) in 10mL of culture medium.

In vitro cytotoxicity experiments. *In vitro* cytotoxicity was evaluated for Free-DOX, Lipo-DOX, Poly-DOX and Poly (negative control) in B16F10 murine melanoma. Around 80% confluent cells were harvested and seeded onto 96 well tissue culture plates at a density of 10^4 cells per well and incubated for 24 h in saturated humid conditions at 5% CO_2 and 37^{o}C. Spent medium was then replaced by fresh medium containing formulations with graded concentrations of DOX ranging from 0.75-90.5 μM, and plates were further incubated for 48 h. Cells treated with medium only served as viability control. At the end, mitochondrial activity was measured by MTT assay.

In vivo experiments - B16-F10 metastatic lung cancer mice induction and treatment with free-DOX, Poly-DOX, Lipo-DOX and controls. All the experiments were performed with the approval of the Institute of Biomedical Sciences

Ethics Committee, from University of São Paulo, (CEUA-ICB/USP), under the protocol number 70/2017. Treatment Schedule. Animals were divided into 5 groups, with 4 mice total/group. Group 1 was kept as normal control and Group 2, 3, 4, 5 were injected with $1x10^4$ B16-F10 melanoma cells (per mice) intravenous by tail vein on day zero. The free-DOX was administered in Group 3, Lipo-DOX in Group 4 and Poly-DOX in Group 5 at the dose of 1 $mg.kg^{-1}$. The schedule was start the treatment 5 days after melanoma injection and make the first treatment with 30 μL of 1$mg.mL^{-1}$ DOX formulations followed by other 3 doses with 7-day waiting period totalizing 90 μg DOX/animal. Group 2 served as experimental control without DOX treatment, and PBS buffer was used as control formulation. Mice in all groups were sacrificed 2 days after the experimental schedule.

Mice lung biodistribution in vivo. To investigate the lung biodistribution of PEG-b-PLA polymersomes and compare them to PS particles, 30 μL samples were intranasal injected, having standadized fluorecence intensities. All the experiments were performed with the approval of the Institute of Biomedical Sciences Ethics Committee, from University of São Paulo, (CEUA-ICB/USP), under the protocol number 70/2017. After 2 hours of treatment, euthanasia was performed and lungs were excised, frozen and analyzed.

*Cryo-microtome, histological assessment and confocal microscopy***.** Samples immersed, immediately after excision, in Neg-50™ Frozen Section Medium (Thermo Scientific). NEG-tissue blocks were cut to 15-50 μm thickness using a microtome (Thermo Scientific™ HM525 NX Cryostat) and stained with Fast Panoptic LB Kit (Centerlab), for conventional microscope observation. The isolated epithelia and lung were also examined without staining to assure the presence of tested particles in the sample and by light microscopy. High-resolution confocal imaging was promoted using a 5× and 10× dry objective on a confocal microscope (Leica), using 480 nm laser intensity. Images were processed using ImageJ.

Statistical Analysis. Using Origin Software, One-Way ANOVA test was used to compare formulations in the treatment of B16-F10 murine lung metastasis. Statistical significance was determined using $p<0.05$.

4. RESULTS AND DISCUSSION

4.1 Poly-DOX preparation and in vitro release

The production methodology used for DOX loading was performed by the top-down approach, which means that the drug was added to the polymeric system wile structures were been formed, i.e. during film hydration. This strategy was chosen based on the fact that production method that relies on organic solvents is less desirable while developing pharmaceutical formulations.

Notably, modifications on the expected particles morphology were herein detected when these polymer films are rehydrated in the presence of DOX. According to the micrographs shown in Figure 48, both vesicles and tubular structures were produced. Moreover, the amount of bulk produced in the drug-loaded sample was greater in comparison to unloaded one. For that reason, we believe that the ionized amine groups of DOX (pKa=8.2) in neutral condition can electrostatic interact with the glycol hydrophilic portion of the polymer, increasing the hydrophilic fraction (f) of the polymeric molecule. Thus, the interaction of the former with the block co-polymer could favor the formation of other morphologies.

Table 9 Synthesis and characterization of PEG-PLA polymersomes

Entry	Production technique	Drug load	Size[a] (nm)	PDI[a]	Size[b] (nm)	Morphology
1	film hydration	-	198.5	0.263	~55	vesicles
2	film hydration	DOX	208.6	0.287	~45	vesicles + rods

[a]measured by DLS. [b]measured by TEM micrograph analysis.

Figure 48 – Poly-DOX formulation. A. NS-TEM micrographs of Poly-DOX polymersomes with *62 kx and ***100 kx magnification after extrusion (0.2 µm). B. DLS distribution, and C.Commonly obtained zeta potential for the Poly-DOX formulation.

A

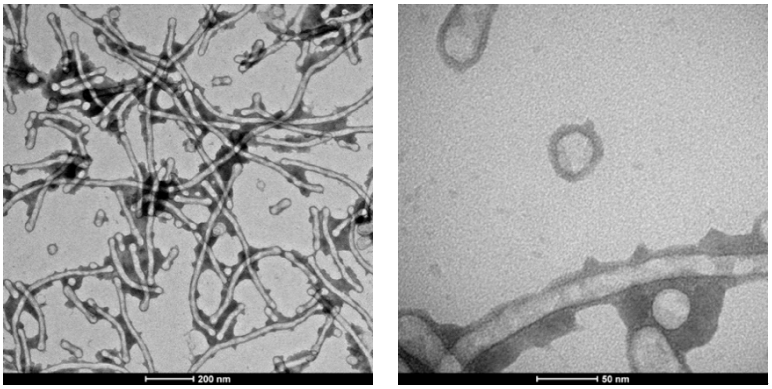

B

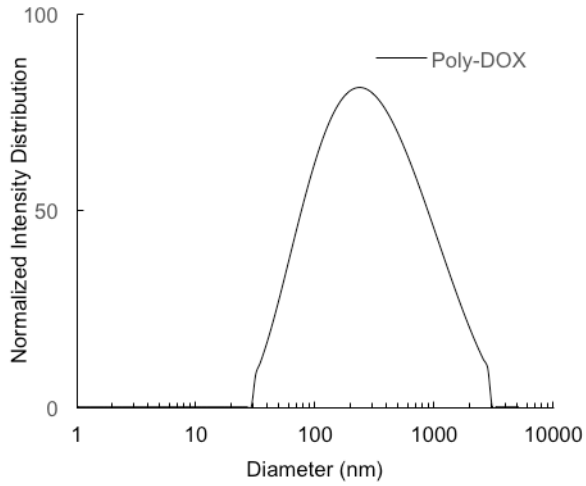

C

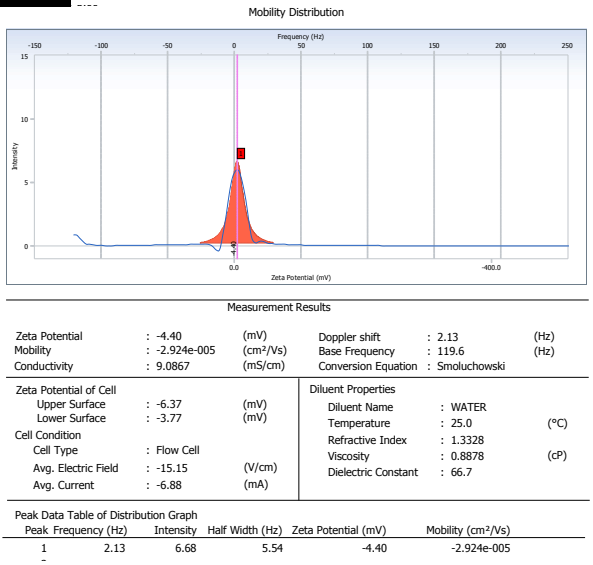

Source: Beatriz N. M. Miranda

Moreover, the strong electrostatic interactions between DOX and pluronic-based co-polymer systems were previously reported.[156–158] Even though here we dont have COOH or SO_3^- moieties in the hydrophilic portion, the hydrolysis of PLA originates carboxilic acid, as previously discussed in Chapters 2-3, which may be influencing the formation of such complex. Another explanation could be that the anthraquinone lipophilic moietie of the drug entangles among the hydrophobic polymer chains, aggregating within the membrane instead of localized in the vesicle core. Once and for all we undertand why most of the reports in the literature use a bottom up approach for DOX loading, i.e. either form the vesicle by film hydration and then use remote transmembrane loading procedures (such as pH swich) to induce DOX loading or use other production method such as nanoprecipitation or

solvent swich, as vastly shown in Table 8. Such approaches, as claimed by the literature, would increase final DOX loading in polymersomes as well as encapsulation efficiency; besides prevent that the DOX loading interfeer in the self-assemble process. At the same time, the same way that a cargo permeates through the membrane for loading issues, it should also be readly release.[40] pH-related strategies also include the increase in the systems pH above the DOX pKa to improve the loading capacity of the carrier by decreasing the solubility of the drug.[53,148]

Ahmed and coworkers, 2006 also observed the presence of other morphologies in the PEG-PLA/PEG-PBD (PEG-butadiene) polymersomal-DOX system, which they claim to be due hydrolysis of PLA in the core of vesicles.[150] This polymer-drug interaction will be further discussed; meanwhile, to better explore these hypothesis, initial thermal analysis were performed.

Figure 49 – Thermograms of the 1st heat of PEG-PLA (black), PEG-PLA+DOX (green), and DOX (red). Signs of PEG-PLA decomposition observed at ~50 ^{o}C, and for PEG-PLA+DOX at ~116 ^{o}C.

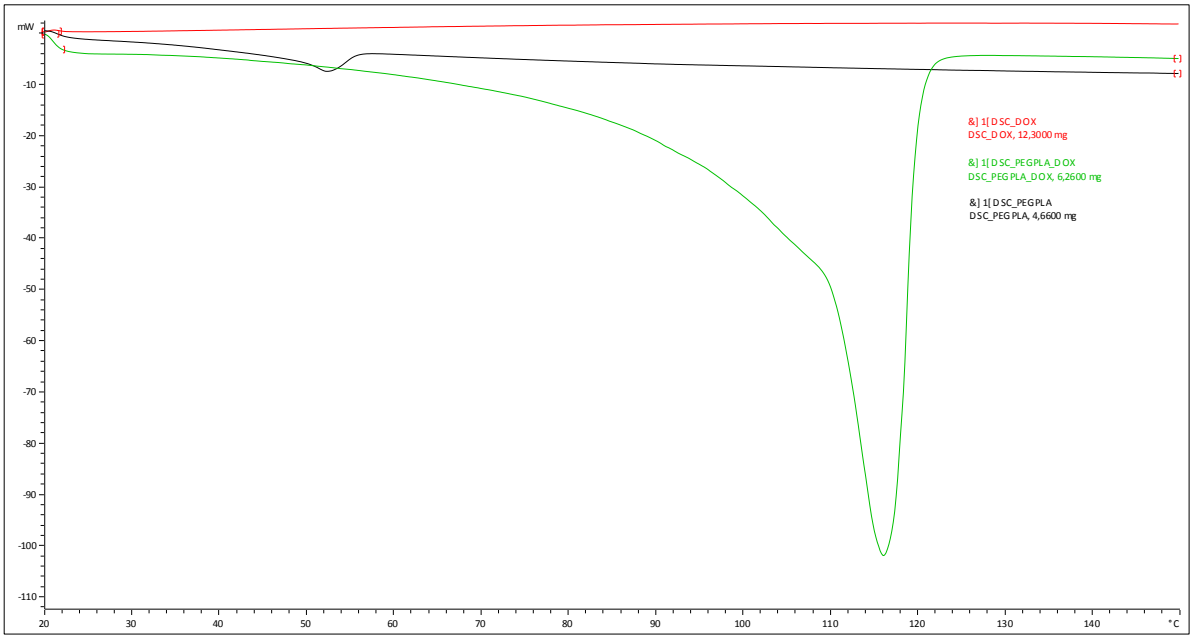

Source: Beatriz N. M. Miranda

After DSC scans, the thermogram for the 1st sample heat is shown in Figure 50. Even though the Tg temperature was not well determined using this heating program, signs of a shift in an endothermic peak at ~50 ^{o}C to ~116 ^{o}C was

observed, indicative of pure polymer and PEG-PLA+DOX decomposition, respectively. This observation most likely indicates the interaction between the drug and the polymer. Doxorubicin's melting point is 250 ^{o}C, which was not covered in this program. Further, additional runs with broader temperature ranges should provide us more insignts such as if there is any change is DOX thermal properties. Still, these preliminary results once again indicates the apparent interaction between the drug and the polymer.

Figure 50 – Poly-DOX formulation. A. NS-TEM micrograph 100 K× after dialysis experiment, scale bar 50 nm. B. In vitro release behavior of DOX from POLY-DOX at PBS (pH 7.2). Data represent mean ±SD (n=2). The data points are average of at least three experiments. Bars represent the range over which the values were observed.

A

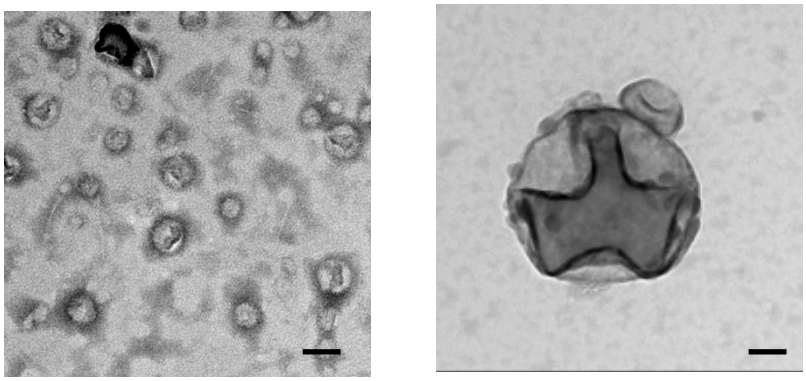

B

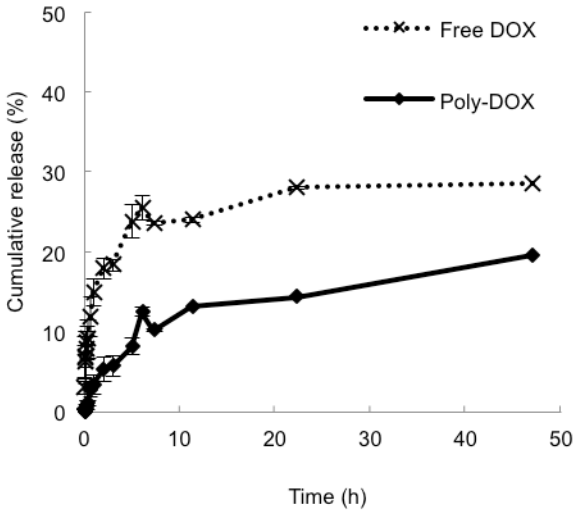

Source: Beatriz N. M. Miranda

Drug-releasing studies were still promoted by dyalisis and NS-TEM characterization of the inner content revealed the clearly existance of vesicles in the system, as shown in Figure 50 A. Drug release studies demonstrated that Free DOX release was accelerated in comparison to Poly-DOX, in physiological pH, 37^{o}C, as shown in Figure 50 B. DOX was released from polymersomes following first order kinetics. At this point, the a pH-dependent release was not evaluated, but according to what was previously observed by confocal for microsized polymersomes, described in Chapter 2, it is thought that a faster release profile should be observed in our system, hypothesized to be due PLA hydrolysis. Figure 50 shows an initial drug burst release at physiological pH, followed by extended release release rate than the free drug, which is thought to be caused by transmembrane diffusion, i.e., permeation. The controled DOX release profile observed in vitro for our Poly-DOX formulation is in accordance to the literature as well as release liposomal profiles, delivering less than 20 % of the drug after 50 h.[40,147,159]

Since unencapsulated drug was not removed the encapsulation efficiency was not established. The use of SEC as a method to quantify the amount of encapsulated was tested, although owing to the amount of drug-polymer aggregation, specially after stocking in colder teperatures (as well as speed-vaccum procedure) and therefore low amount of vesicles in solution, the diluted sample could not be analyzed by this mean.

Owing to their potential as drug delivery, the in vitro effect of freshly prepared Poly-DOX was promoted in comparison to lipo-DOX formulation as well as the free drug.

4.2 In vitro cytotoxicity experiments

Therefore, we studied dose dependency of biocompatibility and cell killing efficiency of the polymersome *in vitro*. As shown in Figure 51, cell viability remained greater than 90% even at high polymersome concentration, for B16-F10 murine cancer cells. These cytotoxicity studies revealed that free DOX was more potent than both PolyDOX and Lipo-DOX formulations, with IC_{50} (inhibitory concentration to produce 50% cell death) what could be attributed to delayed DOX release when

encapsulated. Therefore, free DOX was more toxic than liposomal and polymersomal formulations at the same drug concentration, while the blank polmersomes showed no cytotoxic effect up to the tested concentration. Our results are in accordance to the literature and explained by the fact that free DOX rapidly accumulated in nucleus, while the encapsulated drug is released from cytosolic compartments in a controlled manner. [140,154]

Figure 51 – Relative viabilities of B16-F10 murine tumor cells exposed to Free-DOX, polymersomes and Poly-DOX. Data are represented as mean±SE of six wells per group.

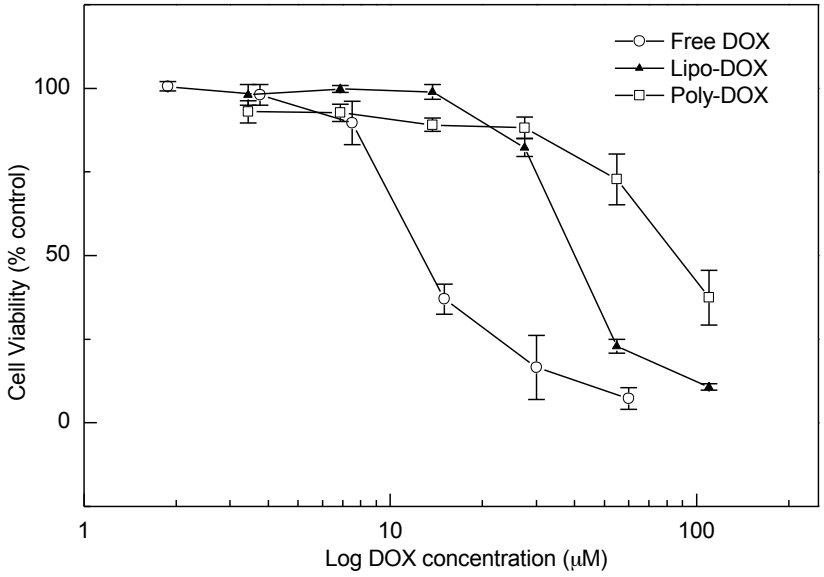

Source: Beatriz N. M. Miranda

4.3 Biodistribution tests

Having polymersomes shown potential regarding safety over the free DOX, a first strategy tested regarding pulmonary delivery was to understand if these nanoencapsulated systems would reach their site of action, therefore the lung. To explore the biodistribution of liposomes and polymersomes, a single dose of Poly-Rhod, Lipo-Rhod in 30 μL PBS was administrated intranasaly into mice. At 2 h post injection, the treated mice were were sacrificed and frozen at −20 ^{o}C for further

analysis. After sample preparation using a cryomicrotome, fluorescence images were acquired using confocal microscopy.

Figure 52 – In vivo distribution of Polymersomes and Liposomes formulations in mice lung. Photomicrographs show localization of fluorescent (red) in sections of bronchioles and alveolar ducts. Negative sample was used to remove backgoud noize. The images reported in the figure are representative of 2 slides per animal; containing at least 3 sections (2 animals per group), scale 50 μm.

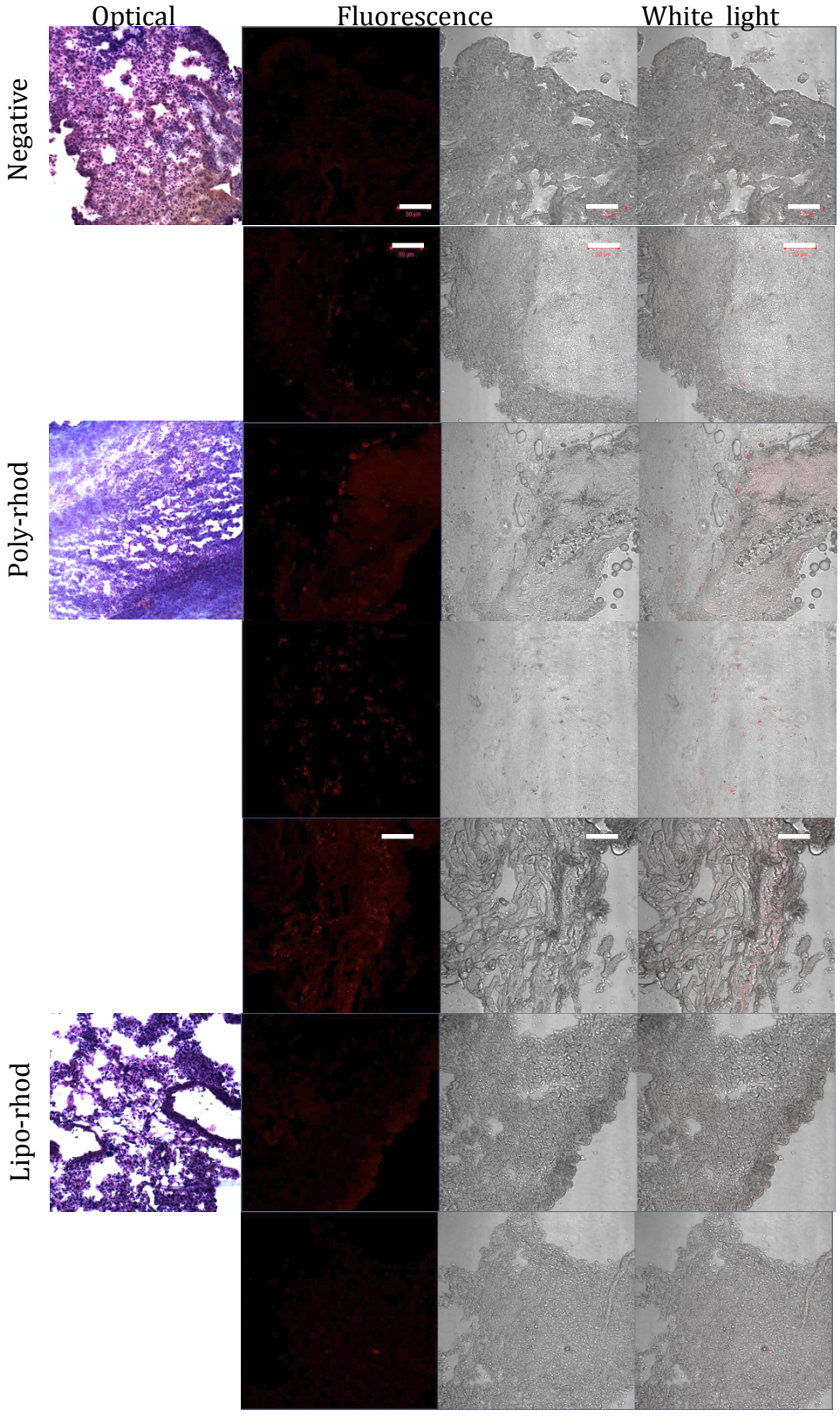

Source: Beatriz N. M. Miranda

The results indicate that most liposomes were co-localized with airway tubes or blood vessels, while polymersomes were more evenly distributed over the samples, as shown in Figure 52.

4.4 In vivo anti-cancer tests

We further investigated the *in vivo* tumor treatment efficacy of Lipo-DOX, Poly-DOX formulations and free drug in mice B16-F10 lung metastasis by tail injection of cancer cells and nasal formulation injection. At 5 days post-tumor injection, the animals were treated with correlating amount of drug. One group was kept as positive and the other as negative controls. After finishing the treatment schedule, euthanasia was promoted and lung was extracted. Lung tumor sites were counted (as the sample shown in Figure 53 B) randomly and undisclosed, and data was plotted, Figure 53 A. Interesting information can be taken from analyzing Figure 53, Poly-DOX was more effictive than the liposomal drug formulation and the free drug. Even though statilstical analysis demonstrates that Poly-DOX treatment is significantly different from Free-DOX and Lipo-DOX ($p<0.05$), although no statistically difference was observed when compared to positive control samples. Noteworthy to say that some unexpected issues regarding the mortality of tumor bearing mice were encontered in our experiment, 2 animals for the positive control were dead before the last treatment schedule, while Poly-DOX and Lipo-DOX groups had 1 animal dead in each group. Therefore, further analyses are needed to assure the antitumor activity of the Poly-DOX.

Figure 53 – Treatment of B16-F10 murine lung metastasis. (A). Number of tumor spots per animal found for each group and (B) sample of spots found in mouse lung. Statistical analysis was performed by One-way ANOVA, $p < 0.05$.

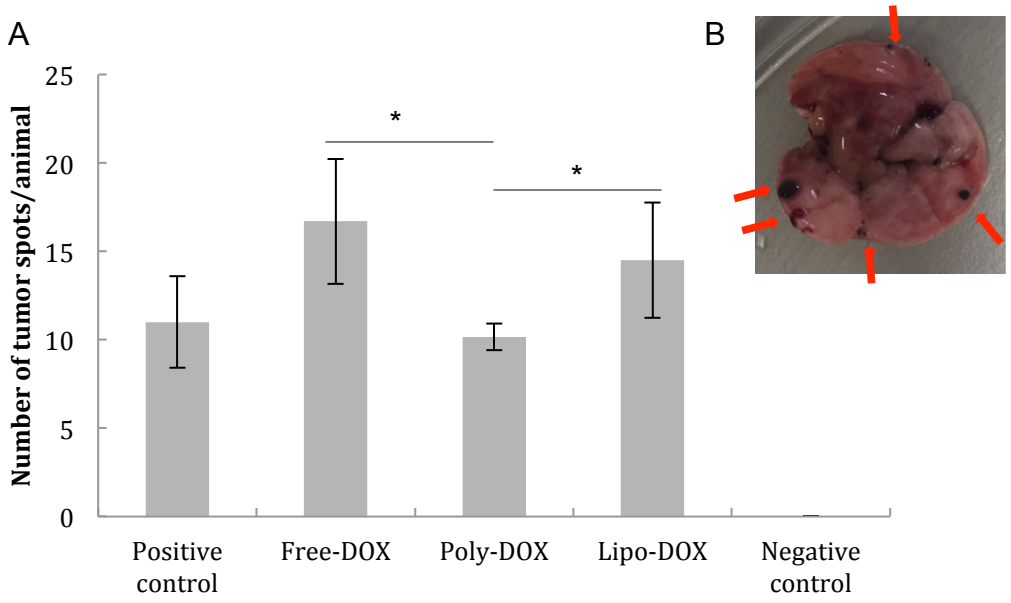

*Significant difference for $p<0.05$

Source: Beatriz N. M. Miranda

5. Conclusion and Remarks

We developed a robust platform for mucosal drug delivery based on pH-sensitive polymersomes. As shown in *ex-vivo* experiments as well, a prominent advantage of this platform over mucus-penetrating nanoparticles is its weaker interaction with the mucus mesh, which imparted by the highly dense PEG outer layer of the polymersome membrane. Another main benefit comes from the hollow structure of the polymersomes; unlike solid particles, these contain an aqueous core that can be loaded with cargo. Furthermore, the cargo can be controllably released using an external trigger. In particular, the PLA core of these polymersomes is designed to respond to acidic pH environments, such as solid tumors. This characteristic was employed to treat locally B16-F10 murine lung metastasis and polymersomes proving to be an important drug delivery carrier. These advantages, their biocompatibility and their ease of fabrication make them

excellent candidates for clinical management of different diseases, including cancers. The effect of the DOX loading in the mucus-penetration capability should still be addresed. An extensive encapsulation efficiency discussion regarding the characteristic of the encapsulated drug should also be followed, as initial thermogravimetric experiments already suggests drug-polymer interaction. Therefore, forther studies should help us determine by the specific thermal properties of the drug such as Doxorubicin in its original (crystalline) form or encapsulated within the polymersome and their interaction that may be interfering in the self-assembly process. Further enhancement of this platform including drug loading and active delivery will further overcome challenges encountered for the trans-mucus drug delivery, enabling locally administration, decreasing side effects and enhancing drug effectiveness.

Still, based on previous experiments, this platform would offer an ease of fabrication, a core-shell robust platform for mucosal drug delivery based on polymersomes.

CHAPTER 7

Final conclusion and outlook

1. Conclusion and Outlook

In conclusion, block copolymers were self-assembled into polymersomes of different size regimes, either by film hydration or by employing a microfluidic approach. Using the microfluidic-produced polymersomes, the drug release was studied after a pH change, indicating that the release is most likely driven by the hydrolysis of the ester groups from PLA. Downstream techniques were employed to achieve relevant size and morphology to the desired application, as mucus penetrating particles. Since these polymersomes exhibit a hindered surface carrying glycol groups, regardless of the need of coating process.

Looking forward to industrial polymersome production, low-energy production method based on the use water-soluble organic solvents were tested and demonstrated its potential. Scale-up experiments should still be promoted and should support the polymersome use in clinical trials.

By changing the membrane composition, we observed that the chemical stability of the vesicle, under acidic conditions, can also be tunned. The addequate membrane polymer composition should provide greater efficiency in vesicle production as well as higher amount of hydrophilic cargo, as our results related to blended PEG-PLA/Soluplus® polymersomes provided promissing results. Further studies related to the dynamical process of cargo reallocation from inside to outside the vesicles may be promoted to monitor its distribution kinetics, since dilution is frequently resulted after in vivo applications. Downstream techniques should still be promoted for blended systems, as well as mucus-penetration, but we antecipate that the preservation of the PEG surface should provide similar results from pure PEG-PLA polymersomes.

Mucosal entrapment was less acentuated for polymersomes than conventional uncoated particles, what contributes permeation capability and locally delivering drugs, as observed by particle tracking experiments as well as biodistribution tests. Moreover, preliminary in vivo results for the local treatment of B16-F10 murine lung metastasis using DOX-loaded polymersomes demonstrated

promissing results when compared to the liposomal formulation and free drug. The effect of the DOX loading in the mucus-penetration capability should still be addressed. Advantages related to the vesicle structure come from the existance of an aqueous core that enables the loadeding of hydrophilic cargo, while hydrophobic molecules can be loaded within the membrane. These advantages, their biocompatibility and their ease of fabrication make them excellent candidates for clinical management of different diseases, including cystic fibrosis and cancers. To our knowledge, this is the first report of the application of polymersome structure as a trans-mucosal drug delivery carrier. Further enhancement of this platform including drug loading and active delivery will further overcome challenges encountered for the trans-mucus drug delivery, enabling locally administration, decreasing side effects and enhancing drug effectiveness.

REFERENCES

1. Schultsz, C., Van den Berg, F. M., Kate, F. W. T., Tytgat, G. N. J. & Dankert, J. The intestinal mucus layer from patients with inflammatory bowel disease harbors high numbers of bacteria compared with controls. *Gastroenterology* **117,** 1089–1097 (1999).
2. Bansil, R., Celli, J. P., Hardcastle, J. M. & Turner, B. S. The influence of mucus microstructure and rheology in Helicobacter pylori infection. *Front. Immunol.* **4,** 1–12 (2013).
3. Ensign, L. M., Cone, R. & Hanes, J. Nanoparticle-based drug delivery to the vagina: A review. *J. Control. Release* **190,** 500–514 (2014).
4. Hollingsworth, M. A. & Swanson, B. J. Mucins in cancer: protection and control of the cell surface. *Nat. Rev. Cancer* **4,** 45–60 (2004).
5. Boegh, M. & Nielsen, H. M. Mucus as a Barrier to Drug Delivery - Understanding and Mimicking the Barrier Properties. *Basic Clin. Pharmacol. Toxicol.* (2015). doi:10.1111/bcpt.12342
6. Bansil, R. & Turner, B. S. Mucin structure, aggregation, physiological functions and biomedical applications. *Curr. Opin. Colloid Interface Sci.* **11,** 164–170 (2006).
7. Cornelis, G. R. *et al.* Colorectal Cancer in Mice Genetically Deficient in the Mucin Muc2. **1322,** 1–5 (2001).
8. Shibahara, H. *et al.* Pathobiological implications of mucin (MUC) expression in the outcome of small bowel cancer. *PLoS One* **9,** 1–8 (2014).
9. Williams, S. J. *et al.* Two novel mucin genes down-regulated in colorectal cancer identified by differential display. *Cancer Res.* **59,** 4083–4089 (1999).
10. Qingguo Xu, Laura M. Ensign, Nicholas J. Boylan, Arne Scho, Xiaoqun Gong, Jeh-Chang Yang, Nicholas W. Lamb, Shutian Cai, Ta o Yu ,X, Ernesto Freire, and J. H. Impact of Surface Polyethylene Glycol (PEG) Density on Biodegradable Nanoparticle Transport in Mucus ex Vivoand Distributionin Vivo. *ACSNano* **9,** 9217–9227 (2015).
11. Juhie Bhatia. New model tackles sticky problem of getting drugs past mucus. **21,** 301 (2015).
12. Lai, S. K., Wang, Y. Y., Wirtz, D. & Hanes, J. Micro- and macrorheology of mucus. *Adv. Drug Deliv. Rev.* **61,** 86–100 (2009).

13. Cone, R. a. Barrier properties of mucus. *Adv. Drug Deliv. Rev.* **61,** 75–85 (2009).
14. Min Liu, Jian Zhang, Wei Shan & Yuan Huang. Developments of mucus penetrating nanoparticles. *Asian J. Pharm. Sci.* **10,** 275–282 (2015).
15. Hanes, J., Dawson, M. R., Wirtz, D., Fu, J. & Krauland, E. M. Drugs and gene carrier particles that rapidly move through mucous barriers. (2005).
16. Wang, Y.-Y. *et al.* Addressing the PEG Mucoadhesivity Paradox to Engineer Nanoparticles that “Slip” through the Human Mucus Barrier. *Angew Chem Int Ed* **47,** 9726–9729 (2008).
17. Tang, B. C. *et al.* Biodegradable polymer nanoparticles that rapidly penetrate the human mucus barrier. *Proc. Natl. Acad. Sci. U. S. A.* **106,** 19268–19273 (2009).
18. Lai, S. K. *et al.* Rapid transport of large polymeric nanoparticles in fresh undiluted human mucus. *Proc. Natl. Acad. Sci. U. S. A.* **104,** 1482–1487 (2007).
19. Yang, M. *et al.* Nanoparticle penetration of human cervicovaginal mucus: The effect of polyvinyl alcohol. *J. Control. Release* **192,** 202–208 (2014).
20. Shum, H. C., Kim, J.-W. & Weitz, D. a. Microfluidic fabrication of monodisperse biocompatible and biodegradable polymersomes with controlled permeability. *J. Am. Chem. Soc.* **130,** 9543–9 (2008).
21. Du, J. Z., Mao, C. Q., Yuan, Y. Y., Yang, X. Z. & Wang, J. Tumor extracellular acidity-activated nanoparticles as drug delivery systems for enhanced cancer therapy. *Biotechnol. Adv.* **32,** 789–803 (2014).
22. Liu, J. *et al.* pH-Sensitive nano-systems for drug delivery in cancer therapy. *Biotechnol. Adv.* **32,** 693–710 (2014).
23. Yu, S., Azzam, T., Rouiller, I. & Eisenberg, A. “Breathing” vesicles. *J. Am. Chem. Soc.* **131,** 10557–10566 (2009).
24. Chen, W., Meng, F., Cheng, R. & Zhong, Z. pH-Sensitive degradable polymersomes for triggered release of anticancer drugs: A comparative study with micelles. *J. Control. Release* **142,** 40–46 (2010).
25. Lomas, H. *et al.* Biomimetic pH sensitive polymersomes for efficient DNA encapsulation and delivery. *Adv. Mater.* **19,** 4238–4243 (2007).
26. Lee, J. S. & Feijen, J. Polymersomes for drug delivery: Design, formation and

characterization. *J. Control. Release* **161,** 473–483 (2012).

27. Couvreur, P. Nanoparticles in drug delivery: Past, present and future. *Adv. Drug Deliv. Rev.* **65,** 21–23 (2013).
28. Cho, K., Wang, X., Nie, S., Chen, Z. & Shin, D. M. Therapeutic nanoparticles for drug delivery in cancer. *Clin. Cancer Res.* **14,** 1310–1316 (2008).
29. Torchilin, V. Tumor delivery of macromolecular drugs based on the EPR effect. *Adv. Drug Deliv. Rev.* **63,** 131–135 (2011).
30. Allen, T. M. Liposomal Drug Formulations. *Drugs* **56,** 747–756 (1998).
31. McNeil, S. E. Nanoparticle therapeutics: A personal perspective. *Wiley Interdiscip. Rev. Nanomedicine Nanobiotechnology* **1,** 264–271 (2009).
32. Jatzkewitz, H. An ein kolloidales Blutplasma-Ersatzmittel (Polyvinylpyrrolidon) gebundenes Peptamin (Glycyl-L-leucyl-mezcalin) als neuartige Depotform für biologisch aktive primäre Amine (Mezcalin). *Zeitschrift fur Naturforsch. - Sect. B J. Chem. Sci.* **10,** 27–31 (1955).
33. Petros, R. a & DeSimone, J. M. Strategies in the design of nanoparticles for therapeutic applications. *Nat. Rev. Drug Discov.* **9,** 615–627 (2010).
34. Nicolas, J., Mura, S., Brambilla, D., Mackiewicz, N. & Couvreur, P. Design, functionalization strategies and biomedical applications of targeted biodegradable/biocompatible polymer-based nanocarriers for drug delivery. *Chem. Soc. Rev.* **42,** 1147–235 (2013).
35. Mai, Y. & Eisenberg, A. Self-assembly of block copolymers. *Chem. Soc. Rev.* **41,** 5969 (2012).
36. Discher, B. M. *et al.* Polymersomes: Tough vesicles made from diblock copolymers. *Science (80-.).* **284,** 1143–1146 (1999).
37. Discher, D. E. & Eisenberg, A. Polymer vesicles. *Science* **297,** 967–973 (2002).
38. Discher, D. E. & Ahmed, F. Polymersomes. *Annu. Rev. Biomed. Eng.* **8,** 323–41 (2006).
39. Meng, F., Zhong, Z. & Feijen, J. Stimuli-responsive polymersomes for programmed drug delivery. *Biomacromolecules* **10,** 197–209 (2009).
40. Ahmed, F. & Discher, D. E. Self-porating polymersomes of PEG-PLA and PEG-PCL: Hydrolysis-triggered controlled release vesicles. *J. Control. Release* **96,** 37–53 (2004).

41. Ahmed, F. *et al.* Shrinkage of a rapidly growing tumor by drug-loaded polymersomes: pH-triggered release through copolymer degradation. *Mol. Pharm.* **3,** 340–350 (2006).
42. Christian, D. a. *et al*. Polymersome carriers: From self-assembly to siRNA and protein therapeutics. *Eur. J. Pharm. Biopharm.* **71,** 463–474 (2009).
43. Lee, J. S. *et al.* Circulation kinetics and biodistribution of dual-labeled polymersomes with modulated surface charge in tumor-bearing mice: Comparison with stealth liposomes. *J. Control. Release* **155,** 282–288 (2011).
44. Discher, D. E. & Eisenberg, A. Polymer vesicles. *Sceince, Polym.* **297,** 967–973 (2002).
45. Ahmed, F., Photos, P. J. & Discher, D. E. Polymersomes as Viral Capsid Mimics. *Drug Dev. Res.* **67,** 4–14 (2006).
46. Christian, D., Cai, S., Photos, P. & Ahmed, F. Molecular Dynamics to Shrinkage of Tumors. **32,** 838–857 (2014).
47. Hocine, S. & Li, M.-H. Thermoresponsive self-assembled polymer colloids in water. *Soft Matter* **9,** 5839 (2013).
48. Cho, H. K., Cheong, I. W., Lee, J. M. & Kim, J. H. Polymeric nanoparticles, micelles and polymersomes from amphiphilic block copolymer. *Korean J. Chem. Eng.* **27,** 731–740 (2010).
49. Shum, H. C., Kim, J.-W. & Weitz, D. A. Microfluidic Fabrication of Monodisperse Biocompatible and Biodegradable Polymersomes with Controlled Permeability. *J. Am. Chem. Soc.* **130,** 9543–9549 (2008).
50. Shih, C. A Graphical Method for the Determination of the Mode of Hydrolysis of Biodegradable Polymers. *Pharm. Res. An Off. J. Am. Assoc. Pharm. Sci.* **12,** 2036–2040 (1995).
51. Meng, F. H., Hiemstra, C., Engbers, G. H. M. & Feijen, J. Biodegradable polymersomes. *Macromolecules* **36,** 3004–3006 (2003).
52. Discher, B. M. *et al.* Polymersomes: Tough vesicles made from diblock copolymers. *Science (80-.).* **284,** 1143–1146 (1999).
53. Ayen, W. Y., Garkhal, K. & Kumar, N. Doxorubicin-loaded $(PEG)_3$-PLA nanopolymersomes: effect of solvents and process parameters on formulation development and in vitro study. *Mol. Pharm.* **8,** 466–78 (2011).
54. Meng, F. *Artificial Cells Based on Biodegradable Polymersomes*. *Thesis*

(2003).

55. Nahire, R. *et al.* Multifunctional polymersomes for cytosolic delivery of gemcitabine and doxorubicin to cancer cells. *Biomaterials* **35,** 6482–6497 (2014).
56. Kita-Tokarczyk, K., Grumelard, J., Haefele, T. & Meier, W. Block copolymer vesicles - Using concepts from polymer chemistry to mimic biomembranes. *Polymer (Guildf).* **46,** 3540–3563 (2005).
57. Battaglia, G. & Ryan, A. J. Pathways of polymeric vesicle formation. *J. Phys. Chem. B* **110,** 10272–10279 (2006).
58. Tyrrell, Z. L., Shen, Y. & Radosz, M. Fabrication of micellar nanoparticles for drug delivery through the self-assembly of block copolymers. *Prog. Polym. Sci.* **35,** 1128–1143 (2010).
59. Hayward, R. C., Utada, A. S., Dan, N. & Weitz, D. a. Dewetting instability during the formation of polymersomes from block-copolymer-stabilized double emulsions. *Langmuir* **22,** 4457–61 (2006).
60. Shum, H. C. *et al.* Dewetting-induced membrane formation by adhesion of amphiphile-laden interfaces. *J. Am. Chem. Soc.* **133,** 4420–4426 (2011).
61. Shum, H. C., Zhao, Y., Kim, S.-H. & Weitz, D. a. Multicompartment polymersomes from double emulsions. *Angew. Chem. Int. Ed. Engl.* **50,** 1648–51 (2011).
62. Cone, R. A. Barrier properties of mucus ☆. *Adv. Drug Deliv. Rev.* **61,** 75–85 (2008).
63. Duncanson, W. J. *et al.* Microfluidic Fabrication of Perfluorohexane-Shelled Double Emulsions for Controlled Loading and Acoustic-Triggered Release of Hydrophilic Agents. (2014). doi:10.1021/la502473w
64. Amstad, E., Kim, S.-H. & Weitz, D. a. Photo- and thermoresponsive polymersomes for triggered release. *Angew. Chem. Int. Ed. Engl.* **51,** 12499–503 (2012).
65. Arriaga, L. R. *et al.* Ultrathin Shell Double Emulsion Templated Giant Unilamellar Lipid Vesicles with Controlled Microdomain Formation. *Small* 1–7 (2013). doi:10.1002/smll.201301904
66. Tuguntaev, R. G. *et al.* Nanoscale Polymersomes as Anti-Cancer Drug Carriers Applied for Pharmaceutical Delivery. 2857–2865 (2016).

67. Chierico, L. Polymersomes mediated intracellular delivery of antibodies: implication in anticancer therapy. (University College London, 2015).
68. Malvern. Dynamic Light Scattering. (2016). Available at: http://www.malvern.com/en/products/technology/dynamic-light-scattering/.
69. Instruments, M. Zeta potential: An Introduction in 30 minutes. *Zetasizer Nano Serles Technical Note. MRK654-01* **2,** 1–6 (2011).
70. Kim, S.-H., Kim, J. W., Cho, J.-C. & Weitz, D. a. Double-emulsion drops with ultra-thin shells for capsule templates. *Lab Chip* **11,** 3162–6 (2011).
71. Robertson, J. D. *et al.* Purification of Nanoparticles by Size and Shape. *Sci. Rep.* **6,** 27494 (2016).
72. do Nascimento, D. F. *et al.* Microfluidic Fabrication of Pluronic Vesicles with Controlled Permeability. *Langmuir* **32,** 5330–5355 (2016).
73. Mason, M. N., Metters, A. T., Bowman, C. N. & Anseth, K. S. Predicting Controlled-Release Behavior of Degradable PLA-b-PEG-b-PLA Hydrogels. *Macromolecules* **34,** 4630–4635 (2001).
74. Brunner, A., Mäder, K. & Göpferich, A. pH and Osmotic Pressure Inside Biodegradable Microspheres During Erosion. *Pharm. Res.* **16,** 847–853 (1999).
75. Schliecker, G., Schmidt, C., Fuchs, S. & Kissel, T. Characterization of a homologous series of D, L-lactic acid oligomers; a mechanistic study on the degradation kinetics in vitro. *Biomaterials* **24,** 3835–3844 (2003).
76. Codari, F. *et al.* Kinetics of the hydrolytic degradation of poly (lactic acid). *Polym. Degrad. Stab.* **97,** 2460–2466 (2012).
77. Lazzari, S., Codari, F., Storti, G., Morbidelli, M. & Moscatelli, D. Modeling the pH-dependent PLA oligomer degradation kinetics. *Polym. Degrad. Stab.* **110,** 80–90 (2014).
78. Dunne, M., Corrigan, O. I. & Ramtoola, Z. Influence of particle size and dissolution conditions on the degradation properties of polylactide-co-glycolide particles. *Biomaterials* **21,** 1659–1668 (2000).
79. Rydz, J., Sikorska, W., Kyulavska, M. & Christova, D. Polyester-Based (Bio) degradable Polymers as Environmentally Friendly Materials for Sustainable Development. *Int. J. Mol. Sci.* **16,** (2015).
80. Hocine, S. *et al.* Polymersomes with PEG corona: structural changes and

controlled release induced by temperature variation. *Langmuir* **29,** 1356–69 (2013).

81. Habel, J. *et al.* Selecting analytical tools for characterization of polymersomes in aqueous solution. *RSC Adv.* **5,** 79924–79946 (2015).
82. Silverman, L. & Glick, D. THE REACTIVITY AND STAINING OF TISSUE PROTEINS WITH PHOSPHOTUNGSTIC ACI. *J. Cell Biol.* **40,** 761–767 (1969).
83. Zhu, Y., Yang, B., Chen, S. & Du, J. Polymer vesicles: Mechanism, preparation, application, and responsive behavior. *Prog. Polym. Sci.* **64,** 1–22 (2017).
84. Lai, S. K. *et al.* Rapid transport of large polymeric nanoparticles in fresh undiluted human mucus. *Proc. Natl. Acad. Sci.* **104,** 1482–1487 (2007).
85. Lieleg, O., Vladescu, I. & Ribbeck, K. Characterization of Particle Translocation through Mucin Hydrogels. *Biophys. J.* **98,** 1782–1789 (2010).
86. Men, Y., Peng, F., Tu, Y., van Hest, J. C. M. & Wilson, D. A. Methods for production of uniform small-sized polymersome with rigid membrane. *Polym. Chem.* **7,** 3977–3982 (2016).
87. Ruiz-Perez, L. *et al.* Molecular engineering of polymersome surface topology. *Sci. Adv.* **2,** e1500948–e1500948 (2016).
88. Habel, J. *et al.* Selecting analytical tools for characterization of polymersomes in aqueous solution. *RSC Adv.* **5,** (2015).
89. Grillo, D. A. *et al.* Mechanical properties of drug loaded diblock copolymer bilayers: A molecular dynamics study. *J. Chem. Phys.* **148,** 214901 (2018).
90. Kempe, S., Metz, H. & Mäder, K. Application of Electron Paramagnetic Resonance (EPR) spectroscopy and imaging in drug delivery research - Chances and challenges. *Eur. J. Pharm. Biopharm.* **74,** 55–66 (2010).
91. Rübe, A. & Mäder, K. Electron Spin Resonance Study on the Dynamics of Polymeric Nanocapsules. *J. Biomed. Nanotechnol.* **1,** 208–213 (2005).
92. Batrakova, E. V. & Kabanov, A. V. Pluronic block copolymers: Evolution of drug delivery concept from inert nanocarriers to biological response modifiers. *Journal of Controlled Release* (2008). doi:10.1016/j.jconrel.2008.04.013
93. Rodríguez-García, R. *et al.* Polymersomes: smart vesicles of tunable rigidity and permeability. *Soft Matter* (2011). doi:10.1039/c0sm00823k

94. Jones, R. A. L. The efficiency of encapsulation within surface rehydrated polymersomes. *Faraday Discuss.* **143,** 9–14 (2009).
95. Basf. Technical Information Soluplus. *BASF, Pharma Ingredients & Services* 1–8 (2010).
96. Yang, H. *et al.* Investigation of a nanosuspension stabilized by Soluplus®to improve bioavailability. *Int. J. Pharm.* **477,** 88–95 (2014).
97. Thornton, D. J. & Sheehan, J. K. From Mucins to Mucus Toward a More Coherent Understanding of This Essential Barrier. **1,** 54–61 (2004).
98. Voynow, J. A. & Rubin, B. K. Mucins, Mucus, and Sputum. *Chest* **135,** 505–512 (2009).
99. Cai, L. *et al.* STRUCTURE AND FUNCTION OF AIRWAY SURFACE LAYER OF THE HUMAN LUNGS & MOBILITY OF PROBE PARTICLES IN COMPLEX FLUIDS. (2012).
100. Corfield, A. P. Mucins: A biologically relevant glycan barrier in mucosal protection. *Biochim. Biophys. Acta - Gen. Subj.* **1850,** 236–252 (2015).
101. Rose, M. C. Respiratory Tract Mucin Genes and Mucin Glycoproteins in Health and Disease. *Physiol. Rev.* **86,** 245–278 (2006).
102. Berry, M., Corfield, A. P. & Mcmaster, T. J. Mucins: a dynamic biology. doi:10.1039/c2sm26453f
103. Moniaux Nicolas , Escande Fabienne, Porchet Nicole, J.-P. A. and S. B. Structural organization and classification of the human mucin genes. *Syst. Biol.* **61,** i1 (2001).
104. Sheehan, J. K. *et al.* Identification of Molecular Intermediates in the Assembly Pathway of the MUC5AC Mucin. *J. Biol. Chem.* **279,** 15698–15705 (2004).
105. Perez-vilar, J. & Hill, R. L. Secreted Mucins * □. *Biochemistry* 31751–31754 (1999).
106. Wickström, C., Davies, J. R., Eriksen, G. V, Veerman, E. C. & Carlstedt, I. MUC5B is a major gel-forming, oligomeric mucin from human salivary gland, respiratory tract and endocervix: identification of glycoforms and C-terminal cleavage. *Biochem. J.* **334 (Pt 3,** 685–93 (1998).
107. Wang, Y.-Y. *et al.* The Microstructure and Bulk Rheology of Human Cervicovaginal Mucus Are Remarkably Resistant to Changes in pH. *Biomacromolecules* **14,** 4429–4435 (2013).

108. Levitin, F. *et al.* The MUC1 SEA module is a self-cleaving domain. *J. Biol. Chem.* **280,** 33374–33386 (2005).
109. Johansson, M. E. V. & Hansson, G. C. Immunological aspects of intestinal mucus and mucins. *Nat. Rev. Immunol.* (2016). doi:10.1038/nri.2016.88
110. Walji, N. A Systematic Correlation of Nanoparticle Size with Diffusivity through Biological Fluids. (Imperial College London, 2010).
111. Dawson, M., Wirtz, D. & Hanes, J. Enhanced Viscoelasticity of Human Cystic Fibrotic Sputum Correlates with Increasing Microheterogeneity in Particle Transport. *J. Biol. Chem.* **278,** 50393–50401 (2003).
112. Sanders, N. N. *et al.* Cystic fibrosis sputum: A barrier to the transport of nanospheres. *Am. J. Respir. Crit. Care Med.* **162,** 1905–1911 (2000).
113. Christopher J. Cheng;, Gregory T. Tietjen;, Jennifer K. Saucier-Sawyer & W. Mark Saltzman. A holistic approach to targeting disease with polymeric nanoparticles. *Nat. Rev.* **14,** 239–247 (2015).
114. Nordgård, C. T. & Draget, K. I. Co association of mucus modulating agents and nanoparticles for mucosal drug delivery. *Adv. Drug Deliv. Rev.* **124,** 175–183 (2018).
115. Araújo, F., Martins, C., Azevedo, C. & Sarmento, B. Chemical modification of drug molecules as strategy to reduce interactions with mucus. *Adv. Drug Deliv. Rev.* **124,** 98–106 (2018).
116. Lai, S. K., Wang, Y. Y. & Hanes, J. Mucus-penetrating nanoparticles for drug and gene delivery to mucosal tissues. *Adv. Drug Deliv. Rev.* **61,** 158–171 (2009).
117. Ensign, L. M., Schneider, C., Suk, J. S., Cone, R. & Hanes, J. Mucus penetrating nanoparticles: Biophysical tool and method of drug and gene delivery. *Adv. Mater.* **24,** 3887–3894 (2012).
118. Mü ller, C. *et al.* Preparation and characterization of mucus-penetrating papain/poly(acrylic acid) nanoparticles for oral drug delivery applications. doi:10.1007/s11051-012-1353-z
119. Dünnhaupt, S., Kammona, O., Waldner, C., Kiparissides, C. & Bernkop-Schnürch, A. Nano-carrier systems: Strategies to overcome the mucus gel barrier. *Eur. J. Pharm. Biopharm.* (2015). doi:10.1016/j.ejpb.2015.01.022
120. Shan, W. *et al.* Overcoming the Diffusion Barrier of Mucus and Absorption

Barrier of Epithelium by Self-Assembled Nanoparticles for Oral Delivery of Insulin. **9,** 2345–2356 (2015).

121. Yang, M. *et al.* Biodegradable nanoparticles composed entirely of safe materials that rapidly penetrate human mucus. *Angew. Chemie - Int. Ed.* **50,** 2597–2600 (2011).
122. Cu, Y. & Saltzman, W. M. Controlled surface modification with poly(ethylene)glycol enhances diffusion of PLGA nanoparticles in human cervical mucus. *Mol. Pharm.* **6,** 173–181 (2008).
123. Schuster, B. S., Ensign, L. M., Allan, D. B., Suk, J. S. & Hanes, J. Particle tracking in drug and gene delivery research: State-of-the-art applications and methods. *Adv. Drug Deliv. Rev.* (2015). doi:10.1016/j.addr.2015.03.017
124. Grießinger, J. *et al.* Methods to determine the interactions of micro-and nanoparticles with mucus. *Eur. J. Pharm. Biopharm.* **96,** 464–476 (2015).
125. Li, L., Lieleg, O., Jang, S., Ribbeck, K. & Han, J. A microfluidic in vitro system for the quantitative study of the stomach mucus barrier function. *Lab Chip* **12,** 4071–4079 (2012).
126. Valentine, M. T. *et al.* Investigating the microenvironments of inhomogeneous soft materials with multiple particle tracking. *Phys. Rev. E - Stat. Physics, Plasmas, Fluids, Relat. Interdiscip. Top.* **64,** 9 (2001).
127. MIT. What is multiple particle tracking? 3–4 (2012). Available at: http://web.mit.edu/savin/Public/.Tutorial_v1.2/Introduction.html. (Accessed: 9th September 2016)
128. Lee, C. H., Crosby, A. J., Emrick, T. & Hayward, R. C. Characterization of Heterogeneous Polyacrylamide Hydrogels by Tracking of Single Quantum Dots. *Macromolecules* **47,** 741–749 (2014).
129. Dawson, M., Krauland, E., Wirtz, D. & Hanes, J. Transport of Polymeric Nanoparticle Gene Carriers in Gastric Mucus. *Biotechnol Prog* **20,** 851–857 (2004).
130. Yu, T. *et al.* Liposome-based mucus-penetrating particles (MPP) for mucosal theranostics: Demonstration of diamagnetic chemical exchange saturation transfer (diaCEST) magnetic resonance imaging (MRI). *Nanomedicine Nanotechnology, Biol. Med.* **11,** 401–405 (2015).
131. Suh, J., Wirtz, D. & Hanes, J. Real-time intracellular transport of gene

nanocarriers studied by multiple particle tracking. *Biotechnol. Prog.* **20,** 598–602 (2004).

132. Xu, Q. *et al.* Scalable Method to Produce Biodegradable Nanoparticles that Rapidly Penetrate Human Mucus. *J. Control. Release* **170,** 279–286 (2014).
133. Hanes, J. & Demeester, J. Drug and gene delivery to mucosal tissues: the mucus barrier. *Adv. Drug Deliv. Rev.* **61,** 73–74 (2009).
134. Maisel, K., Ensign, L., Reddy, M., Cone, R. & Hanes, J. Effect of surface chemistry on nanoparticle interaction with gastrointestinal mucus and distribution in the gastrointestinal tract following oral and rectal administration in the mouse. (2014). doi:10.1016/j.jconrel.2014.10.026
135. Ensign, L. M. *et al.* Mucus-Penetrating Nanoparticles for Vaginal Drug Delivery Protect Against Herpes Simplex Virus. *Sci. Transl. Med.* **4,** 138ra79-138ra79 (2012).
136. Nance, E. A. *et al.* A Dense Poly(ethylene glycol) Coating Improves Penetration of Large Polymeric Nanoparticles within Brain Tissue. *Sci. Transl. Med.* **4,** (2012).
137. Del Consuelo, I. D., Pizzolato, G. P., Falson, F., Guy, R. H. & Jacques, Y. Evaluation of pig esophageal mucosa as a permeability barrier model for buccal tissue. *J. Pharm. Sci.* **94,** 2777–2788 (2005).
138. Mohan, P. & Rapoport, N. Doxorubicin as a molecular nanotheranostic agent: Effect of doxorubicin encapsulation in micelles or nanoemulsions on the ultrasound-mediated intracellular delivery and nuclear trafficking. *Mol. Pharm.* **7,** 1959–1973 (2010).
139. Ayen, W. Y. & Kumar, N. In vivo evaluation of doxorubicin-loaded (PEG)3-PLA nanopolymersomes (PolyDoxSome) using DMBA-induced mammary carcinoma rat model and comparison with marketed LipoDox??? *Pharm. Res.* **29,** 2522–2533 (2012).
140. Upadhyay, K. K. *et al.* The intracellular drug delivery and anti tumor activity of doxorubicin loaded poly(γ-benzyl l-glutamate)-b-hyaluronan polymersomes. *Biomaterials* **31,** 2882–2892 (2010).
141. Liao, J. F. *et al.* Combined cancer photothermal-chemotherapy based on doxorubicin/gold nanorod-loaded polymersomes. *Theranostics* **5,** 345–356 (2015).

142. Alibolandi, M. *et al.* The chemotherapeutic potential of doxorubicin-loaded PEG-b-PLGA nanopolymersomes in mouse breast cancer model. *Eur. J. Pharm. Biopharm.* **94,** 521–531 (2015).
143. Du, Y., Chen, W., Zheng, M., Meng, F. & Zhong, Z. PH-sensitive degradable chimaeric polymersomes for the intracellular release of doxorubicin hydrochloride. *Biomaterials* **33,** 7291–7299 (2012).
144. Kumar Upadhyay, K. *et al.* Biomimetic doxorubicin loaded polymersomes from hyaluronan-block- poly(γ-benzyl glutamate) copolymers. *Biomacromolecules* **10,** 2802–2808 (2009).
145. Upadhyay, K. K. *et al.* The in vivo behavior and antitumor activity of doxorubicin-loaded poly(γ-benzyl l-glutamate)-block-hyaluronan polymersomes in Ehrlich ascites tumor-bearing BalB/c mice. *Nanomedicine Nanotechnology, Biol. Med.* **8,** 71–80 (2012).
146. Yassin, M. A., Appelhans, D., Mendes, R. G., R??mmeli, M. H. & Voit, B. PH-Dependent release of doxorubicin from fast photo-cross-linkable polymersomes based on benzophenone units. *Chem. - A Eur. J.* **18,** 12227–12231 (2012).
147. Katz, J. S. *et al.* Membrane stabilization of biodegradable polymersomes. *Langmuir* **25,** 4429–4434 (2009).
148. Sanson, C. *et al.* A simple method to achieve high doxorubicin loading in biodegradable polymersomes. *J. Control. Release* **147,** 428–435 (2010).
149. Xu, J., Zhao, Q., Jin, Y. & Qiu, L. High loading of hydrophilic/hydrophobic doxorubicin into polyphosphazene polymersome for breast cancer therapy. *Nanomedicine Nanotechnology, Biol. Med.* **10,** 349–358 (2014).
150. Ahmed, F. *et al.* Biodegradable polymersomes loaded with both paclitaxel and doxorubicin permeate and shrink tumors, inducing apoptosis in proportion to accumulated drug. *J. Control. Release* **116,** 150–158 (2006).
151. Sanson, C. *et al.* Doxorubicin Loaded Magnetic Polymersomes: Theranostic Nanocarriers for MR Imaging and Magneto-Chemotherapy. *ACS Nano* **5,** 1122–1140 (2011).
152. Zou, Y., Meng, F., Deng, C. & Zhong, Z. Robust, Tumor-Homing and Redox-Sensitive Polymersomal Doxorubicin: A Superior Alternative to Doxil and Caelyx? *J. Control. Release (2016),* (2016). doi:10.1016/j.jconrel.2016.08.022

153. Zhu, D. *et al.* Bubble-generating polymersomes loaded with both indocyanine green and doxorubicin for effective chemotherapy combined with photothermal therapy. *Acta Biomater.* **75,** 386–397 (2018).
154. Yildirim, T. *et al.* Polymersomes with Endosomal pH-Induced Vesicle-to-Micelle Morphology Transition and a Potential Application for Controlled Doxorubicin Delivery. (2017). doi:10.1021/acs.biomac.7b00931
155. Alibolandi, M. *et al.* Extensive preclinical investigation of polymersomal formulation of doxorubicin versus Doxil-mimic formulation. *J. Control. Release* **264,** 228–236 (2017).
156. Tian, Y., Bromberg, L., Lin, S. N., Alan Hatton, T. & Tam, K. C. Complexation and release of doxorubicin from its complexes with pluronic P85-b-poly(acrylic acid) block copolymers. *J. Control. Release* **121,** 137–145 (2007).
157. Tian, Y., Ravi, P., Bromberg, L., Hatton, T. A. & Tam, K. C. Synthesis and aggregation behavior of Pluronic F87/poly(acrylic acid) block copolymer in the presence of doxorubicin. *Langmuir* **23,** 2638–2646 (2007).
158. Waters, L. J., Swaine, T. S. & Lewis, A. L. A calorimetric investigation of doxorubicin-polymer bead interactions. *Int. J. Pharm.* **493,** 129–133 (2015).
159. Lohade, A. A. *et al.* A Novel Folate-Targeted Nanoliposomal System of Doxorubicin for Cancer Targeting. *AAPS PharmSciTech* **17,** 1298–1311 (2016).